

SDPO.20.002.m.

Parameter identification of full-scale propulsion systems

by T. A. (Tom) Martinus



SHIP FINGERPRINTING

Parameter identification of full-scale propulsion systems

by T.A. (Tom) Martinus

to obtain the degree of Master of Science in Marine Technology
at the Delft University of Technology,
to be defended publicly on Monday March 16, 2020 at 15:00.

Student number: 4317343
Project duration: May 1, 2019 – March 16, 2020
Thesis committee: Ir. K. Visser, Rear Admiral (ME) ret., TU Delft, chair
Dr. ir. A. Vrijdag, TU Delft, daily supervisor
Dr. ir. K. Batselier, TU Delft
Ir. E. J. Boonen, Damen Shipyards Group

This thesis is confidential and cannot be made public until March 16, 2022.

An electronic version of this thesis is available at
<http://repository.tudelft.nl/>.



ACKNOWLEDGEMENTS

First I want to thank Damen Shipyards Gorinchem for giving me the opportunity of completing my master thesis at their R&D department. A great atmosphere and the open doors helped me a lot when I was facing a new problem. I want to thank all of my colleagues for helping me along the way.

In special I want to thank Marnix Bockstael for proofreading the different chapters and for doing a gremmer tjeck. Furthermore I want to thank Arthur Vrijdag & Erik-Jan Boonen for introducing me to this topic and offering me opportunity of doing full scale experiments. Doing this was an unique learning experience and gave me a sneak preview on how full scale experiments in practice are executed.

ABSTRACT

That what makes simulation models useful and especially interesting, is simultaneously what makes building them so difficult. Involving the correct dynamic behaviour in a simulation model is hard and rarely done for commercial purposes. A way of identifying dynamic model parameters within commercial purposes can possibly be done by using parameter identification techniques. The in- and output signal are simultaneously measured, while the input signal contains the correct amplitude and frequencies so that the whole dynamic behaviour of the system will be exposed. When the in- and output are known, this tells something about the system and hopefully the system's parameters can be identified which enables you to have a correct dynamic model in a short time.

First of all, it is tried to identify model parameters of a nonlinear simulation model. Then, this experience is used to avoid pitfalls on the way to parameter identification of a physical propulsion drive train on full-scale. Parameter identification generally requires three things: an information-rich data set, a model structure representing different relations between the system parameters and finally an optimization program.

A nonlinear model is built for the generation of different information-rich datasets. Subsequently, this nonlinear model is linearized so that it can be used as a model structure for parameter estimation. Using an existing Matlab tool for optimization a successful virtual parameter estimation is executed. The parameter estimation was successful, because the initial parameters are known as they are implemented in the nonlinear model and the estimated parameters are identical to the implemented ones. This succeeded for multiple input signals, which means that different information-rich datasets were generated and used for parameter identification. It is important to note that not all individual parameters could be estimated as absolute values. Due to limitations in the model structure, some parameters were only estimated relatively to each other.

Due to the success of the virtual parameter estimation, full-scale experiments were executed on the 5th of November using a stock vessel, namely the Stan Tug 1205 of Damen. During this experiment, full-scale information-rich datasets were generated. A document containing execution details of this experiment, 'experiment protocol', is delivered separately from this thesis, so that origin of the data is known and it can be used for other researches or a repetition of this research.

Apart from some minor changes are for the full-scale parameter identification the same model structure and optimization program used as during the virtual parameter identification. The estimated parameter sets of different parameter estimations with the full-scale data are showing less promising results. The differences between the estimations are so big that results of the different parameter estimations are not trustworthy.

One single parameter of the estimated parameter set is 'known', because it can be obtained from a different kind of experiment. However, the value of this parameter according to the other experiment is completely different than when the value is estimated by parameter identification. Additionally, some of the estimated parameters and/or relations show unexpectedly high or low values. However, when the estimated parameter set is implemented in the model structure it shows step response behaviour similar to step response data from the full-scale experiments. During manoeuvring the most common input signals by the captain are steps, so the relevant responses can now be simulated to some extent.

CONTENTS

List of Symbols	xvii
1 INTRODUCTION	3
1.1 Motivation	3
1.2 Research questions	6
1.3 Research approach	7
1.4 Outline	9
2 LITERATURE REVIEW	11
2.1 Simulation model	11
2.2 Parameter identification	12
3 SIMULATION MODEL	15
3.1 Nonlinear model	15
3.2 Static validation nonlinear model	18
3.2.1 Vessel specification of virtual vessel	18
3.2.2 Static validation	20
3.3 Linearized model	22
3.3.1 DAE of linearized model	22
3.3.2 Transfer functions	23
3.3.3 State space notation	27
3.4 Nominal operation point	29
3.5 Verification of linearized model	30
3.5.1 Verification in time domain	30
3.5.2 Verification in frequency domain	32
3.6 Conclusion	34
4 PARAMETER IDENTIFICATION	35
4.1 Searching algorithm	35
4.1.1 Problem statement time domain	35
4.1.2 Cost function	36
4.1.3 Optimisation	38
4.1.4 Estimated fit	39
4.1.5 Problem statement frequency domain	40
4.2 Model structure	41
4.2.1 Parameter constraints	41
4.2.2 Internal relations	41
4.3 Information-rich data sets	43
4.3.1 Data set generation	43
4.3.2 Input signals	43
4.3.3 Signal requirements	45
4.4 Conclusion	46
5 VIRTUAL PARAMETER ESTIMATION	47
5.1 Data generation from nonlinear model	47
5.1.1 Multiple sine waves	47
5.1.2 Chirp signal	49
5.1.3 Step responses	54
5.2 Searching algorithm	55

5.3	Model structure	55
5.4	Results parameter identification	56
5.5	Conclusion	60
6	FULL-SCALE EXPERIMENTS	61
6.1	Description of experimental set up	61
6.1.1	Situation sketch	61
6.1.2	Ship and the propulsion system description	63
6.1.3	Measurement system description	65
6.2	Description of experiments	71
6.2.1	Multiple sine waves	72
6.2.2	Chirp waves	72
6.2.3	Step responses sequences	72
6.3	Signal inspection	74
6.3.1	Global analysis	74
6.3.2	Detailed analysis	79
6.4	Data pre-processing	83
6.5	Conclusions & Recommendations	85
6.5.1	Conclusion	85
6.5.2	Recommendations experiments	86
7	FULL-SCALE PARAMETER ESTIMATION	87
7.1	Data from pre-processing	87
7.1.1	Multiple sine wave	87
7.1.2	Short chirp signal	92
7.1.3	Long chirp signal	93
7.1.4	Step responses	95
7.2	Model structure & searching algorithm	95
7.3	Results parameter identification	96
7.3.1	Frequency domain behaviour	98
7.3.2	Time domain validation	99
7.3.3	Parameter validation	103
7.4	Conclusion & Recommendations	104
7.4.1	Conclusion	104
7.4.2	Recommendations full-scale estimation	105
8	CONCLUSION & RECOMMENDATIONS	107
8.1	Conclusion	107
8.1.1	First sub question	107
8.1.2	Second sub question	108
8.1.3	Third sub question	109
8.2	Recommendations	110
A	LINEARIZATION	117
A.1	Normalization of Governor	117
A.2	Derivation shaft torque and engine set point	117
B	RELATIONS MODELSTRUCTURE	119
C	STAN TUG 1205	121
D	SHAFT TORQUE FACTOR	123
E	TIME TO FREQUENCY DOMAIN	125

LIST OF FIGURES

Figure 1.1	Model parameter identification.	5
Figure 1.2	Location of subquestions in block diagram.	7
Figure 1.3	Thesis outline in block diagram.	9
Figure 2.1	Clarification categories of model parameter identification.	13
Figure 3.1	Block diagram of the nonlinear model.	16
Figure 3.2	Validation nonlinear model in bollard pull with a sea trial.	20
Figure 3.3	Validation nonlinear model of the engine with a sea trial.	21
Figure 3.4	Linearized parameters from nonlinear model.	29
Figure 3.5	Comparison between nonlinear model and linearized model of shaft speed response.	31
Figure 3.6	Comparison between nonlinear model and linearized model of shaft torque response.	31
Figure 3.7	Comparison between nonlinear model and linearized model of integrated error response.	32
Figure 3.8	Verification of $\frac{\delta n^*}{\delta n_{set}^*}$	33
Figure 3.9	Verification of $\frac{\delta M_s^*}{\delta n_{set}^*}$	33
Figure 3.10	Verification of $\frac{\delta E_{fl}^*}{\delta n_{set}^*}$	33
Figure 4.1	Explanation of unavoidable error in linear parameter estimation.	36
Figure 4.2	Data set generation of nonlinear model.	43
Figure 5.1	Multiple sine waves as input signal.	48
Figure 5.2	Multiple sine waves as input signal and shaft speed as output signal.	48
Figure 5.3	Multiple sine waves as input signal and shaft torque as output signal.	49
Figure 5.4	Chirp signal logarithmic divided over time as input signal.	50
Figure 5.5	Chirp signal logarithmic divided over time as input signal and shaft speed as output signal.	50
Figure 5.6	Chirp signal logarithmic divided over time as input signal and shaft torque as output signal.	51
Figure 5.7	Chirp signal linear divided over time as input signal.	51
Figure 5.8	Chirp signal linear divided over time as input signal and shaft speed as output signal.	52
Figure 5.9	Chirp signal linear divided over time as input signal and shaft torque as output signal.	52
Figure 5.10	Chirp signal with higher amplitude logarithmic divided over time as input signal.	53
Figure 5.11	Chirp signal with higher amplitude logarithmic divided over time as input signal and shaft speed as output signal.	53
Figure 5.12	Chirp signal with higher amplitude logarithmic divided over time as input signal and shaft torque as output signal.	53

Figure 5.13	Step response signal as input signal and shaft speed as output signal.	54
Figure 5.14	Step response signal as input signal and shaft speed as output signal.	54
Figure 5.15	Comparison parameter estimation frequency domain for $\frac{\delta n^*}{\delta n_{set}^*}$	57
Figure 5.16	Comparison parameter estimation frequency domain for $\frac{\delta M_s^*}{\delta n_{set}^*}$	58
Figure 5.17	Comparison parameter estimation in time domain.	59
Figure 5.18	Comparison parameter estimation time domain zoomed in on third step.	59
Figure 6.1	The experimental vessel set up.	62
Figure 6.2	Sailing Stan Tug 1205.	63
Figure 6.3	Set up of the MCC system on board of the Stan Tug 1205.	64
Figure 6.4	Schematic overview measurement set up during the experiments.	66
Figure 6.5	Explanation of the sampling rate DEWESoft Dual Core (1).	67
Figure 6.6	Explanation of pulse time modulation (PTM).	69
Figure 6.7	Board of the MCC system	70
Figure 6.8	Detailed propulsion layout	70
Figure 6.9	Test set up of input signal validation.	74
Figure 6.10	Correlation between input voltage and output current.	75
Figure 6.11	Shaft speed comparison between one pulse measurement and four pulse measurement.	75
Figure 6.12	Explanation pulse difference with a cross section of the shaft line, where the blue rectangles represents the reflectors glued on the shaft.	76
Figure 6.13	Shaft torque signal with constant input signal.	77
Figure 6.14	Shaft torque in frequency domain, with RMS of torque signal in Nm.	78
Figure 6.15	Shaft speed in time domain.	80
Figure 6.16	Shaft speed in time domain.	80
Figure 6.17	Shaft torque in time domain with detailed crest.	81
Figure 6.18	Shaft torque in time domain with detailed crest.	82
Figure 6.19	Signal 'C21' of table 6.7.	82
Figure 6.20	Shaft speed as function of input voltage.	83
Figure 7.1	Multiple sine wave input signal.	88
Figure 7.2	Multiple sine wave input signal and shaft speed 4 pulse measurement.	88
Figure 7.3	High frequency part of multiple sine wave input signal and shaft speed 4 pulse measurement.	88
Figure 7.4	Multiple sine wave input signal and shaft torque	89
Figure 7.5	Shaft torque response in full-scale measurement.	90
Figure 7.6	Bode plot of $\frac{\delta n^*}{\delta n_{set}^*}$	91
Figure 7.7	Bode plot of $\frac{\delta M_s^*}{\delta n_{set}^*}$	92
Figure 7.8	Chirp input signal 'C11' of table 6.7.	92
Figure 7.9	Chirp input signal 'C11' of table 6.7 and shaft speed response.	93

Figure 7.10	Chirp input signal 'C11' of table 6.7 and shaft torque response.	93
Figure 7.11	Chirp input signal 'C21','C22' and 'C23' of table 6.7 and the shaft speed response.	94
Figure 7.12	Chirp input signal 'C21','C22' and 'C23' of table 6.7 and the shaft speed response.	94
Figure 7.13	Chirp input signal 'C21','C22' and 'C23' of table 6.7 and the shaft torque response.	94
Figure 7.14	Step response data St1 of table 6.7. Upper graph shaft speed response, middle graph shaft torque response and lower graph input signal.	95
Figure 7.15	Frequency domain comparison $\frac{\delta n_s^*}{\delta n_{set}^*}$	98
Figure 7.16	Frequency domain comparison $\frac{\delta M_s^*}{\delta n_{set}^*}$	99
Figure 7.17	Comparison parameter estimation time domain.	99
Figure 7.18	Comparison parameter estimation time domain zoomed in on third step	100
Figure 7.19	Validation parameter estimation iii and iv with multiple sine waves.	100
Figure 7.20	Validation parameter estimation ii and iv with short chirp signal.	101
Figure 7.21	Validation parameter estimation ii and iii with long chirp signal.	102
Figure 7.22	Explanation of influence of shaft torque measurement on the value τ_n	103
Figure 7.23	Reasons for incorrect parameter estimation	105
Figure A.1	Closed loop linearization	117
Figure E.1	Input signal validation 3.433 Hz in time domain	127
Figure E.2	Input signal validation 3.433 Hz in frequency domain	127
Figure E.4	Input signal validation 3.433 Hz in frequency domain.	128
Figure E.6	Input signal validation 7.19 Hz in frequency domain.	129
Figure E.7	Torque signal wrongly estimated amplitude at input frequency 3.44 Hz in time domain.	130
Figure E.8	Torque signal wrongly estimated amplitude at input frequency 3.44 Hz in frequency domain.	130
Figure E.9	Torque signal wrongly estimated amplitude at input frequency 7.19 Hz in frequency domain.	130

LIST OF TABLES

Table 3.1	Main particulars of virtual vessel.	18
Table 3.2	Additional input of nonlinear model with values. . .	18
Table 3.3	Highest reflected mass moment inertia's in propulsion drive train of virtual vessel seen from propeller side.	19
Table 3.4	Summary of different transfer function.	27
Table 3.5	Values of system variables with constant input signal of $n_{set} = 1300rpm = 21.7rps$	29
Table 3.6	Values of linearized model parameters with constant input signal of $n_{set} = 1300rpm$ on nonlinear model. .	29
Table 3.7	The applied step responses.	30
Table 4.1	Definition of different linearized model parameters.	41
Table 4.2	System of linear equations of the internal relations within the model structure.	42
Table 5.1	Different frequencies of sine signal presented in Hz. .	48
Table 5.2	Results of virtual experiments.	57
Table 6.1	Dimensions of pontoon and the aft of the Stan Tug 1205.	62
Table 6.2	Main particulars of Stan Tug 1205.	63
Table 6.3	Clarification of the abbreviation in figure 6.3.	64
Table 6.4	Clarification symbols in figure 6.4.	66
Table 6.5	Logged signals on the different logging devices. . . .	68
Table 6.6	Conversion factor provided by JVS B.V.	69
Table 6.7	Overview of executed experiments with the names of the logfiles.	71
Table 6.8	Shaft torque analysis	77
Table 6.9	Peak frequencies obtained from figure 6.14.	78
Table 6.10	Different signals with their 'errors'.	79
Table 6.11	Relationship between input signal and engine speed derived from JVS logging.	83
Table 6.12	Normalisation points of logging device of JVS, with $U_{setpoint} = -5V$	84
Table 7.1	Results of full-scale parameter estimations.	97
Table 7.2	Fit percentage shaft speed of different parameter estimations according to different validation sets. . . .	102
Table 7.3	Fit percentage shaft torque of different parameter estimations according to different validation sets. . . .	102
Table E.1	Setpoint engine speed determined by 'SineFit'	125
Table E.2	Shaft speed determined by 'SineFit'	126
Table E.3	Shaft torque determined by 'SineFit'	126

LIST OF SYMBOLS

NONLINEAR MODEL

M_s	Shaft torque	$[Nm]$
M_p	Propeller torque	$[Nm]$
M_b	Engine torque	$[Nm]$
n_{set}	Set point of engine speed	$[rpm]$
n_e	Engine speed	$[rpm]$
n_s	Shaft speed	$[rps]$
e_n	Error between n_{set} and n_e	$[rpm]$
X_f	Fuel rack	$[mm]$
X_{set}	Set point fuel rack	$[mm]$
K_p	Proportional part gain	$[-]$
K_i	Integral part gain	$[-]$
i_{gb}	Gearbox ratio	$[-]$
Q	Propeller open water torque	$[Nm]$
T	Thrust force	$[N]$
K_q	Torque coefficient	$[-]$
K_t	Thrust coefficient	$[-]$
D_p	Propeller diameter	$[m]$
v_a	Advanced velocity	$[m/s]$
η_{trm}	Transmission losses	$[-]$
η_r	Relative rotative efficiency	$[-]$
$I_{p,tot}$	Total mass moment of inertia	$[kgm^2]$
ρ	Water density	$[kg/m^3]$

LINEARIZED MODEL

τ_n	Integration constant	$[s]$
g	Relation engine speed and engine torque	$[-]$
v	Relation fuelrack and engine torque	$[-]$

SEARCHING ALGORITHM

Ψ	Parameter set of nonlinear model	$[-]$
θ	Parameter set of linear model	$[-]$
y	Output signals, where n_y is number of output channels	$[Nm, rpm]$
R	Confidence in prior knowledge of unknown parameters	$[-]$
e	Error between output experiments and model response	$[Nm, rpm]$
W	Weighted function	$[-]$
N	Amount of samples	$[-]$
ω	Frequency	$[Hz]$

EXPERIMENTS

R	Resistance	$[\Omega]$
U	Voltage	$[V]$
I	Current	$[A]$
T_p	Pulse period	$[s]$

NOTATIONS

Scalar	$x \in \mathbb{R}$	-
Dimensionless Scalar	$x^* \in \mathbb{R}$	-
Vector	$\bar{x} \in \mathbb{R}^{m \times 1}$	$\begin{bmatrix} x_1 \\ x_2 \\ \vdots \\ x_m \end{bmatrix}$

1

INTRODUCTION

This chapter contains four different main parts, where the motivation for this research is outlined in the first main part. The second main part contains the main research question, which is then divided into several subquestions. The third main part contains the research approach, which describes how the different subquestions can be answered. During the definition of this approach also a great part of the scope is implicitly defined. In the last main part the report outline is given, clarifying the structure of this thesis.

1.1 MOTIVATION

Computer simulation models play a more important role in every field of engineering nowadays. Furthermore the desire of having a simulation model is increasing. A simulation model is an imitation of the reality. In the marine industry, this can be a simple waste-heat system but also a complex propulsion drive train with different configuration modes. The main reason for having a simulation model is that every kind of dynamic propulsion behavior can be tested in a cheaper and safe environment (2). Especially for the propulsion drive train, where high forces are involved.

The definition of dynamic behavior is the 'path' taken from a starting point A to a new point B, instead of the static values of those two points. To put this in marine propulsion terms: It is common practice nowadays that an engineer calculates the power in different static operating points of the engine. But it is much harder for the engineer to calculate how the propulsion system behaves between the operating points. In other words, what is the 'path' between the operating points A and B?

The reason what makes the simulation models especially useful and interesting. Is also the reason why the building of the simulation models is really difficult. Involving the *correct* dynamic behaviour in a simulation model is hard and rarely done for commercial purposes. The difficulty is that the suppliers of the equipment in the drive train are often not willing to share the correct dynamic behaviour of their components.

But for a shipyard, the urge of having such a dynamic simulation is still there. What kind of simulation studies does a shipyard want to do and which commercial advantages can this have? First of all, the ability for testing the *control system* of the ships propulsion in a simulated environment can decrease the required testing time in a sea trial, since fine-tuning of the control system is one of the most time-consuming activities. This is shown in the testing results of aircraft carrier 'Cavour', built for the Italian navy. The final tuning at sea lasted less than half of the time that is normally scheduled (3). Furthermore the complexity of the propulsion drive train

is increased in the last decade, due to the building of vessels with hybrid propulsion plants and/or more redundancy. As a consequence, the control system becomes even more critical. In the near future, more vessels will be equipped with different propulsion systems, due to an increase of different emission zones all around the world, which again results in more complex control systems.

Another example where simulation models can play a key role, is in the answering to the new IMO requirements. Vessels built today are quite often installed with less power, because they have to comply with the new rules of the international maritime organization (IMO), the energy efficiency design index (EEDI). Potentially, the EEDI could affect the safety in adverse conditions as the installed power is lowered for complying with the EEDI rule (2). For some vessels the EEDI is a design driver, so the installation of less power is beneficial for the complete ship design.

A good control system can also play an important role during the purchase of a vessel by a shipping company. Because sailing with the correct control system can be economically beneficial. For example, economical benefit is achieved by tuning the control system such that the system is less aggressive to small errors. This results in less accelerations which reduces the total amount of energy required for the voyage.

The last possibility is adjusting an existing control systems for a certain situation. During manoeuvring, for example, the captain wants a more aggressive vessel behaviour, so a button can be created which makes the propulsion system more aggressive. But also, one can adjust the control system during sea trials for better results, such as during turning circles and crash stops.

The four reasons mentioned here above indicate the importance of simulation models. But one should understand that the opportunities from having a simulation model are tremendous and some possibilities are still unknown, e.g. condition monitoring. The *problem statement*: 'The model parameter identification of a simulation model requires a lot of time, but the urge is increasing.'

As stated before, the dynamic behaviour of propulsion systems is often not identified, due to the fact that the parameters that are responsible for this dynamic behavior are unknown. Some parameters, as far as known, which are influencing the dynamic behaviour are so far never been known, such as the gain settings of the PID controller. Of course, some dynamic parameters of the components can be derived by doing individual experiments or by getting in touch with product specialists within the supply company. Nevertheless, the gathering of model parameters is very time-consuming task and asks for improvement.

A way of identifying model parameters is by data-driven models (DDM's) (4) (5). These models are built on historical data collected by on-board sensors and they estimate the parameters without requiring any priory knowledge of the system. But there are two really big disadvantages. First of all, the logging of the data on board is quite often too low sampled to make thrust worthy conclusions of the dynamic behaviour. The sampling rates

are low, because otherwise you get a tremendous amount of data. Another big disadvantage is that it is unknown if the information in the data sets is 'rich enough'. For example when a container vessel is sailing for two weeks with constant speed from harbour A to B, than these data sets are not containing enough dynamic behaviour.

Another way of identifying model parameters is by using parameter identification techniques. Nowadays, identification techniques are often used in other fields of engineering, e.g. sound and vibrations, where they excite the system with certain frequencies and measure the response somewhere else which tells you something about the system in between. For example when you put a speaker in room one and measure the noise in room two, than this says something about the wall in between room one and two. Figure 1.1 explains parameter identification, where an input signal is put on an unknown system, in our case a propulsion drive train. During the excitation of the system, the input and output from the propulsion drive train will be simultaneously measured and parameters can hopefully be identified.

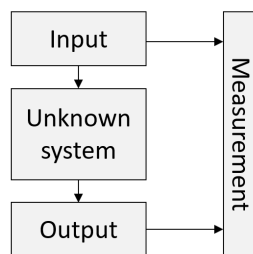


Figure 1.1: Model parameter identification.

The input signal on the propulsion drive train is chosen such that it is a short but information-rich signal, which contains different frequencies so that the whole dynamic behaviour of the vessel can be identified. From this dynamic behaviour the vessel parameters can be calculated. The experiment can take place just before a sea trial or after docking where big maintenance is carried out. Differences between previous gained parameters can point out improvements or installation errors in the maintenance work.

The research goal is to use parameter identification techniques to determine parameters of a full-scale marine propulsion system.

1.2 RESEARCH QUESTIONS

The research goal is defined in the previous section. This research goal leads to the following main research question:

“How to determine propulsion model parameters with identification techniques on a full-scale propulsion system in limited time?”

This main research question will be the common thread throughout this research and will be divided into several subquestions. Below, the different sub-questions are listed with a brief explanation on how this subquestion will contribute to the main research question.

- *‘Which parameter identification techniques are suitable for model parameter estimation of a ship propulsion plant?’* This subquestion involves different mathematical approaches on how the parameters can be identified.
- *‘Which experiments are suitable for the full-scale determination of model parameters?’* The goal of this subquestion is to gain knowledge for the full-scale experiments, where the emphasis lies on safety and pragmatically. Furthermore is the feasibility of full-scale parameter identification discussed.
- *‘What is the uncertainty of an estimated full-scale model parameter?’* The goal of this subquestion is to gain knowledge about the error in the estimated parameter. Also, the uncertainty in the estimated parameter is an important factor in making the concluding statement more thrust worthy.

1.3 RESEARCH APPROACH

The research approach is describing how the answers to the research questions are obtained, this implies that conditions are set. The research approach is split up into three parts, where every part contains one research subquestion.

The global lines of the research is summarized in figure 1.2. In this figure is also illustrated how the answering on the different subquestion is achieved.

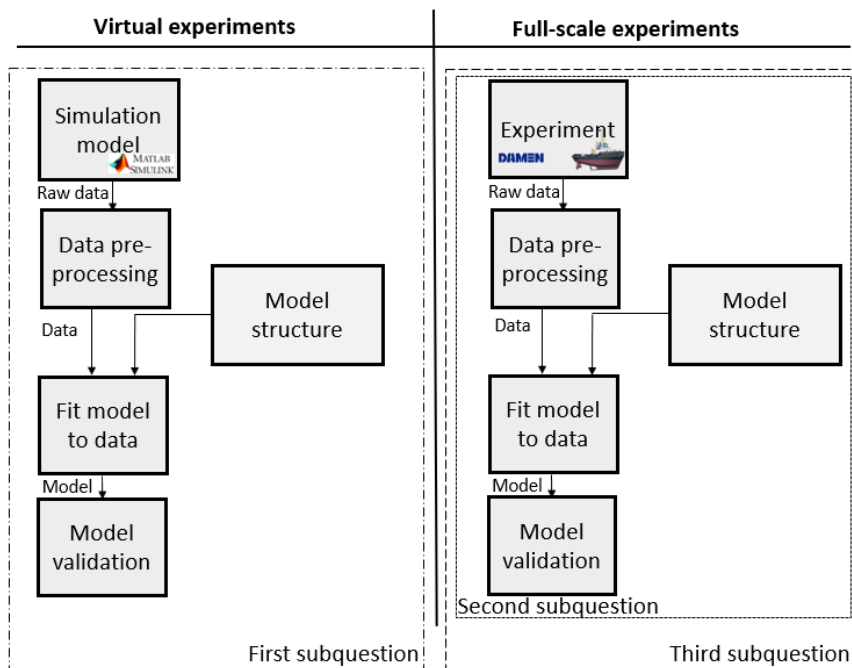


Figure 1.2: Location of subquestions in block diagram.

The '*first subquestion*' is answered with a computer simulation model of a propulsion system, so this is defined as virtual experiments in figure 1.2. In general can be stated that parameter estimation requires three things: data (input and output signals), model structure and an optimization program (fit model to data).

The answering of the first subquestion is done with virtual experiments for several reasons. First of all, different kind of datasets can be generated with the simulation model. Second of all the generation of these data sets in a computer model is faster than gaining them on full-scale. Furthermore using the simulation model is a lot cheaper and safer than doing this on a full-scale vessel. The third reason for building a computer simulation model is that it can be used as basis for the 'model structure' that is required for parameter estimation. Please note that the simulation model is built in Matlab Simulink in the same conditions as the full-scale experiments are executed.

Now the information rich dataset can be generated from the nonlinear model and the model structure can be derived from the nonlinear model, the only thing that is required for parameter estimation is the optimization program. The optimization program is discussed in chapter 4.1 'Methods', were more

in depth research is done on different optimization program and how this optimization works in practice. Using these three pillars, the answering of the first subquestion can be done. Namely, how and to which extent the model parameters can be determined in a theoretical way.

The *second subquestion* is answered with a more pragmatic approach. This is exactly one of the goals of this research question, as after the answering of this question an experiment protocol is delivered for the full-scale experiments. First, the limitations of a propulsion drive train should be dealt with. The limitations are safety and the system's physical response on the input signal. These limits can express themselves into ramps in the different control units and the follow up question is where are these control units are placed.

For the full-scale experiment is full control of the input signal required. This will be achieved in cooperation with VOLVO Penta Netherlands, where the possibilities for the implementation of the input signal will be discussed. The difficulty lies here that the engine should think that the lever is attached to the control system, while in practice it is replaced by a computer or signal generator. Apart from the input signals, the output signal is as important. The output signal is measured in cooperation with JVS B.V., who are specialized in measuring and calculating the vibration and noise levels for maritime installations. In cooperation with JVS B.V. the possibilities will be discussed for the measurement of the output signals, e.g. precision and amount.

In the end is also knowledge required for the correct logging of the data. But if the outlined points here above are done correctly than different information rich datasets can be generated of a full scale propulsion drive train. The second part of the answering contains the results, to see if it is possible with the used input signals to identify the parameters. The approach used during the second subquestion is based on the derived methodology in the first subquestion.

The *'third subquestion'* will be answered with a review of the mathematical approach that is used during the answering of the first and second subquestion. In this review, different errors and their uncertainties on the parameter estimation will be discussed. In this discussion, the errors of the different input signals and different identification techniques will be reviewed. The goal of this research question is to substantiate the conclusion that can be with drawn from this research.

1.4 OUTLINE

The thesis outline clarifies the contents of all the chapters in this thesis. Furthermore, figure 1.3 shows a block diagram which contains the interaction of the vital chapters leading to the research goal. Figures 1.3 and 1.2 are nearly identical, indicating that Chapters 1-5 contain the answering of the first subquestion, that Chapter 6 and 7 answer the second subquestion and the third subquestion.

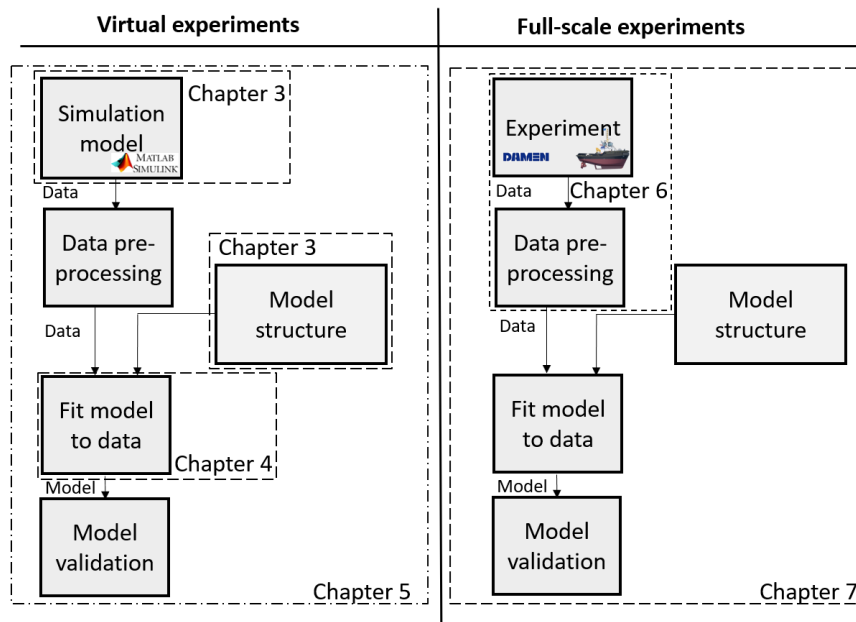


Figure 1.3: Thesis outline in block diagram.

- Chapter 1 'Introduction' contains motivation, research questions and an approach to the answering of the research questions.
- In Chapter 2 'Literature review' a brief literature review is given on the literature that is used for the simulation model. Furthermore, literature about the basic knowledge/principles of signals, systems and parameter identification techniques is given.
- Chapter 3 'Simulation model' contains the building of the simulation model that is used for the 'virtual experiments'. After that, this simulation model is linearized which results in the model structure for the parameter estimation.
- In Chapter 4 'Parameter identification' the input signal and parameter estimation methods are discussed. Furthermore the requirements for the input signal are derived. Also, it is discussed how the parameter estimation program could be optimized.
- In Chapter 5 'Virtual parameter estimation', the model structure, information-rich data sets and parameters estimation algorithms from the previous chapters leads to different virtual parameter estimation. From these virtual parameter estimations, lessons are learned which are used for the full-scale experiments.

- Chapter 6 '*Full-scale experiments*' contains a detailed explanation of how the experiments are executed, how the input signal is put on the system and finally how the data is measured and pre-processed.
- In Chapter 7 '*Full-scale parameter estimation*', the different model parameters are estimated with the obtained data during the experiments. The estimated parameter vector is evaluated and the quality of the estimation is determined. Chapter 7 is based on Chapters 3, 4 and 6.
- In Chapter 8 '*Conclusion & Recommendation*', a conclusion is given on the main research question that is formulated in Chapter 1. After that recommendations for further research are given.

2 | LITERATURE REVIEW

During this research different fields of engineering are touched, such as model building and identification techniques. The two different main parts in this literature review correspond with these two fields, respectively. First the model building is discussed, followed by the main part about 'identification techniques'.

2.1 SIMULATION MODEL

This main part on simulation models can be separated into two parts. The first part covers literature which is used for the building of the nonlinear simulation model. The second part discusses the literature which is used for the linearization of the nonlinear model.

In the past, different simulation models have been built, that imitate the propulsion system of a vessel. These models are a good starting point for the building of a new simulation model. An example of such a propulsion model, is a CODLAG configuration in free sailing, made by Martelli, M (6). Another simulation model is the COGAG configuration by Altosole, M. (3). The basis of simulation models in general are the same, namely all of them consist out of a shaft and speed loop. These two loops are discussed in quite some detail in the work of Makrygiannis, N (7). The differences between simulation models is quite often found in the level of detail of the (sub)-components.

An approach of simulating the diesel engine is found in a publication of Vrijdag, A. (8). Here, the brake torque is a function of fuel rack [mm] and shaft speed [rpm]. Also, it is stated that an increase of the engine speed, while keeping a constant fuel rack position, reduces the brake engine torque slightly. A reason for this is that a higher rpm increases the friction between the piston and the cylinder wall per cycle. Another reason for this phenomenon is that an old fuel injector pump can lead to more fuel leakage at higher engine speeds per cycle.

If one wants to simulate a crash stop, which means 'negative' engine speed and forwards sailing, more quadrants should be added. To do this, one could introduce polynomials that describes the open water diagrams. The polynomial's parametric values are different for every type of propeller and are presented in the book *Marine Propellers and Propulsion*, J. Carlton (9).

Next to the propeller and diesel engine, the governor is also an important component that has a big influence on the dynamic behavior of the vessel. The calculation that is made in the governor determines the error between the set point engine speed and engine speed. This error should then be

minimized over time. This approach is visible in the work of 'Marine diesel engine governor identification', P Matic (10). Next to that, this approach is also used in Martelli, M (6).

For the building of a simulation model it also requires parameters. Parameters are based on a reference vessel, these are supplied by Damen Gorinchem and also partly derived from *sea trails*. A vessel description of the vessel which is used for simulation model is elaborated on in Chapter 3.2.1. Furthermore torsion vibration calculations are provided which are used for the determination of the mass moment of inertia. Not all dynamic parameters can be derived, so then estimations are made based on existing values from other vessels and experience.

In the second part is the linearization of the nonlinear model discussed. The reason for linearization is that there are more identification techniques available in a linearized environment. This can be confirmed by all the different system identification books, where the linearized parameter identification technique methods are enormous (11) (12).

Due to the assumptions in a linearized model, there is a possibility that some nonlinear behavior is not captured and makes the model less valuable (12). Determining the parameters of a nonlinear system can be a major mathematical and time-consuming identification, compared to when the system is linear. Nonlinear system identification comes into picture where linear system identification fails to address the users questions (13). Nevertheless, for this proof of concept, a linearized parameter identification will be satisfying, so that it simplifies the math (12) and is easier to execute parameter estimation which results in less computational time.

Linearization of a nonlinear model is done more often in the literature. In this thesis this is partly done according to work of Vrijdag, A (14) (8). These two examples are executing the linearization for free sailing conditions, while during this research the linearization should be made for bollard pull. In the literature are also additional constraint/reasons between governor settings found, e.g. reduces cavitation or pitch changes (7) (15). These extra relations/constraints can lead to a more solvable set equations and/or speeds up the algorithm that is estimating the parameter.

2.2 PARAMETER IDENTIFICATION

This second main part 'parameter identification' contains two parts. First of all, a literature review is given on what parameter identification is and which literature is used to get a basic understanding of parameter identification, with respect to '*systems and models*'. More information about the existing methods that are available for parameter identification can be found in Chapter 4.1 'Methods'. The second part of the parameter identification literature review is about applied parameter identification techniques in marine engineering specifically.

First of all, a basic understanding of model identification should be gained, which is done with the help of different identification books (16) (11) (12)

and (17). As mentioned in the previous section, there is a large difference between linearized parameter estimation and nonlinear parameter estimation. Another important separation is made between a *time-variant* (TV) system and a *time invariant* (TIV) system. In the case of a short and information-rich experiment of a vessel in bollard pull (BP), it can be assumed that the system will be time-invariant because the system will not change a lot during the experiment (assumed constant weather conditions). An example of a time-variant system could be an aircraft losing weight during a flight, due to the combustion of fuel. As a result of this, the system will also react differently over time, because the system weight is changing over time.

An unknown system, in this case the marine propulsion drive train, can be classified into three categories: White, grey and black box, illustrated in figure 2.1.

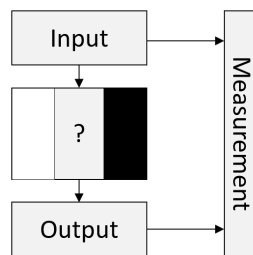


Figure 2.1: Clarification categories of model parameter identification.

First of all, a white box means that everything is known about the system, including all the internal relations. The grey box represents that some relations are known and the black box represents that nothing inside the system is known. In this particular case, the marine propulsion system can be classified as a grey box, as some relations are known, but not everything. This also clarifies the statement, made in the beginning of this thesis, that says that parameter identification requires three things: Data sets, searching algorithm and a model structure. The model structure defines the relations that are required in this grey box.

The model structure is equal to the linearized model, but it can be represented in different mathematical forms. For some parameter identification techniques, it is easier to work with a transfer function, but for some it is easier to work with state space notation. The conversion from one mathematical representation to the other can easily be done with different techniques (12).

Now that there is a basic understanding of parameter identification in general. The second part is about how parameter identification has played a role in marine engineering. This can be split up into two different fields, namely full-scale and model scale.

In model scale, there are some different researches done on identification techniques. First of all, identification techniques were applied on maneuvering models. For optimizing an autopilot, a certain signal (zig-zag) was sent to the steering system and parameters were identified (18). Next to that, the parameters of a whole nonlinear maneuvering model were identified

by doing short and information-rich experiments on the model 'Cybership II' (19) (20). The 'Cybership II' is a model scale vessel, which is used for experiments by the Norwegian University of Science and Technology (NTNU).

Identifying the propulsion drive train characteristics using identification techniques is so far only applied on model scale. The model parameters of the educational model ship 'The Tito Neri' are identified with system identification (21) (22). From this literature, it is understood that the parameter estimation on model scale was successful. In these papers, recommendations are written for full-scale parameter identification, as listed here below:

- Avoid own frequencies in the drive system
- Different nonlinear effects should be taken into consideration when the model is linearized such as:
 - The engine ignition frequency relates to the upper limit of a meaningful excitation frequency.
 - The discrete behavior of the controller

Another thing that is addressed in these papers, is the time duration of the full-scale experiments. A way of reducing the required time for the experiments is by the implementation of a multi sinus, which means that multiple frequencies will be exciting the system at the same time. When the value of the own frequency of the drive system is known, a multi sinus can also easily avoid this own frequency.

There are also different full-scale identification techniques carried out in the marine engineering. For example ship resistance and propeller efficiency identification.

The use of identification techniques on full-scale manoeuvring models started with the PhD thesis of Wei-Yuan Hwang, (23). After that, in May 1987, Lui G. (24) performed different experiments on the 'Exxon' San Francisco, which were used to identify the ship resistance coefficient with the help of system identification. The experiments only took 40 minutes while the ship was heading into the desired direction of the voyage. The procedure during the 40 minutes was first to maintain ship equilibrium. After that, the ship speed was slowed down by cutting the power of the propeller, allowing windmilling. Then this was followed by slow to half speed and reverse the propeller to bring the ship to a stop. After remaining at stop for a few minutes, the ship was speed up by calling for cruise speed to be reached as quickly as possible. With this collected data the ship resistance coefficient was identified with an accuracy probably within 1%. Furthermore the full-scale wake fraction, w , and full-scale thrust deduction factor, t , were determined.

3 | SIMULATION MODEL

This chapter is divided into six different main parts. The first main part describes the formulation of a nonlinear model of the ship propulsion plant in bollard pull conditions. The second main part is about the static validation of the nonlinear model. In the third main part, this nonlinear model is linearized for bollard pull. In the fourth main part is a static operating point selected, which is required for the verification of the linearized model. The fifth main part consists a verification of the linearized model. In the last and final part the conclusions from this chapter are outlined.

3.1 NONLINEAR MODEL

The build of the nonlinear model is structured in the following way. First a brief introduction is given about the full-scale experiment set up, which influences the building of the nonlinear model. This is followed by a block diagram of the simulation model, where every block represent a component of the propulsion drive train. After that a set of differentials and algebraic equations (DAE) is given, where the equations correspond to the different blocks in a block diagram. Finally, the equations for the different blocks are discussed.

The vessel that is used during the full-scale experiments is a small tug, because it's relatively simple propulsion drive train, which suits for this proof of concept. Furthermore, to the writer's knowledge, there are no results of similar experiments. Because it is all-new, a small ship is chosen, so if something unexpected happens that will damage the vessel, e.g. excite own frequencies, gearbox hammering, then the consequences and costs on a smaller vessel are minimized. Most of Damen's smaller tugs are equipped with a fixed pitch propeller (FPP). This leads to an important consequence for this research, namely that no input signal can be put on the pitch of the propeller. This means that the only input signal in the model is the engine speed set point.

For safety reasons and for the simplification of the full-scale experiments, it is chosen to carry out the experiments while the vessel is moored to the shore. It should be noted that in theory this is not equal to bollard pull condition. However in a simulation environment they are equal so the nonlinear model is built for bollard pull. This is a simplification as the vessel speed loop can be neglected.

The three mentioned constraints, namely small tug vessel with simple drive train, bollard pull condition and only single input signal on the system namely shaft speed are taken into account in the simulation model.

In figure 3.1, a block diagram of the nonlinear model is presented, which consists out of a governor, fuel actuator, diesel engine, gearbox, propeller and shaft loop. The reference vessel is equipped with a damper, but this is neglected in this model, because the influence on dynamic behaviour is minimal.

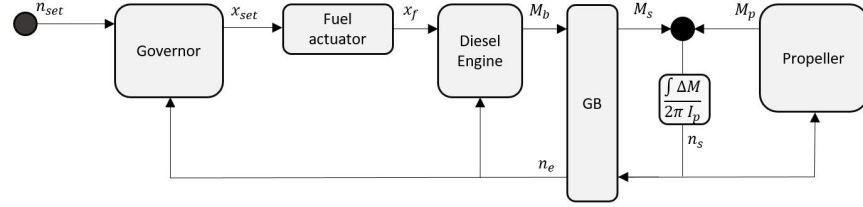


Figure 3.1: Block diagram of the nonlinear model.

The nonlinear model is built in Matlab Simulink, where the blocks in figure 3.1 represent sub systems in Matlab Simulink model. The DEA of the components of this nonlinear simulation model are listed in box here below.

$$2\pi \frac{d I_p n_s}{dt} = M_s - M_p \quad (3.1)$$

$$\frac{d E_n}{dt} = n_{set} - n_e \quad (3.2)$$

$$x_{set} = K_p \delta e_n + K_i \delta E_n \quad (3.3)$$

$$x_f = x_{set} \quad (3.4)$$

$$M_b = A_1 x_f + A_2 n_e + A_3 \quad (3.5)$$

$$M_s = M_b i_{gb} \eta_{trm} \quad (3.6)$$

$$n_e = n_s i_{gb} \quad (3.7)$$

$$Q = D_p^5 \rho n_s^2 K_q(J) \quad (3.8)$$

$$T = D_p^4 \rho n_s^2 K_t(J) \quad (3.9)$$

$$M_p = \frac{Q}{\eta_r} \quad (3.10)$$

$$J(v_a = 0) = \frac{v_a}{n_s D_p} = 0 \quad (3.11)$$

The *shaft loop* is a first order differential which is presented in equation 3.1, (14). The shaft speed loop is a balance between the shaft torque and propeller torque. The shaft rotation dynamics are considered by implementing the mass moment of inertia and the shaft speed.

In equations 3.2 and 3.3, the two equations of the *governor* are presented. In equation 3.2, the error is calculated between the actual engine speed and the requested engine speed by the operator. In equation 3.3, the set point of the fuel rack actuator is determined by using a PI regulator. This set point is

calculated by multiplying the error with a gain, K_p , and the time-integrated error with another gain, K_i . It is unknown if the actual vessel is equipped with a PID or PI regulator.

The *fuel actuator* is a component which makes sure that the fuel goes inside the cylinder, quite often under high pressure. This actuator is controlled by the governor and in practice there is a delay between the governor sending signal, x_{set} and the fuel actuator doing this, x_f . Due to the fact that this response is small compared to the full shaft speed loop, this delay is neglected. So the fuel actuator is assumed ideal, which means mathematically that equation 3.4 is applicable.

The *diesel engine* is simulated in such a way that the brake torque is dependent on the fuel rack and the engine speed, see equation 3.5. In practice this dependency is also the case but than for every engine cycle. Furthermore, limiters are implemented in the diesel engine. This is because the turbocharger first needs power to achieve an increased air pressure. Furthermore is the engine limited, because at high engine speeds the internal forces are becoming too high. Figure 3.3, shows all the engine limits with the black line and these are also implemented inside the simulation model. The engine brake torque is in relation with shaft torque, gearbox ratio and gearbox efficiency, see equation 3.6. In practice there are more limitations in the engine for example the discrete firing frequency. Furthermore are the step sizes of the calculation of the engine governor and possible the engine management system not implemented. This is assumed because it is expected that the response of shaft speed loop occurs already at lower frequencies so these components only play a role at higher frequencies. Furthermore is obtaining the correct discrete behaviour from these components really difficult.

The *propeller* is simulated according to equations 3.8, 3.9 and 3.11. J is zero, because the ship speed is zero, which also results in the fact that K_t and K_q are constants. As a consequence is the torque and thrust only function of the shaft speed and a multiplication with some constants. With the relative rotative efficiency, which presents wake field disturbances, the propeller torque can be calculated, see equation 3.10.

3.2 STATIC VALIDATION NONLINEAR MODEL

This main part consists out of two parts, were in the first part the input values of the nonlinear model are presented. In the second part a static validation is executed. The nonlinear model is only statically validated, because there is no dynamic behaviour data available for the reference vessel.

3.2.1 Vessel specification of virtual vessel

In this first part the vessel specifications of nonlinear model is discussed. The virtual vessel is exactly a *Stan Launch 804*, with a VOLVO D5A-B TA, a 'Twin Disc 505 3.00:1' gearbox and a Kaplan FPP 3-70 propeller with no nozzle. This is the same drive train set-up as the vessel that later on will be used for the full-scale experiments. The sea trial data, performance specification and the torsion vibration calculation of the virtual vessel are provided by Damen Gorinchem. The main particulars of the vessel are presented in table 3.1, and more detailed information of the virtual vessel can be found in the product sheet (25).

Symbol	Physical quantity	Value	Unit
L_{oa}	Overall ship length	8.62	m
B	Overall ship width	3.82	m
T_{side}	Draft at the sides	1.3	m
v_s	Ship speed	8.3	Kn
DWT	Dead weight	17.6	t

Table 3.1: Main particulars of virtual vessel.

Next to the vessel dimensions, more values are important for the execution of simulations with the nonlinear model, these are listed in table 3.2. This list contains some general physical quantities, the shaft line characteristic, the propeller parameters, diesel engine and governor settings. The general physical quantities such as water density are based on 'Haven Zuid' in Gorinchem, in where the full-scale experiments take place.

Symbol	Physical quantity	Value	Unit
g	Gravitational constant	9.81	m/s^2
ρ	Water density	1000	kg/m^3
w	Wake factor	0.25	[-]
t	Thrust factor	0.06	[-]
η_{trm}	Mechanical transmission losses	0.95	[-]
i_{gb}	Gearbox ratio	3	[-]
$I_{p,tot}$	Total mass moment inertia	21.2	$kg \cdot m^2$
D_p	Propeller diameter	0.77	m
P/D	Pitch ratio	0.799	[-]
$P_{b,max}$	Maximum engine brake power	89	kW
$n_{e,max}$	Maximum engine speed	1800	rpm

Table 3.2: Additional input of nonlinear model with values.

One of the parameters that is required in the model and needs some additional more clarification is the mass moment of inertia I_p , which is used in shaft loop. The value of I_p is derived from a torsion vibration calculation

(TVC). In this formulation it is assumed that all the contributing moments of inertia of the drive train are reflected to the values as 'seen' from the propeller side.

Due to the fact that there is a rotational speed difference in the drive train, due to the gearbox, the total mass moment of inertia can not be summed up directly. First the components after the reduction gear should be multiplied by the squared value of the reduction ratio. This is presented in equation 3.12, where subscript n represents all the components that are after the reduction gear such as damper, pulley, cylinders, flywheel and flexible coupling. In here is I_{nc} denoted as the corrected moment of inertia for a component, after the gearbox as 'seen' from the propeller side.

$$I_{nc} = I_n \cdot i_{gb}^2 \quad (3.12)$$

In here is I_{nk} in equation 3.13 is denoted as the corrected moment of inertia for a component, before the gearbox as 'seen' from the propeller side.

$$I_{kc} = I_k \quad (3.13)$$

Were in the end the total mass moment of inertia is a summation of all the values of the different corrected components I_{nc} and I_{kc} . The total mass moment inertia 'seen' from the propeller side is $21.2kgm^2$. The biggest contributions of the mass moment of inertia seen from the propeller side is listed in table 3.3.

Description	Mass mom. of inertia	Unit
Flywheel	8.15	$kg \cdot m^2$
Propeller	2.18	$kg \cdot m^2$

Table 3.3: Highest reflected mass moment inertia's in propulsion drive train of virtual vessel seen from propeller side.

From table 3.3 can be seen that the flywheel has a big contribution to the total mass of inertia. By assuming that the total moment of inertia is operating from one engagement point in this nonlinear model at end of the shaft, this will lead to differences with reality. The reason for this is that big contributor of the total mass moment of inertia is placed somewhere else on the drive train. The point of engagement of all the mass moments of inertia can have influence on the precision of the model.

3.2.2 Static validation

The static validation is done for two cases, first an engine power comparison and second a bollard pull comparison. This is done by comparing model results with sea trial results of the reference vessel, which are provided by Damen Gorinchem. Figure 3.2 shows the bollard pull as function of engine speed for the nonlinear simulation model. The dots in figure 3.2 which indicate the bollard pull for a certain engine speed that was obtained during the sea trial. The grey line is the obtained result from the the nonlinear model.

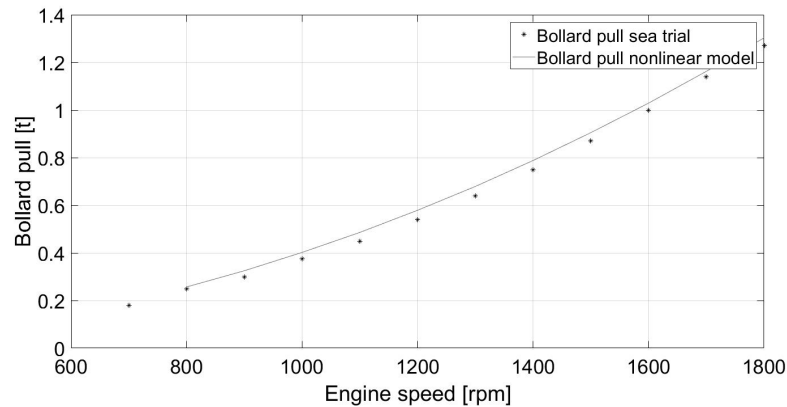


Figure 3.2: Validation nonlinear model in bollard pull with a sea trial.

When the figure is investigated in more depth, the following observations are done:

- The two graphs are identically shaped over the whole rpm range.
- Between 900 and 1700 rpm there is a maximum error of 0.02-0.04 ton.
- The highest relative error occurs at 1100 rpm, where the error is 0.036t, which is 7%.

In figure 3.3 the grey line represents the brake power of the nonlinear model as function of engine speed. As stated in the beginning of this chapter, the black line is the torque and engine speed limit of the diesel engine. Also, the results of the engine brake power during the bollard pull is represented as the different dots. At closer inspection, the following observations are done:

- Until 1200 rpm, the correlation between the two lines is nearly 100%
- Above 1200 rpm, the error is increasing with a maximum at $\pm 1800rpm$ and with a percentage error of 3.5%

From the two different static validations the following can be concluded. The nonlinear model is built correctly, so the model fulfils the requirements, because the static validation between the simulation model and the sea trial are showing the same results. Still there are small differences between sea trials and the simulation model. A reason why the brake power is higher at higher engine speeds in the nonlinear model, could be that the friction is assumed constant. In practice the energy loss in the bearings and transmission

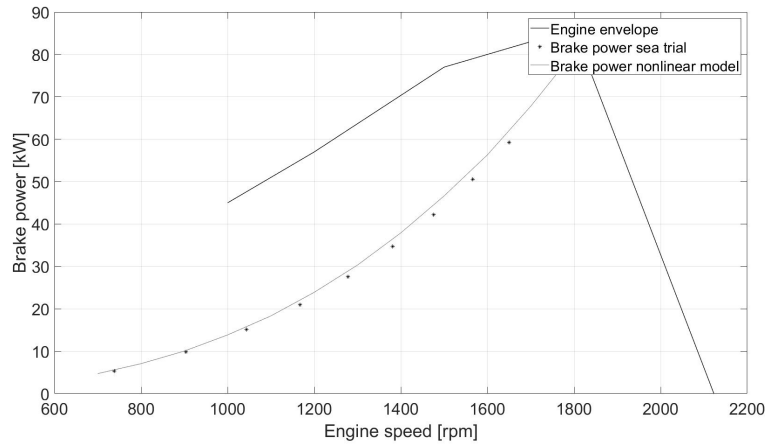


Figure 3.3: Validation nonlinear model of the engine with a sea trial.

increases when the shaft speed increases, so in practice is the brake power slightly less. Furthermore, the bollard pull of the vessel is also higher, which could be caused by the fact that during the sea trial there were disturbances in the wake field, for instance due to shallow water. Literature (26) states that a correction factor is sometimes used to compensate this phenomenon, but this is not taken into account in the nonlinear model. Nevertheless the nonlinear model is capturing the static behaviour correctly and is assumed valid.

3.3 LINEARIZED MODEL

This main part contains three different parts. In the first part, a DAE is given of the linearized model, which is followed by a brief description on how the equations are derived. In the second part different transfer functions are derived from the DAE. In the final part, the transfer functions are transformed to state space notation.

This linearized model can be used as model structure for parameter estimation. So the nonlinearities should be removed from the nonlinear model. The nonlinearities in the model are (14):

- Nonlinearities due to multiplicative action in the mathematical model of the system, e.g. ($T = \rho n_s^2 D_p^4 K_t$)
- Nonlinearities due to a hard limit in the model, e.g. protective engine limits.

Furthermore please note that the equations are also normalized, this is mathematically noted as *.

3.3.1 DAE of linearized model

Before the DAE of the linearized model is shown, it should be mentioned that the linearization is based on the work of D. Stapersma & A. Vrijdag (14). They performed this linearization already for free sailing mode and this is the basis for this linearization. The difference is that this linearization will be done for bollard pull condition. In mentioned reference (14) 'Appendix B Normalisation and linearization', it is explained how to deal with multiplications in a linearized environment. (14) 'Appendix C1 Linearization of shaft speed' is also used. These appendices of this reference are not shown in this thesis and assumed to be known by the reader. The DAE is listed in the box here below:

$$\tau_n \frac{dn^*}{dt} = M_s^* - M_p^* \quad (3.14)$$

$$\frac{dE_n^*}{dt} = \delta n_{set}^* - \delta n^* \quad (3.15)$$

$$\delta X_{set}^* = K_p \delta e_n^* + K_i \delta E_n^* \quad (3.16)$$

$$\delta X_f^* = X_{set}^* \quad (3.17)$$

$$\delta M_b^* = g \delta n^* + v \delta X_f^* \quad (3.18)$$

$$\delta M_s^* = \delta M_b^* \quad (3.19)$$

$$\delta Q^* = 2 \delta n^* \quad (3.20)$$

$$\delta M_p^* = \delta Q^* \quad (3.21)$$

$$\delta T^* = 2 \delta n^* \quad (3.22)$$

The *shaft loop* in a linearized and normalised form is presented in equation 3.14. An integration constant is added, namely τ_n . This is nothing more than the operating point multiplied with the mass moment of inertia 'seen'

from the propeller side and is defined in equation 3.23.

$$\tau_n \equiv \frac{2\pi I_p n_0}{M_{s,0}} \quad (3.23)$$

The *governor* is presented in equation 3.15 and 3.16. A more detailed mathematical derivation of the normalized governor is presented in appendix A.1.

The *diesel engine* is shown in equation 3.18, which is derived from equation 3.5 of the nonlinear model. The parameters A_1 and A_2 are becoming normalized derivatives but still represent a ratio, but to ease the math they are named g and v . The definition of the parameters is presented here below in equation 3.24 and 3.25. As can be seen in the definition, the parameter g represents the influence of a small increase in engine speed on the engine torque multiplied by the linearization point. The parameter v represents the influence of a small increase in the fuel rack on the engine torque and is also multiplied by the linearization point.

$$g \equiv \left. \frac{n_{e,0}}{M_{b,0}} \frac{\delta M_b}{\delta n} \right|_x \quad (3.24)$$

$$v \equiv \left. \frac{X_0}{M_{b,0}} \frac{\delta M_b}{\delta X} \right|_n \quad (3.25)$$

The linearization of the *propeller* is easily derived in bollard pull, because in a linearized environment the quadratic coefficients become a linear multiplier. So in equation 3.8, of the nonlinear model, is visible that the shaft torque is depended on the quadratic shaft speed. In the linearized environment, this means that the quadratic becomes a multiplication of 2, see equation 3.20. The ideal fuel actuator is normalized, see equation 3.17, so it's still a ideal actuator

Equation 3.19 is the normalized shaft torque equal to the normalized brake torque, so their is a constant transmission efficiency. In equation 3.21 is the propeller torque equal to Q^* , so the relative rotative efficiency is assumed constant.

Now all the equations of the nonlinear model are linearized and normalized they can be put in different mathematical forms which represent a relation between a certain input and output.

3.3.2 Transfer functions

A transfer function which can also be called a system function, is a mathematical function, which represents for theoretical models the relation between every possible input and output (27). The transfer function can be presented in graph form, also called a transfer curve or Bode plot. These graphs show the relation between input and output for a certain frequency. The bode plot's behaviour is influenced by the system parameters, because these change the value of the transfer function.

As stated in the research approach, the only input signal on the system is the set point of engine speed, n_{set} . However, a lot of different outputs are

available, in theory all of them, because everything can be measured in the simulation model. For now three different outputs are used and transfer functions with respect to the set point of shaft speed are made. For identifying a system, it is best to place the three outputs at three different places. For the best parameter identification it's better to have an output after every component. As can be seen figure 3.1, the fuel actuator and gearbox can be negligible. Then after the governor, diesel engine and shaft speed loop the three measurements say something about the whole drive train. For this reason, it is decided to make relations between the set point engine speed and the integrated error E_n , the shaft torque M_s and the actual shaft speed n_s .

The shaft speed over set point engine speed is derived from the shaft loop equation 3.14 as a starting point. As stated before δQ^* equals the δM_p^* , so the propeller torque can be implemented in the shaft loop equation 3.14. As can be seen in equation 3.20, the propeller torque is equal to twice the shaft speed, so this can also be implemented. Next to that, the engine brake torque presented in equation 3.18 is also implemented in the shaft loop equation 3.14. This will finally result in equation 3.26.

$$\tau_n \frac{dn^*}{dt} = g\delta n^* + v\delta X^* - 2\delta n^* \quad (3.26)$$

The governor, equation 3.16, and the fuel actuator, equation 3.17, are now implemented in the shaft speed loop of equation 3.26, resulting in equation 3.27.

$$\tau_n \frac{dn^*}{dt} = g\delta n^* + v(K_p\delta e_n^* + K_i\delta E_n^*) - 2\delta n^* \quad (3.27)$$

The integral of the error is as follows:

$$\delta E_n^* = \int_0^t \delta e_n^* dt \quad (3.28)$$

So then equation 3.15 is put in Laplace form which is shown in equation 3.29.

$$\frac{dE_n^*}{dt} = -\delta n^* + \delta n_{set}^* \longrightarrow E_n^* s = -\delta n^* + \delta n_{set}^* \quad (3.29)$$

Next to that, the shaft speed loop is put in Laplace form and the error and the integrated error are replaced with equation 3.29 and 3.15. Then after some mathematical manipulations, equation 3.30 is derived. It is put in this form, because it allows easier derivation of the transfer function.

$$\left(\frac{\tau_n}{vK_i}s^2 + \frac{2-g+vK_p}{vK_i}s + 1\right)\delta n^* = \left(\frac{K_p}{K_i}s + 1\right)\delta n_{set}^* \quad (3.30)$$

The transfer function is shown in equation 3.31.

$$\frac{\delta n^*}{\delta n_{set}^*} = \frac{\frac{K_p}{K_i}s + 1}{\frac{\tau_n}{vK_i}s^2 + \frac{2-g+vK_p}{vK_i}s + 1} = \frac{\frac{vK_p}{\tau_n}s + \frac{vK_i}{\tau_n}}{s^2 + \frac{2-g+vK_p}{\tau_n}s + \frac{vK_i}{\tau_n}} \quad (3.31)$$

The transfer function is analysed by putting in some extreme frequencies to see if the relation in the transfer function is logic. For example the DC gain: When a very low frequency is exciting the system, transfer function 3.31 becomes 1, as can be seen in equation 3.32. This is logical, because when the system is excited very slowly, one can assume that the system is able to follow the changes, so then the input frequency becomes the output frequency.

$$\frac{n^*}{\delta n_{set}^*}(S \rightarrow 0) = 1 \quad (3.32)$$

One can also imagine that this works the other way around, when set point engine speed is excited with high frequencies, the large mass moment of inertia can not be excited in such a short period. Or in other words, the system will not react at all. This is also inline with the math because the result is zero, see equation 3.33.

$$\frac{n^*}{\delta n_{set}^*}(S \rightarrow \infty) = 0 \quad (3.33)$$

Instead of expressing the output in the shaft speed the following transfer function has the integrated error of the governor as output signal. This transfer function can be obtained when some of the previous shaft speed loop is rewritten and some mathematical manipulations are executed. The base is again equation 3.27, in which the error is rewritten to shaft speed and set point shaft speed, as can be seen in equation 3.15. Then after that the shaft speed components on the right hand side are rewritten to set point shaft speed and the integrated error in Laplace form, see equation 3.29. This newly derived shaft loop is then put in Laplace notation and with some manipulations, equation 3.34 is derived.

$$\begin{aligned} \tau_n s \delta n^* &= \delta n_{set}^* (-2 + g - v K_p) + .. \\ &.. + \delta E_n^* s (-2 + g - v K_p) - v K_i \delta E_n^* - v K_p \delta n_{set}^* \end{aligned} \quad (3.34)$$

The δn^* on the left hand side should also be rewritten to shaft speed δn_{set}^* and integrated errors δE_n^* . With some mathematical manipulations the transfer function 3.35 can be derived .

$$\frac{\delta E_n^*}{\delta n_{set}^*} = \frac{\tau_n s + 2 - g}{\tau_n s^2 + (2 - g + v K_p) s + v K_i} = \frac{s + \frac{2-g}{\tau_n}}{s^2 + \frac{2-g+vK_p}{\tau_n} s + \frac{vK_i}{\tau_n}} \quad (3.35)$$

Transfer function 3.35 is also tested to two extreme conditions, namely for infinitely slow frequencies shown in equation 3.36. It is visible that the integrated error is dependent on the engine characteristics g , v and a tuning parameter, K_i . It is logical that the engine parameters have influence on the integrated error, because the speed with which the error decreases has influence on the integrated error. For high frequencies, the quadratic component will dominate the denominator of the fraction, so in the end this will go to zero as well, see equation 3.37. This makes sense, because the integrated error consists of a lot of sinus signals while the system can not react. So,

this integration becomes zero.

$$\frac{\delta E_n^*}{n_{set}^*}(s \rightarrow 0) = \frac{2-g}{vK_i} \quad (3.36)$$

$$\frac{\delta E_n^*}{n_{set}^*}(s \rightarrow \infty) = 0 \quad (3.37)$$

The derivation of the shaft torque as output over the shaft speed set point is derived in a different way to ease the math involved. This derivation is shown in appendix A.2, where H_{ship} is the core propulsion system and C represents the governor. When the procedure in the appendix is followed and some mathematical manipulations are done, the transfer function in equation 3.38 is obtained.

$$\begin{aligned} \frac{\delta M_s^*}{\delta n_{set}^*} &= \frac{\tau_n v K_p s^2 + (v k_i \tau_n + 2v K_p) s + 2v K_i}{\tau_n s^2 + (2-g + v K_p) s + v K_i} = .. \\ &.. = \frac{v K_p s^2 + \frac{v K_i \tau_n + 2v K_p}{\tau_n} s + \frac{2v K_i}{\tau_n}}{s^2 + \frac{v K_p - g + 2}{\tau_n} s + \frac{v K_i}{\tau_n}} \quad (3.38) \end{aligned}$$

When engine set point is a really slow frequency, the shaft speed will follow this frequency. But from the linearization of the torque, we know that this is by a factor 2, see equation 3.20. So the DC gain in equation 3.39 is correct, because it shows that for low frequencies the shaft torque over set point engine speed is a factor 2.

$$\frac{\delta M_s^*}{\delta n_{set}^*}(s \rightarrow 0) = 2 \quad (3.39)$$

When a high frequent signal is put on the engine speed set point then only the quadratic components in the transfer function 3.39 will be effected. So in this case the multipliers vK_p in the nominator will determine the gain at high input frequencies, see equation 3.40. This is because the occurring error in the simulation model is multiplied directly with the proportional part of the the governor, K_p . In the simulation model, the engine will also react directly, because the discrete engine ignitions are not taken into account, which would cause in real life delays. So, the engine will directly deliver the amount of torque requested, namely vK_p .

$$\frac{\delta M_s^*}{\delta n_{set}^*}(s \rightarrow \infty) = vK_p \quad (3.40)$$

Above, three different transfer functions are derived with as input set point engine speed and with different outputs. In table 3.4, a small summary is made of the obtained transfer functions.

Relation	Transfer function	DC-gain
$\frac{\delta n^*}{\delta n_{set}^*}$	$\frac{\frac{vK_p}{\tau_n} s + \frac{vK_i}{\tau_n}}{s^2 + \frac{2-g+vK_p}{\tau_n} s + \frac{vK_i}{\tau_n}}$	1
$\frac{\delta E_n^*}{\delta n_{set}^*}$	$\frac{s + \frac{2-g}{\tau_n}}{s^2 + \frac{2-g+vK_p}{\tau_n} s + \frac{vK_i}{\tau_n}}$	$\frac{2-g}{vK_i}$
$\frac{\delta M^*}{\delta n_{set}^*}$	$\frac{vK_p s^2 + \frac{vK_i \tau_n + 2vK_p}{\tau_n} s + \frac{2vK_i}{\tau_n}}{s^2 + \frac{vK_p - g + 2}{\tau_n} s + \frac{vK_i}{\tau_n}}$	2

Table 3.4: Summary of different transfer function.

3.3.3 State space notation

Another way of presenting a linearized model, is in state space notation. The state space notation is a set of first order differential equations that represent a physical system. The state space notation can be continuous and discrete, but also time variant or invariant. Below, the continuous time invariant state space is shown.

$$\dot{\bar{x}} = A\bar{x} + B\bar{u} \quad (3.41)$$

$$\bar{y} = C\bar{x} + D\bar{u} \quad (3.42)$$

In the state space notation every vector and matrix has its own representation and purpose. Matrix A is the system matrix, matrix B is the input matrix and matrix C and D ensure a physical conversion of certain unities, so that a shaft speed input can be related to a shaft torque. The \bar{x} is the state vector, \bar{u} the input vector and \bar{y} the output vector (14).

A distinguish between transfer function and state space, is that state space notation makes it possible to set different outputs in relation to one single input. In this section, the different transfer functions for shaft speed, shaft torque and integrated error over the set point of the engine speed will be put in state space notation.

The linearized DAE that is defined in the previous section, will also be written differently. The two equations contain all the different components. They are defined here in the box below:

$$\tau_n \frac{dn^*}{dt} = (-2 + g - vK_p)\delta n^* + vK_p \delta n_{set}^* + vK_i \delta E_n^* \quad (3.43)$$

$$\frac{dE_n^*}{dt} = -\delta n^* + \delta n_{set}^* \quad (3.44)$$

For state space notation, the vectors \bar{x} , \bar{u} , \bar{y} are first chosen and that results in matrices A, B, C, D. From here, three different state space derivations are shown, where the first case is defined in equation 3.45.

$$\bar{x} = \bar{y} = \begin{bmatrix} \delta n^* \\ \delta E_n^* \end{bmatrix}, \quad \bar{u} = \delta n_{set}^* \quad (3.45)$$

These state vectors will result in the following matrices 3.46 and 3.47:

$$A = \begin{bmatrix} \frac{-2+g-vK_p}{\tau_n} & \frac{vK_i}{\tau_n} \\ -1 & 0 \end{bmatrix}, \quad B = \begin{bmatrix} \frac{vK_p}{\tau_n} \\ 1 \end{bmatrix} \quad (3.46)$$

$$C = \begin{bmatrix} 1 & 0 \\ 0 & 1 \end{bmatrix}, D = \begin{bmatrix} 0 \\ 0 \end{bmatrix} \quad (3.47)$$

In the previous example, one of the output values was the integrated error and the other shaft speed. In second case, the output signal is shaft torque and shaft speed, see 3.48.

$$\bar{x} = \begin{bmatrix} \delta n^* \\ \delta E_n^* \end{bmatrix}, \bar{u} = \delta n_{set}^*, \bar{y} = \begin{bmatrix} \delta n^* \\ \delta M_s^* \end{bmatrix} \quad (3.48)$$

Then in the C and D matrices the error should be rewritten to the shaft torque. Then equation 3.15, 3.16 and 3.17 should be implemented in 3.18. Which results in equation 3.49.

$$\delta M_b = (g - vK_p)\delta n^* + vK_i\delta E_n^* + vK_p\delta n_{set}^* \quad (3.49)$$

With equation 3.49 and the defined input vector, state vector and output vector, the following A,B,C and D matrices are derived:

$$A = \begin{bmatrix} \frac{-2+g-vK_p}{\tau_n} & \frac{vK_i}{\tau_n} \\ -1 & 0 \end{bmatrix}, B = \begin{bmatrix} \frac{vK_p}{\tau_n} \\ 1 \end{bmatrix} \quad (3.50)$$

$$C = \begin{bmatrix} 1 & 0 \\ g - vK_p & vK_i \end{bmatrix}, D = \begin{bmatrix} 0 \\ vK_p \end{bmatrix} \quad (3.51)$$

For parameter identification one can imagine that the model structure can have great influence on the results of parameter estimation. For example, more data leads to another modelstructure, because more relationships should be implemented in the modelstructure. So the following case still has a single input but now has three outputs. A disadvantage is that the parameter estimation will take longer and requires more computational capabilities. The new input, output and state vector are defined in equation 3.52.

$$\bar{x} = \begin{bmatrix} \delta n^* \\ \delta E_n^* \\ M_s^* \end{bmatrix}, \bar{u} = \delta n_{set}^*, \bar{y} = \begin{bmatrix} \delta n^* \\ \delta E_n^* \\ M_s^* \end{bmatrix} \quad (3.52)$$

With the following vector 3.52, the following matrices 3.53 and 3.54 are derived:

$$A = \begin{bmatrix} \frac{-2+g-vK_p}{\tau_n} & \frac{vK_i}{\tau_n} \\ -1 & 0 \end{bmatrix}, B = \begin{bmatrix} \frac{vK_p}{\tau_n} \\ 1 \end{bmatrix} \quad (3.53)$$

$$C = \begin{bmatrix} 1 & 0 \\ 0 & 1 \\ g - vK_p & vK_i \end{bmatrix}, D = \begin{bmatrix} 0 \\ 0 \\ vK_p \end{bmatrix} \quad (3.54)$$

Above different forms are given on how the state space notation can be adjusted by varying input and output vectors and all representations can be used as model structure for the parameter estimations. In Chapter 4.2 are the amount of internal relations discussed.

3.4 NOMINAL OPERATION POINT

In this main part the determination of a suitable operating point is discussed. For operating point n_0 the nominal value of system variables $X_0, M_{b,0}, M_{s,0}, n_{s,0}, P_{b,0}$ and parameters g, v, τ_n are determined. These values are derived from a constant run of the operating point in the nonlinear model. Subsequently these variables and parameters are implemented in the linearized model, resulting in a linearized model that is verified in the following main part.

It is chosen to select the operating point that occurs when the engine speed set point is set at 1300 rpm . The resulting system variables are listed in table 3.5.

Variable	Normalized value	Unit
n_0	21.677	rps
X_0	13.07	mm
$M_{b,0}$	222.93	Nm
$M_{s,0}$	635.766	Nm
$n_{s,0}$	7.222	rps
$P_{b,0}$	30.3	kW

Table 3.5: Values of system variables with constant input signal of $n_{set} = 1300 \text{ rpm} = 21.7 \text{ rps}$.

The system parameters g, v, K_p, K_i are listed in table 3.6 and derived from the shown locations in figure 3.4. The combined parameter τ_n is calculated according to the definition in equation 3.23 and also presented in table 3.4.

Linearized parameters	Value	Unit
v	1.58	[-]
g	-0.58	[-]
K_p	10	[-]
K_i	1	[-]
τ_n	1.44	s

Table 3.6: Values of linearized model parameters with constant input signal of $n_{set} = 1300 \text{ rpm}$ on nonlinear model.

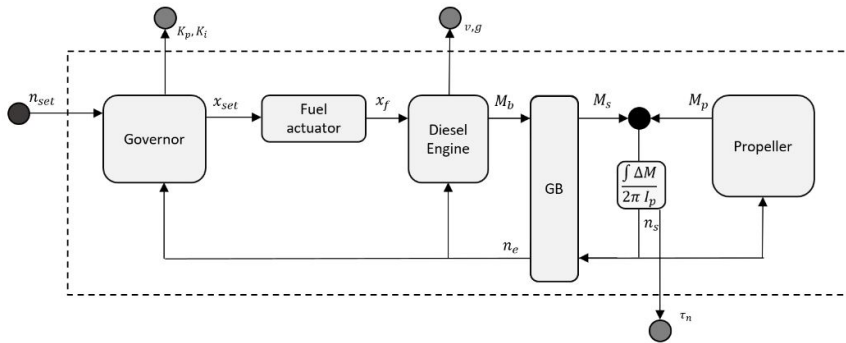


Figure 3.4: Linearized parameters from nonlinear model.

3.5 VERIFICATION OF LINEARIZED MODEL

The verification of the linearized model contains two main parts. The first part contains a verification in time domain, which is followed by a second part where verification in frequency domain takes place. The verification is done twice, because in time domain it is easier to perceive differences between nonlinear model and the linearized model. The second verification is only done to check if the analytical derivation of the linearized model is done correctly.

3.5.1 Verification in time domain

Time domain verification will be done with a step response on engine speed setpoint that is applied on the linearized model and the nonlinear model. It should be stated that the nonlinear model is only statically validated and the linearized model is now dynamically verified to the dynamics of the nonlinear model. But the relevance of doing this dynamic verification is still there, because at which value the system becomes stable after a step response can be compared. Furthermore it can be investigated whether the dynamic behaviour of the linearized model is complete different than the nonlinear model. The step responses that are put on the system are done at the operating point of 1300 rpm. The three different step responses to which the system is exposed are visible in table 3.7.

Step percentage	RPM change
5%	65 rpm
10%	130 rpm
20%	260 rpm

Table 3.7: The applied step responses.

How the shaft speed reacts on the three different step responses in both models is illustrated in figure 3.5. In these three steps it can be seen that the two models show the same shaft speed behaviour. Furthermore it is visible that at higher steps the error between the models is slightly increasing. According to equation 3.32 the DC gain is 1, and this also follows from the graphs in time domain. When the system is stable, around 60 s, the shaft speed approaches $5\% = 0.05$, $10\% = 0.1$ and $20\% = 0.2$ and this is in line with the derived DC gain of the transfer function.

How the shaft torque reacts is shown in figure 3.6. In this graph, it is clearly visible that there are differences between the dynamic behaviour of the two models, especially with high step responses. Figure 3.6 clearly shows that the limiter in the nonlinear model is not applicable for the linearized model, see step response 20%. Next to that, figure 3.6 shows that when the system stabilizes, both models satisfy the DC Gain from equation 3.39. E.g. when a step response of $10\% = 0.1$ is put on the system, then the output of dimensionless shaft torque is $20\% = 0.2$, which equals a DC gain of 2. This is also applicable for the two other step responses. Furthermore, it is visible that the error is a little bit bigger in comparison with the shaft speed when the system is stable. In general, it can be concluded that the linearized model is showing nearly the same results as the nonlinear model.

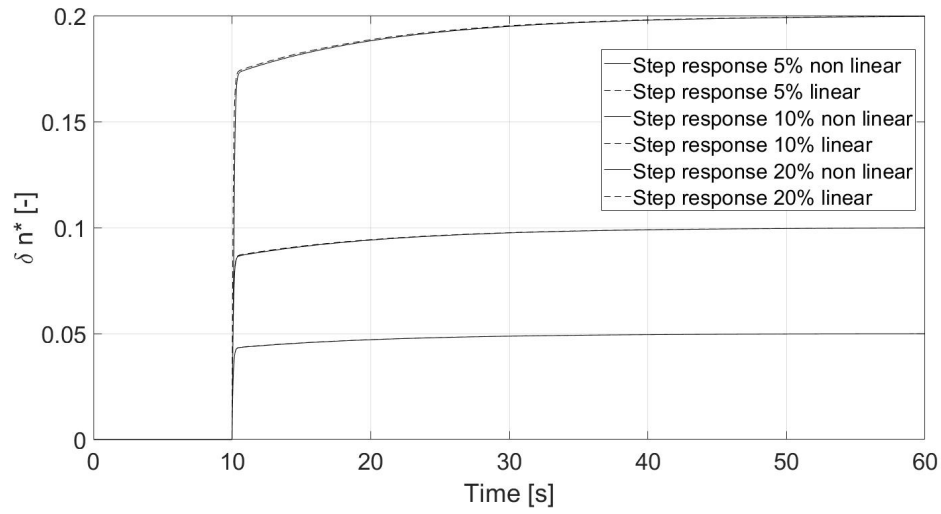


Figure 3.5: Comparison between nonlinear model and linearized model of shaft speed response.

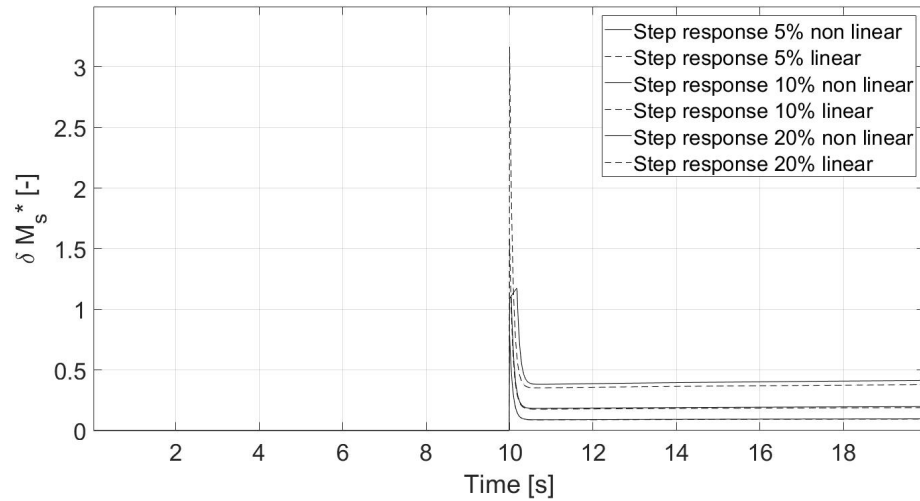


Figure 3.6: Comparison between nonlinear model and linearized model of shaft torque response.

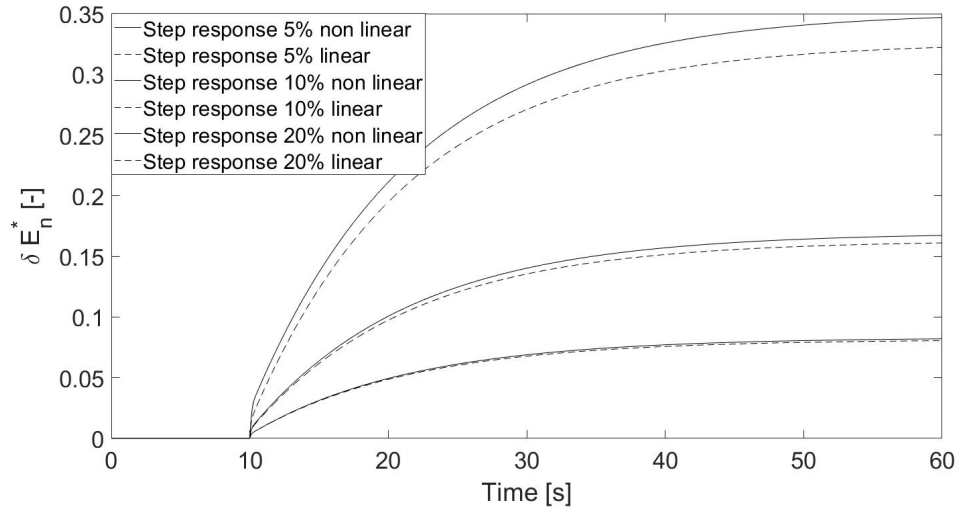


Figure 3.7: Comparison between nonlinear model and linearized model of integrated error response.

The integrated error for the different step responses is presented in figure 3.7. For the integrated error the same applies as for the shaft torque: An increased step responses causes an increased error. When the DC gain of equation 3.36 is filled in with the parameters of table 3.6, the point on which the system stabilizes in figure 3.7 is in line with the expectations.

As can be concluded, the linearized model is showing the same characteristics as the nonlinear model. But at increasing step responses the error between the linearized model and the nonlinear model increases. The non-linearity due to multiplicative action is the reason for this error increase at bigger step responses. $Q = \rho n^2 D^5 K_q \rightarrow \delta Q^* = 2\delta n^*$.

3.5.2 Verification in frequency domain

As was stated earlier, the second verification checks if the analytically derived linearized model is correct. This is checked with the 'Linearization Tool', where the nonlinear model is automatically linearized according to the defined input and output. The results are shown for shaft speed, shaft torque and integrated error in figures ??, 3.9 and 3.10, respectively. As can be seen, the linearization tool of Matlab shows the same results as the analytically derived linearization of the nonlinear model for lower frequencies. At some higher frequencies, a small differences occurs in the phase or gain. The exact reason is unknown but most likely this difference occurs due to the fact that the 'Linearization Tool' is using the pre-programmed linearization of a certain block. Some of the blocks can not be linearized because they do not have a predefined exact linearization. At higher input frequencies, nonlinearities most likely occur, such as in the limiter of the engine. However, the differences are small and it can be concluded that the analytical derivation is done correctly.

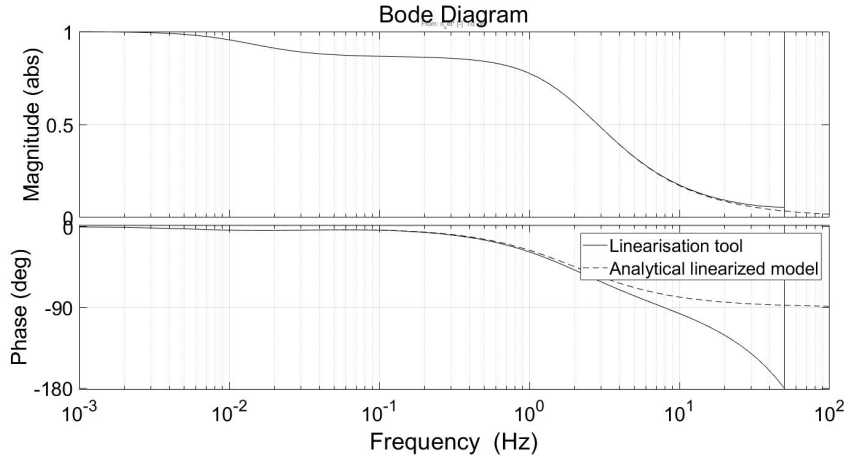


Figure 3.8: Verification of $\frac{\delta n^*}{\delta n_{set}^*}$.

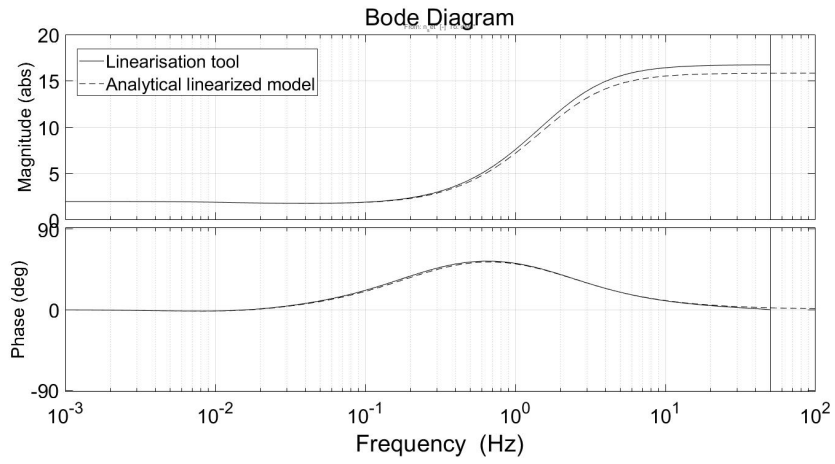


Figure 3.9: Verification of $\frac{\delta M_s^*}{\delta n_{set}^*}$.

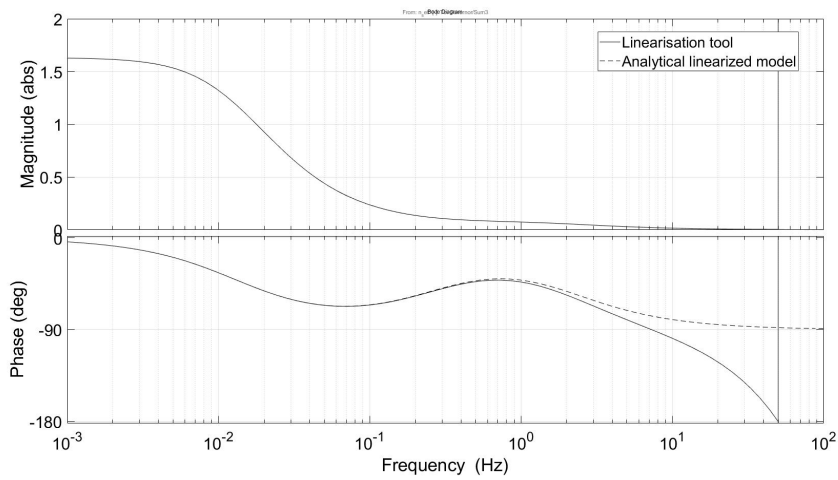


Figure 3.10: Verification of $\frac{\delta E_{pl}^*}{\delta n_{set}^*}$.

3.6 CONCLUSION

The conclusions that can be drawn from this chapter are listed below:

- The nonlinear model is statically validated with data gained from a sea trial and this gives positive results. For this reason, the nonlinear model can be used for data generation, so that different information-rich datasets can be generated for the parameter estimation in the virtual experiments.
- The nonlinear model does not contain any discrete firing frequency or sampling frequency of governor. The governor is also equipped with a PI regulator, but there is a possibility that the vessel is equipped with a PID regulator. Furthermore, the step sizes of engine governor calculations and possible engine management systems are not implemented. Some of these components might play a role at high frequencies.
- The linearized model is made from the nonlinear model by removing the nonlinearities. The first nonlinearity is multiplicative actions e.g. ($T = \rho n_s^2 D_p^4 K_t$) and the second nonlinearity is hard limits, e.g. torque limit.
- The linearized model structure shows the same behaviour as the nonlinear model close to the operating points, so the linearized model is verified according to the nonlinear model.
- The analytical linearized model is derived correctly according to a comparison with the Matlab Linearisation Tool (C).

4

PARAMETER IDENTIFICATION

Chapter 2.2 'Literature Review' states that three things are required for parameter estimation, namely a searching algorithm, a model structure and an information-rich data set. In this chapter, these three necessities and their influence on the parameter estimation are discussed. Every necessity is discussed in its own corresponding main part.

4.1 SEARCHING ALGORITHM

The searching algorithm is divided into five different parts. First of all, a problem statement is made on how parameters are estimated in general with a searching algorithm. After that are different elements from the problem statement discussed in more detail, namely cost function, optimisation and estimated fit in time domain. The fifth part contains a frequency domain problem statement. Most of this theory is based on the book of Ljung, L. (11), which is also the basis for the 'Identification toolbox' in Matlab. Furthermore are only linear parameter identification techniques discussed.

4.1.1 Problem statement time domain

The parameters of the nonlinear model can be defined as a vector $\bar{\Psi}$. When the nonlinear model is linearized, a new set of parameters can be defined, namely parameter vector $\bar{\theta}$. Pay attention to the fact that during this linearization and normalization the parameters will change from unit, so that the value also changes.

The goal of parameter estimation is that the parameter set $\bar{\Psi}$ represents the correct physical quantity. Only linearized parameter estimation will be done in this thesis, so the goal is to optimize the linearized parameter set, $\bar{\theta}$. From full-scale experiments and/or the nonlinear model, different output data sets \bar{y}_{meas} can be derived. Pay attention to the fact that this data set contains nonlinearities.

Now it is imaginable that for a certain parameter set, $\bar{\theta}$ and a certain input signal, an output data set $\bar{y}_{sim}(\bar{\theta})$ can be generated with the linearized model structure. Concluding, the output data set is dependent on the linearized parameter set and input signal and does not contain nonlinearities.

An error can be defined between output of a full-scale measurement or nonlinear model and the output of a certain linearized parameter set in the linearized model. The error defined between those two outputs is defined as \bar{e} , and shown in equation 4.1.

$$\bar{e} = \bar{y}_{meas} - \bar{y}_{sim}(\bar{\theta}) \quad (4.1)$$

The goal is to minimize the total error vector for a certain input signal, because ideally the parameter set estimation is correct when this error is zero. This can be reached by 'fine tuning' the set of linearized parameters $\bar{\theta}$, because the simulated output vector is a function of the linearized parameter set, see equation 4.2.

$$V(\bar{\theta}) = \frac{1}{N} \sum_{t=1}^N \bar{e}^T(t, \bar{\theta}) \cdot \bar{e}(t, \bar{\theta}) \quad (4.2)$$

Please note that the total error is in practice never zero, because linearized parameters are compared to nonlinear data sets, illustrated in figure 4.1.

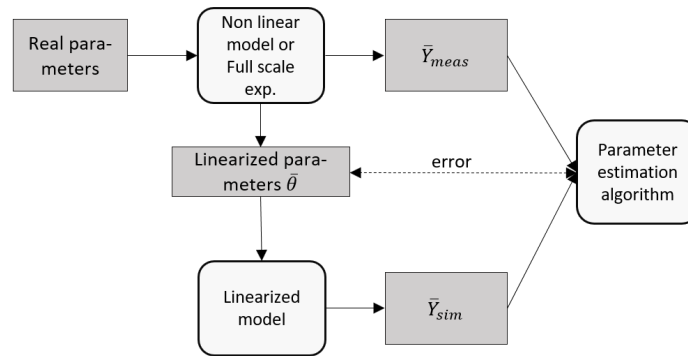


Figure 4.1: Explanation of unavoidable error in linear parameter estimation.

In literature the mathematical expression of equation 4.2 is called a cost function or loss function. During this thesis, different cost functions will be analysed in chapter 4.1.2.

In equation 4.3 the error of the cost function is tried to get minimized. This will be done by changing the values of the linearized parameter set, $\bar{\theta}$. But to which extent and after how many iterations is this minimum achieved? This is discussed in chapter 4.1.3, 'minimization of error'. In the previous part is the parameter identification in time domain defined, in chapter 4.1.5 is a problem statement made in frequency domain.

$$\arg. \min. V(\bar{\theta}) \quad (4.3)$$

The third element that will be discussed after this in more detail is the fit of the estimation. So how can you say that the estimated parameters are correct and how can one say that one technique is better than the other? This part is discussed in chapter 4.1.4.

4.1.2 Cost function

The error, equation 4.1, can be calculated in two different ways. First of all as a prediction error which represents the error one step ahead. The other method is the simulation error. As the name reveals, the prediction error is the best if we want to predict model behaviour. The simulation error

method focuses on making the best fit for the current data set.

The choice of the error calculation results in practice quite oft in an implicit decision of a weighting filter. In practice is the distinguish between the two different error calculation on how the noise is taken into account. While as in the prediction the noise is taken into account as a variable for the parameter estimation, where in the simulation simply the best fit made for the current data set.

After the error vector is derived, a cost function should be made. For example, in equation 4.2 a Least Square Method (LSM) is used as cost function. This is based on literature of Westwick and Kearney (16), chapter 8. LSM methods can be considered as one of the easiest cost functions and is strong for a single input en single output (SISO) system, because it is a straight forward method. The LSM is a summation of the squares of all the different errors (or residues) for every time step, see equation 4.2.

Most likely, the parameter estimation will take place with multiple outputs. Then one should pay attention to the fact that the average of the output signals can vary. With multiple outputs, also in a normalized world, there is still some difference in response of certain output signals, see Bode plots 3.8 and 3.9. This will influence the cost function, because this can induce that the cost function will be optimized for a single output only. A way to avoid this is with a Weighted Least Square method (WLS), because now the cost function is minimized equally for all output signals. This is explained as well in the book *Mathematical Systems Theory* (12). In equation 4.4 the weighted cost function is presented.

$$V(\bar{\theta}) = \frac{1}{N} \sum_{t=1}^N \bar{e}^T(t, \bar{\theta}) \cdot W(\bar{\theta}) \cdot \bar{e}(t, \bar{\theta}) \quad (4.4)$$

The weight function can be fixed or a function of the parameter set. In equation 4.4 the errors are multiplied with $W(\bar{\theta})$, so a function of a parameter set. This can be rewritten to equation 4.5, where the value of W is determined by $\bar{E}(\bar{\theta})$ squared. The capital E is the variance of the error. If the variance is high, the inverse makes sure that this influence is adverse.

$$W(\bar{\theta}) = \left(\frac{1}{N} \bar{E}^T(\bar{\theta}) \bar{E}(\bar{\theta}) \right)^{-1} \quad (4.5)$$

Another modification that can be made on the cost function is 'regularization'. This prevents overestimation of parameters. Overestimation, or over fitting, in practice means that the estimation is fluctuating so much that it fulfils all the data points, but in the end it becomes irregular and useless. To avoid this phenomena, another term is added to the cost functions, which is called the Ridge regression. The ridge term is shown with the conventional weighted cost function in equation 4.6.

$$V(\bar{\theta}) = \frac{1}{N} \sum_{t=1}^N \bar{e}^T(t, \bar{\theta}) \cdot W(\bar{\theta}) \cdot \bar{e}(t, \bar{\theta}) + \frac{1}{N} \lambda (\bar{\theta} - \bar{\theta}^*)^T R (\bar{\theta} - \bar{\theta}^*) \quad (4.6)$$

The last term makes sure that an over fit can not happen. The last term is in fact penalizing the increase of any parameter. The other values in the

additional term of equation 4.6 are: θ^* , which represents the nominal value of θ . R represents the confidence in the prior knowledge of the unknown parameters. So that in the end an trade off occurs which the user should make.

Another interesting adjustment that can be made in the cost function is to penalize for nonlinear behaviour in the data. This can be achieved by adding a threshold, determined by the user, inside the cost function so that the weights of large errors from quadratic behaviour will be penalized in a linear way. When this threshold is added, then the cost function will be written double, this means that i represents the times that the error is below the threshold and j represents the times that the error is above the threshold, see equation 4.7.

$$V(\bar{\theta}) = \frac{1}{N} \left(\sum_{t \in i} \bar{e}^T(t, \bar{\theta}) \cdot W(\bar{\theta}) \cdot \bar{e}(t, \bar{\theta}) + \sum_{t \in j} \bar{v}^T(t, \bar{\theta}) \cdot W(\bar{\theta}) \cdot \bar{v}(t, \bar{\theta}) \right) \quad (4.7)$$

The threshold can be defined as $|e(t) < \rho\sigma|$, where σ stands for the estimated standard deviation of the error and the value of ρ is determined by the user. Here, $v(t, \theta)$ is calculated in equation 4.8.

$$v(t, \theta) = e(t, \bar{\theta})\sigma \frac{\rho}{\sqrt{e(t, \bar{\theta})}} \quad (4.8)$$

4.1.3 Optimisation

The optimisation part contains two different sections. The first section is about different optimisation algorithms. In the second part different stopping criterion's are discussed.

Optimisation and minimisation of the cost function is the same, the difference lies in the constraints. Because 'Optimalisations' is a complete different field of engineering, this topic is only slightly discussed with the only one purpose: to prevent big pitfalls.

For now, especially fixed step size or variable step size algorithms are used for the parameter set estimation. But still, this can lead to a very long optimisation when the starting point is far away from the optimisation point. To speed up the program, one can start with a random search. This means that in the beginning a lot of random but feasible starting sets are made, and the set which results in the lowest error is the starting set.

A point of attention with fixed step size is that there is a possibility that a local minimum is found. A way of avoiding this, is by making a big step so the program steps out of the local minimum and goes to a global minimum. Another approach is by optimizing for different parameter sets and take the lowest local minimum.

In the second section of this optimisation, the stopping criteria are discussed. As stated before, there is no zero optimum, so it should be prevented that the searching algorithm will run forever. The easiest way is to put a maximum criterion in the amount of iterations or the amount of iterations without improvement. Also, a relative improvement can be used, for example that there should be a minimum percentage difference between the current

value of the cost function and its expected improvement after the next iteration (11), otherwise the algorithm will stop.

In practice, the stopping criteria are decided upon the available time of the user for the optimisation. Different tricks can be used to speed up the process so that a better estimation is made in the same amount of time. Some of these tricks include adding additional relations between certain parameters, which are derived from literature and other researches. Another possibility is to set a minimum and maximum value for every parameter, which is determined by logical thinking and experience, this is outlined in chapter 4.2.1.

4.1.4 Estimated fit

This part discusses the question 'What is a good fit?'. The lowest cost function doesn't mean directly that it is the best fit possible. In the full-scale measurement is noise involved, so a possibility exists that the solution is fitted on the noise. So there are different ways in saying that it's a good fit.

First of all, the most easy approach is implement the obtained parameters and put them in the model and compare the response with another data set. The requirement is to have another data set and when this is not the case than different values are defined to say something about the fit. These definitions are outlined here below:

The Normalized Root Mean Squared Error (NRMSE) is defined as a percentage, which can be calculated according to equation 4.9. The fit percentage or NRMSE lies between the minus infinity and 100%.

$$FitPercen = 100(1 - \frac{\|\bar{y}(t)_{meas} - \bar{y}(t)_{sim}\|}{\|\bar{y}(t)_{meas} - \hat{y}(t)_{meas}\|}) \quad (4.9)$$

Equation 4.9 contains first the measured output data set \bar{y}_{meas} , secondly the mean of the measured output data set \hat{y}_{meas} , finally the output of the linearized model for a certain parameter set, $\bar{y}(t)_{sim}$.

The second error is the mean squared error (MSE), an error also shown in the part about the cost function, equation 4.10.

$$MSE = \frac{1}{N} \sum_{t=1}^N \bar{e}^T(t) \bar{e}(t) \quad (4.10)$$

A third way to describe the error is with Akaike's Final Prediction Error (FPE), defined as:

$$FPE = \det\left(\frac{1}{N} E^T E\right) \left(\frac{1 + \frac{n_p}{N}}{1 - \frac{n_p}{N}}\right) \quad (4.11)$$

In equation 4.11 n_p represents the number of free parameters in the model. N represents the number of samples in the estimation data set. E is the $N - b_y - n_y$ matrix of prediction errors, where n_y is the number of output channels. According to Akaike's theory, the most accurate model has the smallest FPE. Next to the Final Prediction Error, there are other ways of expressing the fit. Different examples are the Aikike's Information Criterion (AIC) and the Consistent Akaike's Information Criterion (CAIC) (28).

4.1.5 Problem statement frequency domain

In the previous part the parameter estimation was done in time domain. Parameter estimation in frequency domain is another possibility that is often used in practice. Some advantages of parameter estimation in frequency domain compared to time domain are outlined here below:

- Compression of data, because long time measurements can be rewritten to a short mathematical notation.
- Non-uniformity in the frequency data is allowed, while in time domain the times steps are fixed.
- A pre-filtering takes already place.

The disadvantages of doing parameter estimation in frequency domain are outlined here below:

- Parameter estimation for a nonlinear model is in general impossible.

The data in frequency domain can be presented in different ways. First of all, it is possible to transfer from time to frequency domain for the whole obtained data set. The other notation is that the data is written as a frequency response, where complex notation is used most of the time.

The differences between the domains for the searching algorithms as defined in the previous parts is that the time t is changed to frequency ω . An easy frequency domain optimization for a single in and single out system is presented in equation 4.12.

$$\min \sum_{k=1}^{N_f} |W(\omega)(G(\bar{\theta}, \omega) - f(\omega))|^2 \quad (4.12)$$

In equation 4.12 the $W(\omega)$ is a frequency dependent weight, which makes sure that not on every frequency is fitted, but mostly on the frequencies that are more dominant. N_f is the amount of frequencies that are provided by the data, $G(\omega)$ is the response of the parameter set and $f(\omega)$ is the data itself. In global lines, this looks the same as a time domain parameter estimation, but it speeds up the parameter estimation.

4.2 MODEL STRUCTURE

The model structure main part is split up in two different parts. Firstly, the parameter constraints and, secondly, an analysis of the amount of relations in the model structure.

4.2.1 Parameter constraints

Beforehand, some constraints on parameters are already known. In table 4.1 the linearized parameter set $\bar{\theta}$ is presented with the mathematical expressions in the nonlinear model.

Linearized parameter	Mathematical expression
τ_n	$\frac{2\pi I_p n_0}{M_{s,0}}$
\mathcal{G}	$\frac{n_0}{M_{b,0}} \frac{\delta M_b}{\delta n} \Big _X$
v	$\frac{X_0}{M_{b,0}} \frac{\delta M_b}{\delta X} \Big _n$

Table 4.1: Definition of different linearized model parameters.

With some logical thinking, some boundaries can already be put on the different parameters. This will decrease the optimization time and second of all gives only feasible solutions. A small disadvantage is that more local minimums are created with the extra boundaries. In equation 4.13 different constraints are determined for every parameter i , were the lower bound (lb) and upper bound (ub) are different for every parameter.

$$s.t. \quad lb < \theta(i) < ub, \quad \theta(i) \in \mathbb{R} \quad (4.13)$$

For example, since the governor gains are positive the lower bound is put to zero. The value of v is negative so here the upper bound is put to zero.

Next to putting boundaries on the different linearized parameters, one can imagine that the boundaries can be placed so tight that parameters are practically fixed. In practice this can be used if a parameter is identified by for example another experiments and is 'known'. Fixation of parameters can lead to some big advantages, such as decrease of parameter estimation time and less relations required in the model structure.

4.2.2 Internal relations

In this part the internal relations between the parameters in the linearized model, derived in chapter 3.3, are discussed. This linearized model is the basis for the model structure that is used for the parameter estimation. The relations in the model structure are analyzed according to the transfer functions, $\frac{\delta n^*}{\delta n_{set}^*}$, $\frac{\delta E_n^*}{\delta n_{set}^*}$ and $\frac{\delta M_s^*}{\delta n_{set}^*}$, which is another mathematical presentation of the model structure.

From basic math it follows that the amount of unknowns should equal the amount of equations, if the unknowns need to be identified. The linearized parameter set contains five parameters, which results in the requirement of five equations. Note that then the five different equations should contain all

different parameters.

The transfer functions 3.31, 3.35 and 3.38 are simplified to the following forms, equations 4.14, 4.15 and 4.16. The values of $a, b, c, d, e, f, g, h, i$ are presented in Appendix B 'Terms in transfer functions'.

$$\frac{\delta n^*}{\delta n_{set}^*} = \frac{cs + d}{s^2 + as + b} \quad (4.14)$$

$$\frac{\delta E_n^*}{\delta n_{set}^*} = \frac{es + f}{s^2 + as + c} \quad (4.15)$$

$$\frac{\delta M_s^*}{\delta n_{set}^*} = \frac{gs^2 + hs + i}{s^2 + as + c} \quad (4.16)$$

Table 4.2 presents a 'System of linear equations', where the vertical line represents the mathematical equal sign. If a system identification is made, then the values of a till f are determined. This does not mean that the parameters are estimated, but that a fit is made with the model structure or transfer function on the data. When the values of a till f are known, the individual parameters can be identified. In table 4.2, it can be seen that τ_n can be determined from the first two equations. When the value of τ_n is known, then with help of the third equation the value of g can be calculated.

K_p	K_i	vK_p	vK_i	g	v	-
		1				f
		1				$c\tau_n$
				-1		$e\tau_n - 2$
			1			$b\tau_n$
			2			$i\tau_n$
			1			$d\tau_n$
		$\frac{2}{\tau_n}$	1			h
		1		-1		$a\tau_n - 2$
		1				g

Table 4.2: System of linear equations of the internal relations within the model structure.

As can be seen in the system of linear equations, the parameters of K_p , K_i and v are not expressed individually in an equation, which makes it impossible to identify their absolute values. Only the relations between K_p , K_i and v can be derived with the previous set of equations.

So, if for example one of the values K_p , K_i and v is known, then it is possible to derive the other two parameters. In general, it can be stated that the K_p and K_i are unknown. The value of v can be obtained from a factory acceptance test (FAT) (14), so then K_p and K_i can be calculated.

From this can be concluded that the model structure does not allow identifying all parameters individually. So from here on, only relations can be derived between K_p , K_i and v and not their absolute values. However, the model structure does allow identification of the absolute values of the parameters τ_n and g .

Note that the transfer function 4.15, with values e and f , adds no more relations to the system of linear equations. In other words, the values of e and f are redundant to a and g , because they have the same value. Thus, the transfer function $\frac{\delta E_{\eta}^*}{\delta n_{set}^*}$ can be left out in the model structure.

4.3 INFORMATION-RICH DATA SETS

In the third main part, information-rich data sets are discussed and elaborated upon. The first part contains a brief description of how the data sets are obtained from the nonlinear model. In the second part, different input signals are discussed, whether they are feasible and information-rich. This is done for full-scale and the virtual experiments. The third part is about the frequency and amplitude range, respectively.

4.3.1 Data set generation

In the simulation model it is possible to observe every possible signal, because a log block can be put anywhere in the model. Please note that in reality, some components or values are not measurable, because it is too complicated and/or expensive. From chapter 4.2.2 it is derived that the shaft torque and the shaft speed should be measured during the experiments and the integrated error is left out. The two measurements are indicated as grey circles in figure 4.2. Furthermore, the input signal is also 'logged', the third grey circle. Before the data is logged, the values are first normalized.

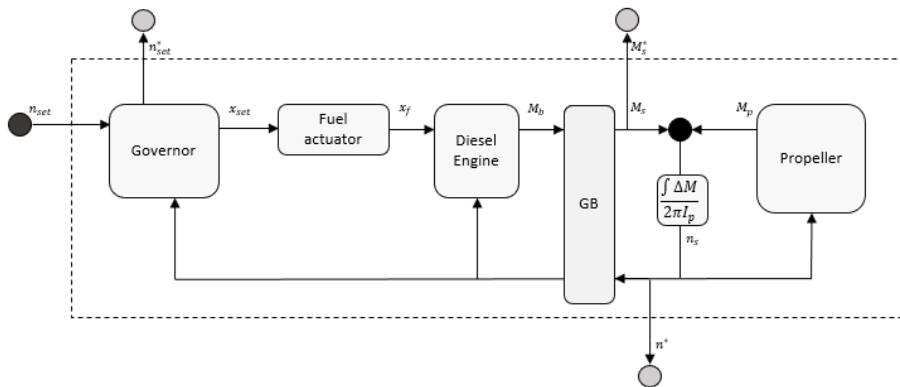


Figure 4.2: Data set generation of nonlinear model.

4.3.2 Input signals

The input signals are discussed based on three different aspects. First of all the practical feasibility of the input signal on a *full-scale* propulsion drive train is discussed. After that the duration of a certain input signal is discussed, because the aim of this research is to obtain the parameters in a short period of time. The last aspect is that the input signal should fulfil some amplitude and frequency requirements. The amplitude should not excite the system unnecessarily much, to avoid damage to the system. Furthermore, the frequency range of the input signal is important for the identification of the whole dynamic behaviour. Below, a list is shown with all the different

input signals that are possible, where some signals are directly classified as unfeasible, according to the three criteria mentioned in this paragraph.

- A *'step response'* is a signal where just a step will be set on an input signal in a very short time. Theoretically, a step response is a summation of an infinite amount of sinus signals. A step response is good for validation, because it covers the whole frequency domain and in time domain the user intuitively gets a feeling whether the estimated response is correct. Furthermore is a step response in time domain perfect to see whether there is a dead time (delay) in the system, what the static gain is and the difference in rise time between the estimated model response and the data. Rise time means how fast the error is minimized over time.
- A *'multiple sine wave'* input signal contains sinus signals with different frequencies. One big advantage is that there is nearly no noise in the input and output signal. And if there is noise, it can be eliminated quite easily, because the input frequency is known. Also the purity of a sine wave is quite high, due to the fact that only one frequency component is put into the system. Another advantage is that one can validate the model structure by plotting the gain and phase lag points for those frequencies, which gives a shape that should cope with the estimated system response. The disadvantage of multiple sine waves is that, when exciting the systems natural frequency, damages to the system can be quite high. Another disadvantage is that low frequencies are time consuming. A way to avoid this is by implementing different sine signals simultaneously. A point of attention here is that the signals have the correct phase difference, otherwise a high peak factor will occur. A high peak factor can lead to unwanted nonlinearities and an increased change of damaging the system.
- A *'chirp signal'* is a sinus signal with a constant amplitude but with a continuously increasing frequency. In this way all frequencies will be present in the input signal. An advantage of implementing the chirp signal is that it decreases the experiment time a lot. A disadvantage is that when there is a measurement error, the output will miss that particular frequency response, because every frequency excites the system only for a very short time span. Another disadvantage is that the natural frequency is always excited, however only for a short amount of time.
- A *'pulse'* with a small pulse width, so that it is not a double step response, is another possible input signal. With the virtual experiments this will make sense, because of limitations of the simulation model. In practice it makes no sense to put a pulse on the engine, because the system can not react due to discrete firing phenomena and moment of inertia. For this reason, it is chosen not to take pulses into account as feasible input signal for the experiments, including variants of pulses (e.g. random binary pulses).
- *'Band limited white noise'* is a random input signal with a constant intensity. Band limited white noise can be a very powerful tool for system identification. In this case, the white noise is not taken into account, because it's the first time for full-scale parameter identification and

there is a possibility that the propulsion drive train will not react on limited white noise. This is because the band limited white noise will most likely be deformed by unknown ramps or limiters in the system. When this deformations occurs, then the actual input of the system is unknown and this makes the parameter identification nearly impossible. Due to a lag of knowledge about the full-scale system the band limited white noise is not taken into account as feasible input signal.

4.3.3 Signal requirements

The last part is split up into two different parts. First the amplitude of the input signal is discussed, and in the second part the characteristics of the input frequency is discussed.

The value of the amplitude of the input signal depends on a trade-off between the signal amplitude/noise ratio and the nonlinearities in the system. The input signal should be visible in the measured data, but the data should not contain to much nonlinearities. During the virtual experiments, the influence of amplitude increase on the total error is analyzed. The results of this analysis are then used during the full-scale experiments, where the amplitude is minimized to avoid strong nonlinearities in the data.

As stated earlier, the input signal should cover a wide range of frequencies. In Bode plots 3.8 and 3.9, two different transfer functions are plotted, namely the $\frac{\delta n^*}{\delta n_{set}^*}$ and $\frac{\delta M_s^*}{\delta n_{set}^*}$. As known from the chapter about internal relations, the poles are identical, but the zeros can variate. The input signal must excite all the different zeros such that the data sets become rich enough. Concluding remarks can be made that the lowest frequency measured in reality depends on how long the available measurement time is and how much prior knowledge is available on the location of the first zero or pole.

The highest frequency in the full scale experiments is limited by the discrete ignition time of the physical system. Nevertheless, in the nonlinear model every offset is directly multiplied with the proportional part of the governor and the engine directly provides the requested torque. From this can be derived that the maximum input frequency for the virtual experiment doesn't exist, because of the limitation in the nonlinear model. During the full scale experiments the highest input frequency should be put on the system to see if any ramps are touched and this theory can be confirmed.

4.4 CONCLUSION

The conclusions that can be drawn from this chapter are listed below:

- Throughout this chapter the knowledge is obtained on how parameter estimation works in theory. Furthermore, the importance of the correct settings of the searching algorithm is discussed. Options and settings such as a weighted cost function, regularization, correct stopping criteria and feasible solutions by adding constraints are recommended to use for the parameter estimation.
- The model structure derived in Chapter 3.3 can be used, but it has some disadvantages. First of all, it is not possible to determine every parameter individually, because the amount of unique relations between the parameters is not equal to the amount of parameters, as presented in table 4.2. This results in the fact that only the values of g and τ_n can be individually determined. The other three model parameters can then only be determined relative to each other by the following two relations vK_p and $\frac{K_p}{K_i}$. Nevertheless, this model structure is used, because the value of v can be derived from a factory acceptance test (FAT) (14). When the value v is known this also implies that the values of K_p and K_i can be determined
- The two most feasible input signals of the system are multiple sine waves and a chirp signal. The advantage of a multiple sine wave is that the model structure can be validated and it contains a relatively high spectral purity, because it is just a range of discrete frequencies, which allows filtering out noise more easily. The chirp input signal is interesting, because it minimizes the duration of the experiments.
- The input signal's amplitude depends on a trade-off between the signal amplitude/noise ratio and the influences of nonlinearities in the data.
- The lowest frequency measured in reality depends on how long the available measurement time is and how much prior knowledge you have about the location of the first zero or pole.

5

VIRTUAL PARAMETER ESTIMATION

In this chapter the virtual experiments and the obtained results are discussed. This chapter is divided into five main parts, where in the first main part the data generation is elaborated on. In here are the input signals and the output signals from the virtual experiments presented. The second main part is about the used searching algorithm for the parameter estimation. In the third main part the used model structure is discussed, explaining how the model fitting on the data is done. In the fourth main part the results are presented and in the fifth main part conclusions are drawn.

5.1 DATA GENERATION FROM NONLINEAR MODEL

First are some references made to previous chapters, because they are relevant for clarity on how the data sets are derived. Next to that, some statements are repeated that concern influences on the virtual experiments.

- In chapter 4.3.1 is explained how the data sets are obtained during a virtual experiment. Figure 4.2 shows that the data contains a input signal δn_{set}^* and output signals δM_s^* and δn_s^* . During the experiments the output signal δE_n^* is not 'measured'. As can be seen from figure 4.2 these data sets are obtained from the nonlinear model.
- The data generation is done with four different input signals. Namely multiple sine waves, chirp signal logarithmic, chirp signal linear and a chirp signal logarithmic with bigger amplitude. These four different input signals were selected in chapter 4.3.2 where different input signals are discussed. One input signal has a bigger amplitude to see the influence on the parameter estimation.
- The nominal operation point is discussed in chapter 3.4 and is 1300 rpm . This operation point leads to the system variables presented in table 3.5. The values from table 3.5 are used for normalisation of the derived data sets.

In the following four parts the input signals and their responses are discussed in more detail.

5.1.1 Multiple sine waves

The frequency range of the multiple sine waves is determined with the help of a Matlab 'Linear Analysis Tool' that is implemented in Matlab Simulink. The input signal has an amplitude of 13 rpm , which leads to normalized value of $\delta n_{set}^* = \frac{13}{1300} = 0.01$ with the current nominal operation point. The sixteen different frequencies of the multiple sine waves are presented in table 5.1.

Freq [Hz]	Begin [s]	End [s]	Freq [Hz]	Begin [s]	End [s]
0.0042	0	954.36	0.1805	2484.52	2506.68
0.0067	954.36	1550.64	0.289	2506.68	2520.52
0.0107	1550.64	1923.2	0.463	2520.52	2529.16
0.0172	1923.2	2155.96	0.7407	2529.16	2534.56
0.0275	2155.96	2301.4	1.19	2534.56	2537.92
0.044	2301.4	2392.28	1.88	2537.92	2540.04
0.0705	2392.28	2449.04	3.03	2540.04	2541.36
0.1127	2449.04	2484.52	4.76	2541.36	2542.2

Table 5.1: Different frequencies of sine signal presented in Hz.

Every frequency in table 5.1 is executed four times for a more trustworthy response of the system. The input signal of the multiple sine signals that is used during the virtual experiment is presented in figure 5.1, where the four periods for every frequency are visible.

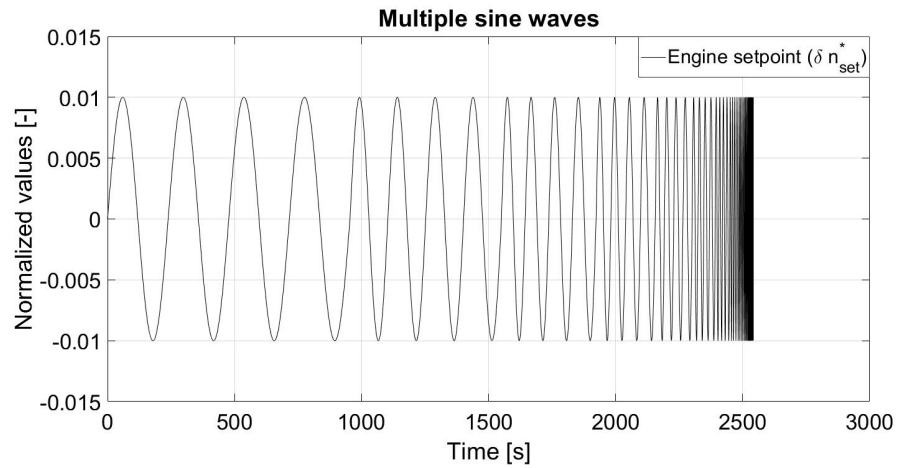


Figure 5.1: Multiple sine waves as input signal.

The input signal set point engine speed δn_{set}^* and output signal shaft speed δn^* are presented in figure 5.2.

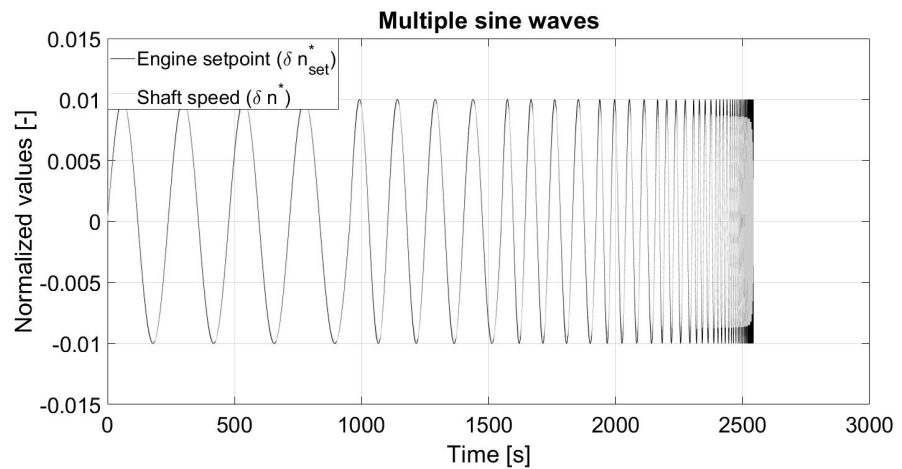


Figure 5.2: Multiple sine waves as input signal and shaft speed as output signal.

The results in figure 5.2 are in line with the expectations from looking at the results of the Bode diagram in figure 3.8. In the Bode diagram it is clearly visible that at higher frequencies the response of the shaft speed becomes zero. This is also visible in the results as presented in figure 5.2, where the grey line in the last 100 s goes rapidly to zero at higher frequency input. Furthermore in chapter 3 is derived that the DC-gain of $\frac{\delta n_{set}^*}{\delta n_{set}^*}$ is 1. This is also clearly visible in figure 5.2 where the shaft speed can follow the set point of the engine speed at lower frequencies. Another phenomena that is slightly visible in figure 5.2 is that at increased input frequency a bigger phase shift occurs. This is also in line with the expectations derived from the Bode diagram.

The input signal δn_{set}^* and the output signal shaft torque δM_s^* are presented in figure 5.3.

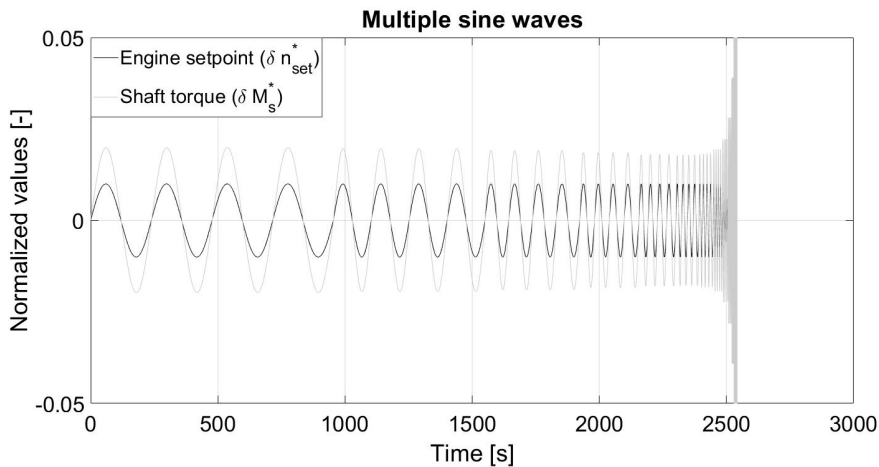


Figure 5.3: Multiple sine waves as input signal and shaft torque as output signal.

The results of the output signal, torque, in relation with set point engine speed are in line with the expectations gained from the Bode diagram in figure 3.9. In the Bode graph can be seen that at higher frequencies, the response drastically increases. The response is even so high that these responses are not plotted, because otherwise the response of the lower frequencies is not visible. The DC-gain $\frac{\delta M_s^*}{\delta n_{set}^*}$ is 2. This is also in line with figure 5.3, where at low frequencies the response of the shaft torque is 0.02, while the input is 0.01. Furthermore is in figure 5.3 also slightly visible that with an increased input frequency a phase shift in the response signal occurs.

From the above mentioned observations it can be concluded that the obtained data sets with multiple sine waves input signal shows behaviour that is, in line with qualitatively the frequency domain behaviour predicted in chapter 3.3.

5.1.2 Chirp signal

During the virtual experiments three different chirp signals are used for parameter estimation. First, the distinguishment is made between linear and logarithmic, which means how the frequency range is divided over time. Another difference between the chirp input signals is the amplitude.

The frequency range for all chirp signals are kept the same and are $w = [0.0014 \dots 20] Hz$. The frequency range is also determined by the toolbox of Matlab.

Chirp logarithmic small amplitude

The chirp signal in which the frequencies are logarithmic divided over time and with normalized amplitude of $\delta n_{set}^* = \frac{13}{1300} = 0.01$ is presented in figure 5.4.

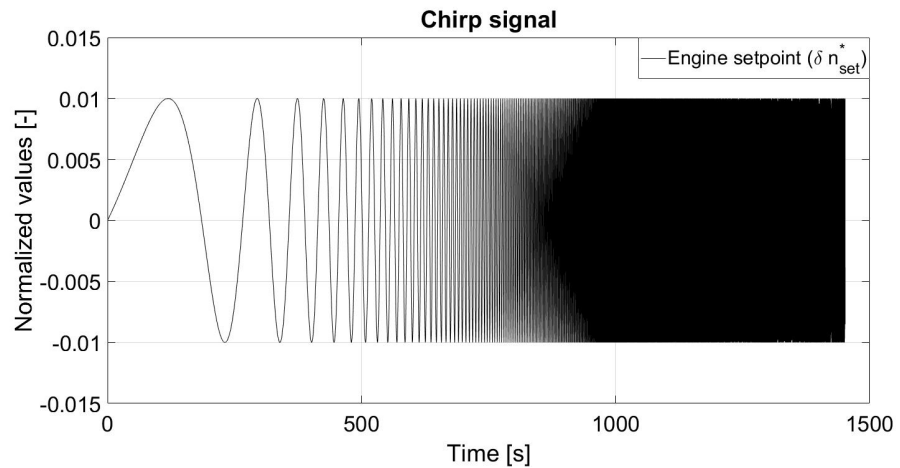


Figure 5.4: Chirp signal logarithmic divided over time as input signal.

The input signal δn_{set}^* and the output signal δn_s^* are presented in figure 5.5.

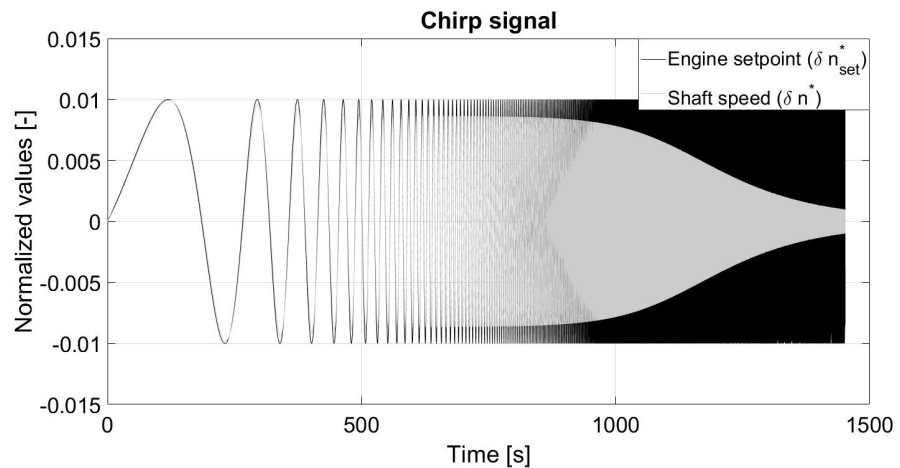


Figure 5.5: Chirp signal logarithmic divided over time as input signal and shaft speed as output signal.

The results of the output signal are in line with the expectations derived from the Bode plot in figure 3.8. The reason for this is the same as stated for the multiple sine wave signal. The shaft torque response and set point engine are presented in figure 5.6.

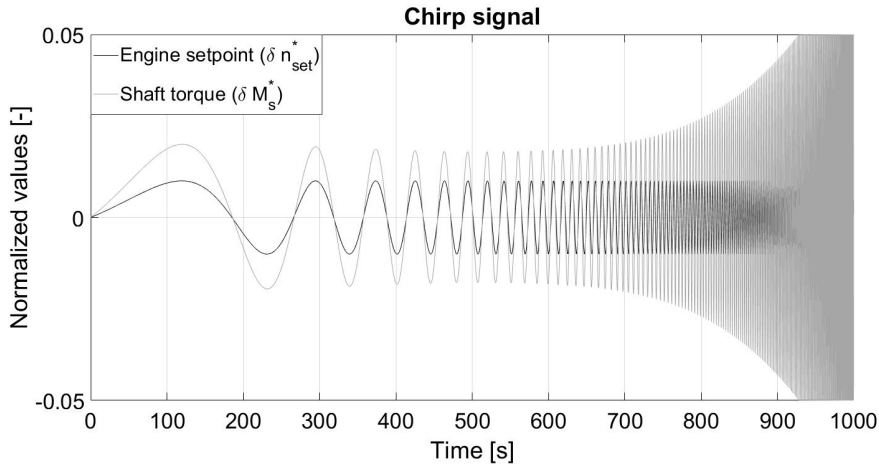


Figure 5.6: Chirp signal logarithmic divided over time as input signal and shaft torque as output signal.

Pay attention to the fact that the actual chirp is an input signal of 1500 seconds, but the shaft torque response is only plotted till 1000 seconds. The reason for this is that at too high input frequencies the shaft torque response dominates figure 5.6 and presenting these results in a figure is not useful. However at higher frequencies is the shaft torque response in line with the expectations. From the above mentioned observations it can be concluded that the obtained data sets with chirp signal logarithmic divided input signal shows behaviour that is, in line with qualitatively the frequency domain behaviour predicted in chapter 3.3.

Chirp linear small amplitude

In figure 5.7 a chirp signal is represented, where the frequencies are linearly divided over the time and the amplitude is as well $\delta n_{set}^* = \frac{13}{1300} = 0.01$. From figure 5.7 can be seen that after 50s the frequency is so high that a chirp signal is not visible anymore.

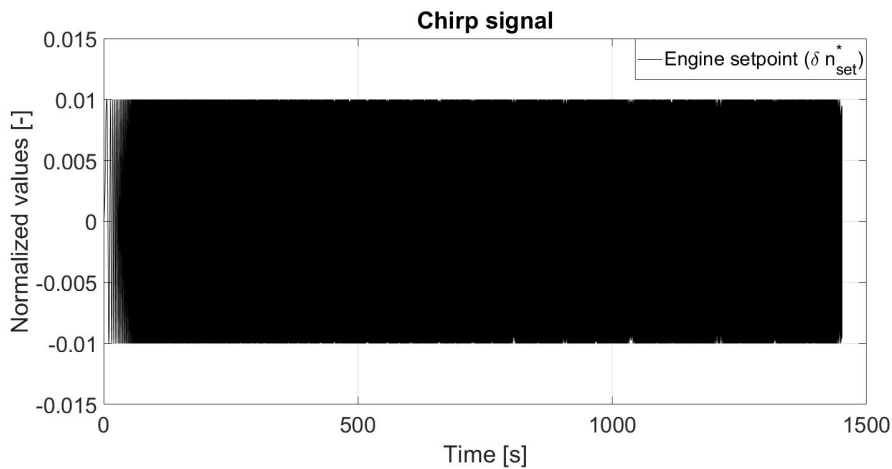


Figure 5.7: Chirp signal linear divided over time as input signal.

To see if the output signals are in line with the expectations only the first 12 seconds are plotted, see figure 5.8 and 5.9.

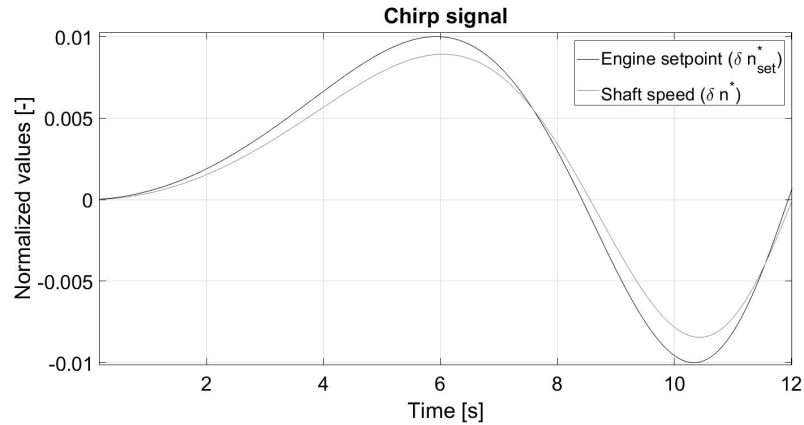


Figure 5.8: Chirp signal linear divided over time as input signal and shaft speed as output signal.

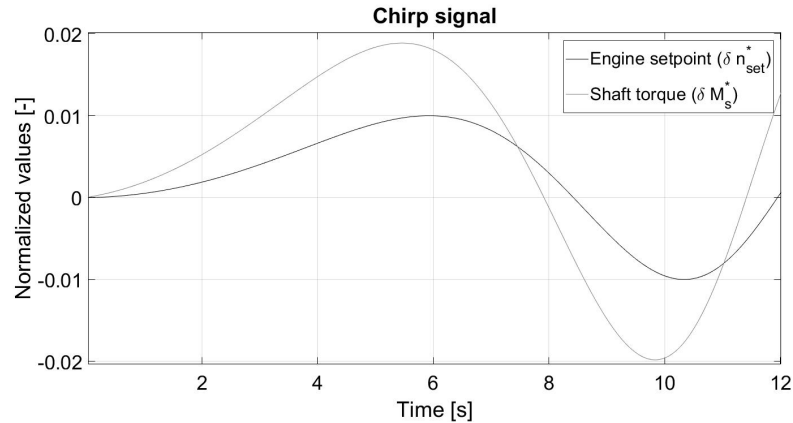


Figure 5.9: Chirp signal linear divided over time as input signal and shaft torque as output signal.

From figure 5.8 can be derived that at zero seconds the shaft speed can follow set point engine speed, but at 6 seconds is the $\frac{\delta n^*}{\delta n_{set}^*} = 0.9$. This is phenomena is also visible in figure 5.9 where at 6 seconds the $\frac{\delta M_s^*}{\delta n_{set}^*} = 1.9$. A reason for this is that the frequency increases so fast that after 5 seconds the shaft is already not able to follow the set point engine speed. Still are the values quite close to what was expected. From the above mentioned observations it can be concluded that the obtained data sets with linear chirp input signal shows behaviour that is, in line with qualitatively the frequency domain behaviour predicted in chapter 3.3.

Chirp logarithmic increased amplitude

In chapter 4 is derived that during the full-scale experiments an increased amplitude should be used so that the input signal is still visible between the expected measurement noise, because the validation should be done with a different data set. For this reason the amplitude is increased to a

normalized value of 0.08. This means a shaft speed amplitude in practice of $n_{set} = 0.08 \cdot 1300 = 104rpm$, see figure 5.10. The responses of the output signals and the input signal are shown figure 5.11 and 5.12.

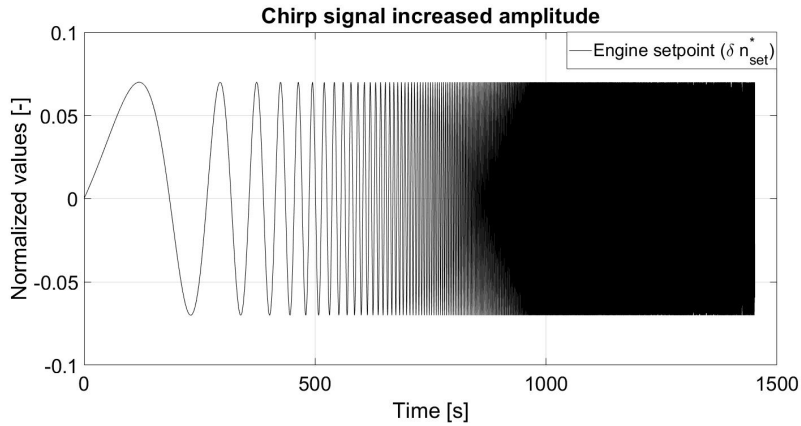


Figure 5.10: Chirp signal with higher amplitude logarithmic divided over time as input signal.

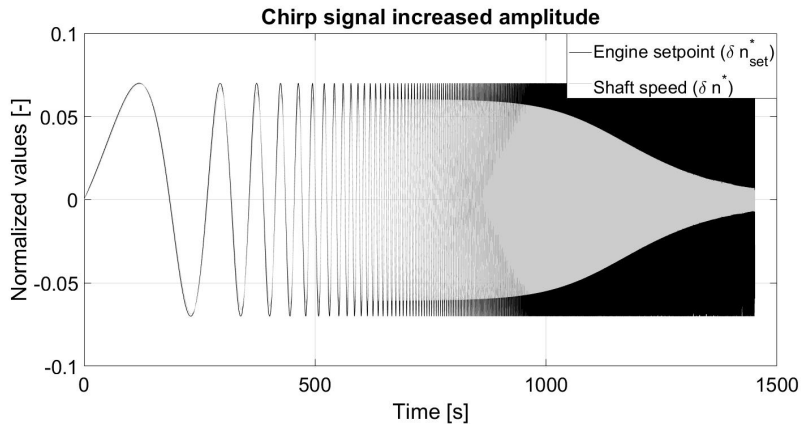


Figure 5.11: Chirp signal with higher amplitude logarithmic divided over time as input signal and shaft speed as output signal.

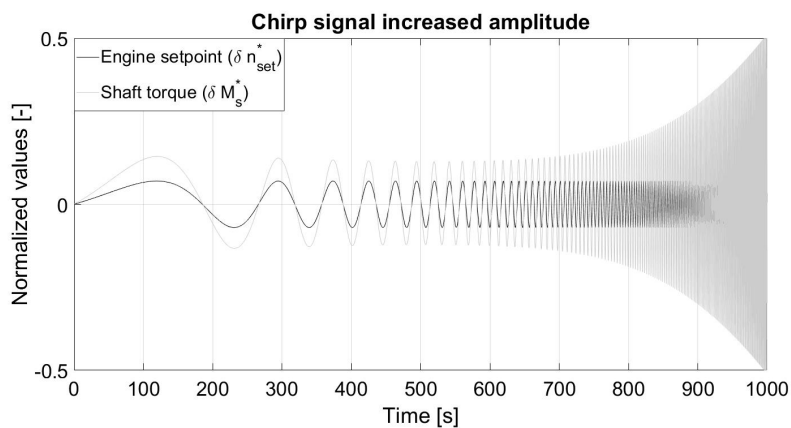


Figure 5.12: Chirp signal with higher amplitude logarithmic divided over time as input signal and shaft torque as output signal.

The responses are also in line with the expectation for the same reason as stated in the multiple sine waves. From the above mentioned observations it can be concluded that the obtained data sets with high amplitude chirp input signal shows behaviour that is, in line with qualitatively the frequency domain behaviour predicted in chapter 3.3.

5.1.3 Step responses

During the virtual experiments there are also step responses executed, they serve for the purpose of validation. The input signal contains three different steps of $\delta n_{set}^* = \frac{13}{1300} = 0.01$ and they are executed every 20 seconds. The input signal and the two different output signals are presented in figure 5.13 and 5.14.

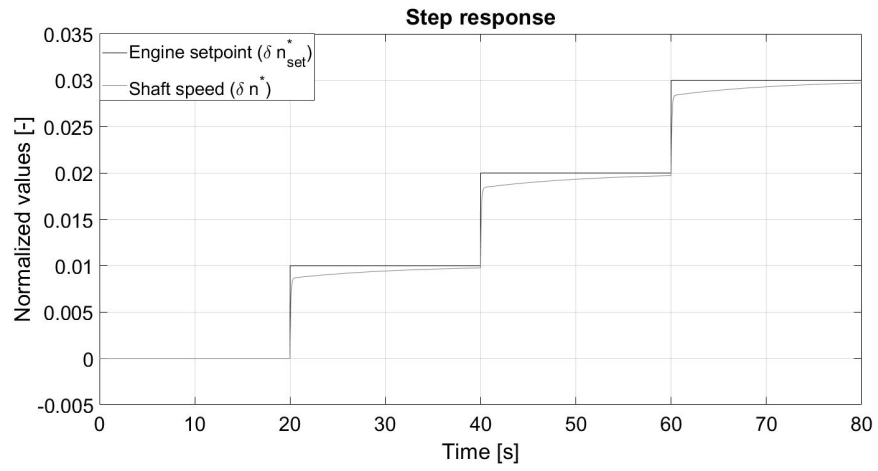


Figure 5.13: Step response signal as input signal and shaft speed as output signal.

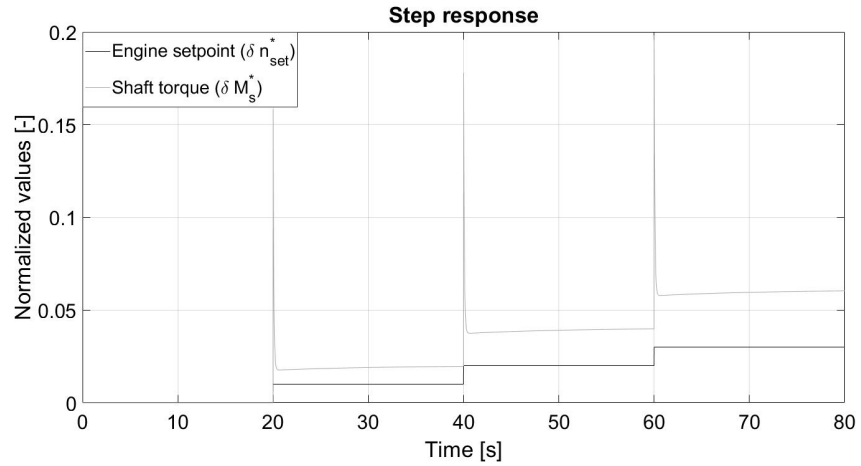


Figure 5.14: Step response signal as input signal and shaft speed as output signal.

5.2 SEARCHING ALGORITHM

In the second main part the settings of the searching algorithm are discussed. In other words: How is the model fitted to the obtained data sets?

The '*Initial State*' of the optimisation algorithm is put to zero. This is the initial state for the searching algorithm; a different initial state can lead to a different fit (29). The '*Disturbance*' in the model is put to zero, this means that there is no disturbance or noise in the data. This is also the case, because the data sets are obtained from the nonlinear computer model. The '*Focus*' of the error function is put to prediction, which results in a better model reponse when a different data set is used. The searching algorithm is obligated to come to '*force stability*', which means that the estimation should be stable, because in reality the propulsion system is also stable. The '*Input/Output offset*' are turned off, because the offsets are automatically cancelled when the data sets are normalized.

The '*Output Weight*' is turned on, which results in a weighted cost function. This is required, because the averages of the output channels are different and the difference at its maximum is ± 15 at high input frequencies. Furthermore: '*Regularization*' is used to remove the 'high' peaks generated by the nonlinearities in the data. The effect of this regularization is not seen in the parameter estimation results. The '*Searching algorithm*' is chosen by the software itself. In practice this means that the parameter estimation program chooses the approach to come to a minimum. The methods that can be used are subspace Gauss Newton Last Squares (GNLS), Levenberg Marquard Last Squares (LMLS) and the Matlab function '*fmincon*'.

The stopping criterion of the searching algorithm is defined as follows: There are a maximum of 100 '*iterations*' during the loss function minimization. The '*tolerance*' is 0.01, which is the minimum percentage difference between the current value of the loss function and the expected improvement after a following iteration. The expected improvement is computed based on the Gauss-Newton vector for the current parameter set. If the improvement ratio is not achieved, the algorithm will stop.

5.3 MODEL STRUCTURE

In chapter 3.3 the linearized model in state space notation is presented and this is also used as model structure for the parameter estimation. In Chapter 4.2.2 is derived that the shaft speed and shaft torque are only measured. This leads to the usage of the model structure which is presented in equation 3.50 and 3.51. It was also concluded that the parameters v , K_p , K_i can not be individually identified. For this reason two relations are estimated during the parameter identification, namely vK_p and $\frac{K_p}{K_i}$. The model structure is able to estimate the parameters g and τ_n , so the parameter estimations gives 2 parameters and 2 relations.

5.4 RESULTS PARAMETER IDENTIFICATION

In the fourth main part the results of several parameter estimations are presented, where every parameter estimation is defined as a small Roman numeral (ii,...,v). First, the starting conditions are defined, which is followed by a description of the four parameter estimations that have been executed. After that the results are presented in a table and figures.

All the parameters of the nonlinear simulation model are known, because the user knows the input, see chapter 3.4. This will result in the real parameter set $\bar{\theta}_r$, presented in equation 5.1.

$$\bar{\theta}_r = [\tau_n \quad g \quad v \quad K_p \quad K_i]^T = [1.442 \quad -0.583 \quad 1.583 \quad 10 \quad 1]^T \quad (5.1)$$

The searching algorithm requires a starting vector, which is presented in equation 5.2. The values have been selected randomly. Other values can also be used for parameter estimation, but for the comparison between the different singals are all the results calculated with the same starting vector $\bar{\theta}_0$.

$$\bar{\theta}_0 = [\tau_n \quad g \quad v \quad K_p \quad K_i]^T = [2.5 \quad -2.5 \quad 3.5 \quad 10 \quad 3]^T \quad (5.2)$$

To speed up the optimization program and to guide the optimization to a feasible solution different boundaries are set for different parameters. The boundaries are defined in equation 5.3, 5.4, 5.5, 5.6 and 5.7.

$$0.01 < \tau_n < 5 \quad (5.3)$$

$$-3 < g < -0.01 \quad (5.4)$$

$$0.01 < v < 5 \quad (5.5)$$

$$0.01 < K_p < 15 \quad (5.6)$$

$$0.01 < K_i < 10 \quad (5.7)$$

Below the different parameter estimations are discussed.

- (i) '*Real parameters from nonlinear model*' are the parameters that are obtained from the nonlinear model, $\bar{\theta}_r$. To be clear, this parameter set is **not** derived from parameter estimation, but this parameter set will be used as a comparison with the other estimated parameter sets (ii - v). In the end, the errors between the real parameter set and the estimated parameter set are determining the quality of the parameter estimation. The reason for this is if you only look at the fit percentages, than you are not sure if the error occurs due to the limitations of the optimization or because you are fitting a linearized model on nonlinear data.
- (ii) '*Multiple sine waves*' are used as input signal, which is illustrated in figure 5.1. The amplitude is 13 rpm and the parameter estimation is executed in frequency domain.
- (iii) '*Chirp signal-lin*' where the frequencies are linearly divided over time, which is illustrated in figure 5.7. The amplitude is 13 rpm and the parameter estimation is executed in time domain.

(iv) 'Chirp signal-log' where the frequencies are logarithmic divided over time, which is illustrated in figure 5.4. The amplitude is 13 and the parameter estimation is executed in time domain.

(v) 'Chirp signal-ampl' where the frequencies are logarithmic divided over time, which is illustrated in figure 5.10. The amplitude is $0.08 \cdot 1300 = 104 \text{ rpm}$ and the parameter estimation is executed in time domain.

In table 5.2 different parameter identifications are listed with their results. In the second column of table 5.2 the total experiment duration is given. In the third till sixth columns the values of the parameters and relations of parameters are presented. In the seventh and eighth column the fitting percentages are presented for the data set with which the parameters are estimated. In the ninth and tenth column validations fitting percentage to step responses signal is shown.

	Duration	Parameters				Fitting		Validation	
		τ_n	g	$\frac{K_p}{K_i}$	vK_p	$\delta n^* [\%]$	$\delta M_s^* [\%]$	$\delta n^* [\%]$	$\delta M_s^* [\%]$
(i)	+	1.442	-0.583	10	15.83	+	+	99.53	90.72
(ii)	2542s	1.349	-0.575	9.99	15.83	99.99	99.98	99.52	90.70
(iii)	1500s	1.349	-0.575	10.03	15.86	99.91	99.91	99.53	90.69
(iv)	1500s	1.349	-0.575	10	15.43	99.98	99.98	99.52	90.70
(v)	1500s	1.321	-0.4616	11.57	15.22	97.84	87.76	99.36	89.99

Table 5.2: Results of virtual experiments.

+ The 'real parameters' are not fitted, so for this reason there is no percentage and no signal time.

From table 5.2 can be derived that all four (ii-v) different parameter estimations are giving promising results. The only parameter estimation that contains a slight error is the parameter estimation with an increased amplitude in the input signal, v. Nevertheless, the five parameter sets are put in a Bode plot, see figure 5.15 and 5.16 to see if the system responses are estimated correctly.

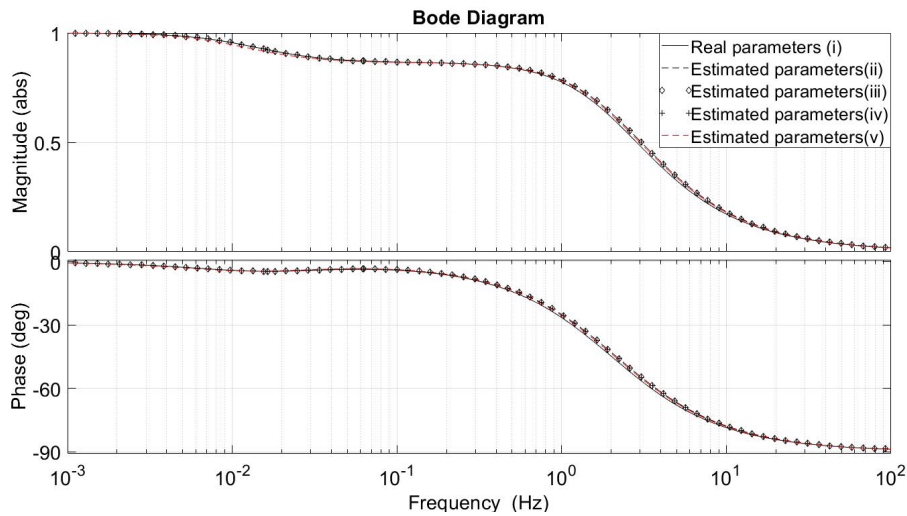


Figure 5.15: Comparison parameter estimation frequency domain for $\frac{\delta n^*}{\delta n_{set}^*}$

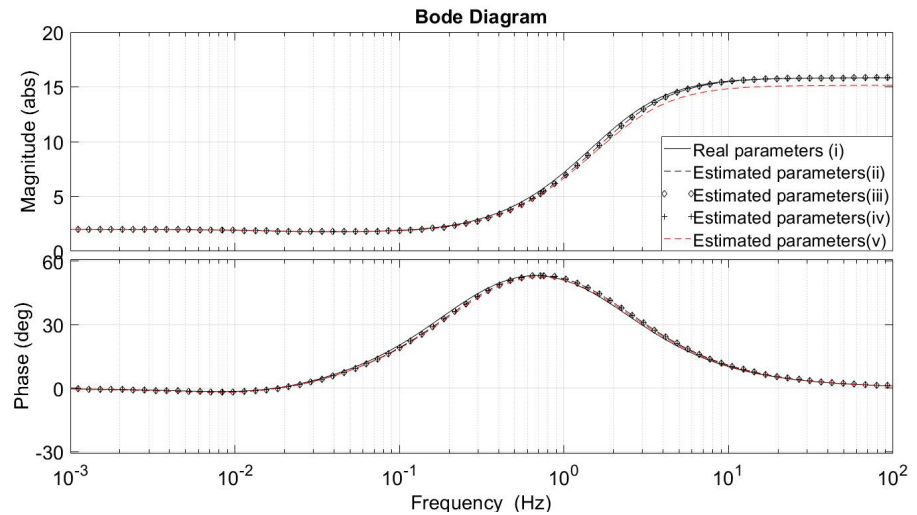


Figure 5.16: Comparison parameter estimation frequency domain for $\frac{\delta M_s^*}{\delta n_{set}^*}$

Figure 5.15 shows a nearly perfect fit between the response of the real parameters and all four (ii-v) different estimated parameters sets responses. Figure 5.16 shows a small offset between the response of different estimated parameters at higher frequencies. When taking a closer look, it can be seen that the response of parameter estimation v is containing a small offset compared to the responses of the other three parameter estimations. The reason for this offset probably has to do with nonlinearities due to the higher amplitude in the input signal used for parameter estimation v. In parameter estimation v, the maximum obtained error in the parameters is $\pm 22\%$, while with smaller amplitude the maximum error 2%. However, this parameter estimation is classified as correct, especially if you look at the simulated response in frequency domain compared to the real system response.

The previous evaluation is performed in frequency domain. The estimated parameter sets responses are also compared to an independent data set to see if the fit in time domain is also correct, namely step responses. The ninth and tenth columns of table 5.2 show the different fit percentages given with the step response data set. The fit percentages are also presented in figure 5.17.

In general lines, the parameter estimations are in line with the real parameter set, as shown in figure 5.17. The biggest difference that occurs is at higher offsets in the shaft torque output. For this reason the rectangular drawn around the third step is observed in more detail in figure 5.18

From figure 5.18 is observed that the only difference occurs is between the nonlinear data and the response of *all* the estimated linearized parameter sets. All the different parameter estimations are on top of each other. So in time domain the difference between parameter estimation with a high or low amplitude of the input signal is not visible.

As concluding remark it can be stated that all used input signals are feasible for parameter estimation. An increase of amplitude decreases the quality of the system estimation, which is visible in the Bode diagram and in the

results of table 5.2. Another criteria is the time duration of the different parameter estimations. From here can be derived that the two chirp signals are shorter than the multiple sine wave and the result is nearly identical.

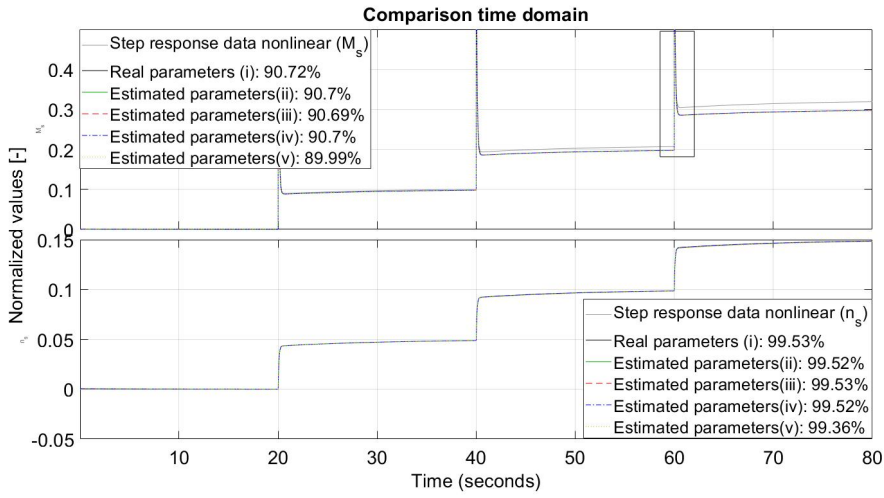


Figure 5.17: Comparison parameter estimation in time domain.

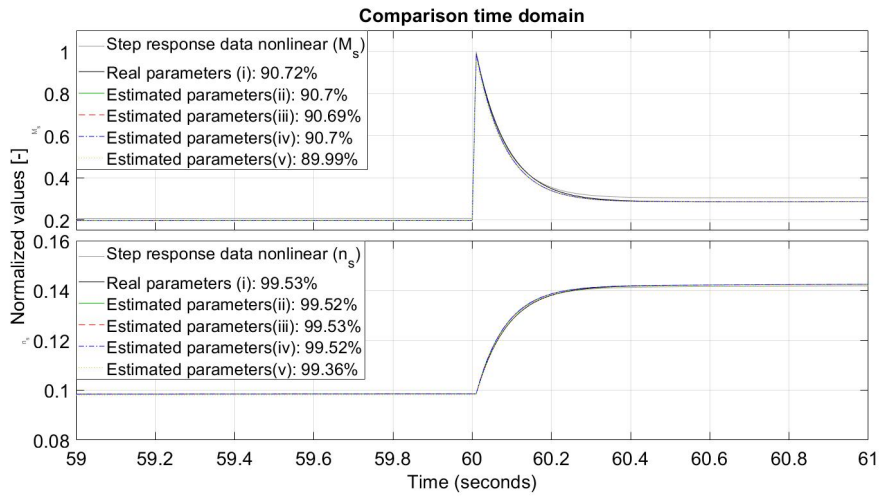


Figure 5.18: Comparison parameter estimation time domain zoomed in on third step.

5.5 CONCLUSION

The conclusions that can be drawn from this chapter are listed below:

- In theory it can be concluded the best parameter estimation can be done with an input signal of multiple sinus waves with a low amplitude. This can be obtained from table 5.2, where the multiple sine waves, ii, has the smallest errors with respect to the real parameter set i. Nevertheless, the differences between the results of parameter estimation cases ii, iii, iv and v compared to real parameter set, i, are so small, that it is not possible to say which is the best input signal result wise.
- A big advantage of using a chirp signal in practice is that it saves quite some time, namely $2500 - 1500 = 1000s$. This is already a 40% decrease of the total experiment time. In practice more time can be saved, because with multiple sine waves the input frequency should be changed during the experiments or it should be programmed beforehand. Please note that in the multiple sine waves, as used now, every frequency is executed for four periods. To decrease the total experiment time of the multiple sine wave, the lower frequencies could be executed only for a duration of two periods instead.
- The chirp signal on full-scale should be logarithmic distributed, which increases the quality of the parameter estimation. The reason for this is that with a logarithmic distribution, the lower frequencies of the system are excited more.
- The amplitude of the input signal has a big influence on the results of the parameter estimation. In parameter estimation v, the maximum obtained error in the parameters is $\pm 22\%$, while with smaller amplitude the maximum errors are 2%. However, this parameter estimation is classified as correct, especially if the simulated response using the whole estimated parameter set is taken into account.

6

FULL-SCALE EXPERIMENTS

In this chapter the full-scale experiments and the analyses of obtained data is reported. The chapter is divided into four main parts, were in the first main part a description of the experimental set up is given. In the second main part is a description of the experiments given and in the third main part is a signal inspection executed were a data set is chosen for the full-scale parameter estimation. In the fourth main part is the pre-processing of the chosen data set discussed. In the last and final main part are the conclusion and recommendations outlined.

6.1 DESCRIPTION OF EXPERIMENTAL SET UP

The description of the experimental set up is divided into three different parts. The first part contains a situation sketch, in which the conditions during the experiments are elaborated on. In the second part, the ship and the propulsion system are discussed. In the third and final part, a measurement description is given.

6.1.1 Situation sketch

The preparations and the building of the test set up for the experiments were carried out on the 4th and the early morning of the 5th of November 2019. The actual experiments were carried out on the 5th and started at 10:29 and the final measurement ended at 14:07.

The experiments took place at 'Haven zuid', which is a mooring location of the stock vessels of Damen Gorinchem in the Netherlands. 'Haven zuid' is surrounded by a break water, which resulted in calm water conditions during the experiments. The 5th of November can be described as a day with average weather conditions.

The experiments are carried out in backwards bollard push, which means that the back of the vessel is pushing against a pontoon moored to the shore. The reason for carrying out the experiment in this way is that the tug was initially moored in this backwards position. Doing backward bollard push eased the preparation of experiments in the way that a captain was not required during the preparation phase. Also, one of the levers was not controllable from the bridge anymore, which would have made the turning of the vessel complex. An advantage is that there are no steering corrections made during the experiments, which would be the case in bollard pull.

In figure 6.1, the experimental ship set up is presented in two different ways. In figure 6.1a a picture of the tug pushing against the pontoon during the experiments is shown. In figure 6.1b, a schematic overview of the aft of

the experimental ship set up is drawn. The schematic also contains symbols representing different distances. The value of these distances can be seen in table 6.1.

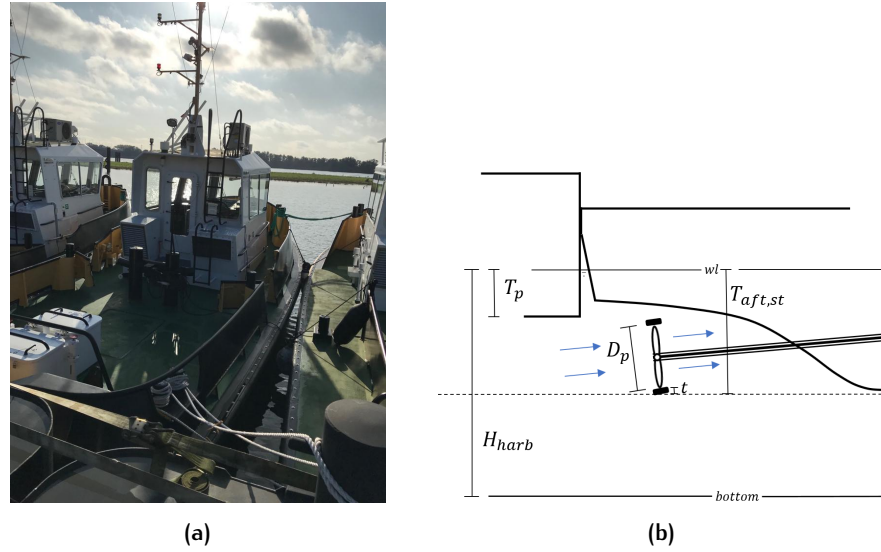


Figure 6.1: The experimental vessel set up. (a) Stan Tug 1205 during the experiments. (b) Schematic overview of experimental ship set up.

Symbol	Physical quantity	Value	Unit
T_p	Draft of pontoon	0.5	[m]
$T_{aft,st}$ [m]	Draft of Stan Tug in the middle of the aft	1.8	[m]
D_p [m]	Propeller diameter	1.05	[m]
t [m]	Nozzle thickness	± 0.1	[m]
H_{harb} [m]	Draft in the harbour	± 4.5	[m]

Table 6.1: Dimensions of pontoon and the aft of the Stan Tug 1205.

Some of the symbols in table 6.1 need some extra clarification. T_p represents the draft of the pontoon, T_{st} , represents the draft of the Stan Tug in the middle aft part and D_p is the propeller diameter, excluding the nozzle. The symbol H_{harb} is the water depth on the position where the experiments were carried out and this value varied a little bit during the experiments. The last symbol is t , which represents the thickness of the nozzle and the tip clearance. The exact thickness of the optima nozzle is unknown but an estimation of $\pm 0.1m$ is used. This estimation is based on a ratio from a drawing of the propeller. The tip clearance, derived from the performance specification of the propeller, is 5 mm for this nozzle and propeller and will be neglected for t .

The importance of having the correct values, is the ability to discuss the influence of the pontoon on the water inflow of the propeller. From the schematic overview, it can be concluded that the pontoon is not horizontally in-line with the propeller tip, but it definitely does have influence on the inflow. This interaction is also slightly influencing the dynamic system behaviour by changing the mass moment of inertia of the propeller, while it influences the displaced water during a propeller rotation. In the end, this effect will influence the total mass moment of inertia of the complete shaft

line and should be taken into account when a parameter comparison will be made with a value taken from an existing torsional vibration calculation (TVC).

6.1.2 Ship and the propulsion system description

The experiments are carried out on a Damen **Stan Tug 1205** (STU1205), with yard number 502522. The main particulars are listed in table 6.2 and in figure 6.2 a picture of a sister ship in free sailing condition is shown. Appendix C contains the product sheet of a sister ship, which is generally equipped with the same mechanical systems as the used vessel. The main difference is the engine control system, but this will be discussed later on.

Symbol	Physical quantity	Value	Unit
L_{oa}	Overall ship length	13.08	m
B	Overall ship width	5.28	m
DWT	Dead weight	54	t
v_d	Design speed	1	Kn
i_{gb}	Gearbox ratio	3.82	[-]
$P_{b,max}$	Maximum engine brake power	221	kW
$n_{e,max}$	Maximum engine speed	1800	rpm
D_p	Propeller diameter	1.05	m
P/D	Pitch ratio	1.110	[-]

Table 6.2: Main particulars of Stan Tug 1205.



Figure 6.2: Sailing Stan Tug 1205.

The vessel is equipped with two drive trains, each consisting of a VOLVO D9-MH in-line 6 cylinder diesel engine, a twin disc gearbox and a 'Kaplan' type fixed pitch propeller in an 'Optima' Nozzle. The 'Optima' nozzle ($L/D = 0.5[-]$) is not steerable and the blade area ratio of the propeller is $\frac{A_F}{A_0} = 0.7[-]$ and $\frac{P}{D} = 1.11[-]$.

The engine control system that is used for controlling the fuel injection from the bridge is an older VOLVO specific system, namely the Marine Commercial Control (MCC) system. This is a control system for both electronic and mechanical engines (30). A schematic overview of this system is presented in figure 6.3. The meaning of the different abbreviations that are used in the figure are clarified in table 6.3.

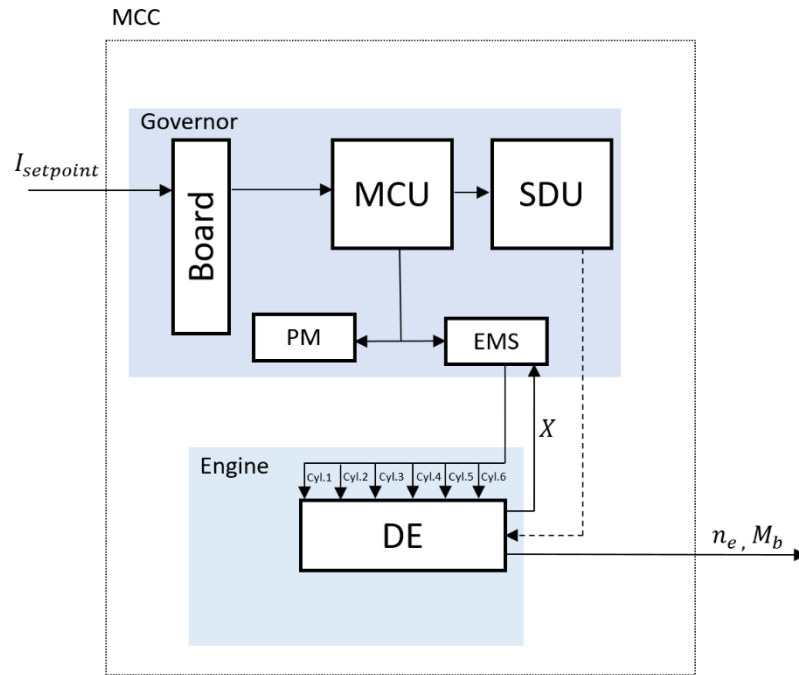


Figure 6.3: Set up of the MCC system on board of the Stan Tug 1205.

Abbreviation	Meaning
MCC	Marine Commercial Control
MCU	Marine Control Unit
SDU	Shutdown Unit
PM	Power module
EMS	Engine Management System
DE	Diesel Engine

Table 6.3: Clarification of the abbreviation in figure 6.3.

The control system starts with receiving an input signal from the lever, namely a current, $I_{setpoint}$. The internal signals between the different components are neglected, but the output of the diesel engine (DE) is engine speed, n_e , and engine brake torque, M_b . In practice, the PM- and EMS units are physically installed on/in the engine. Putting the input signal directly on the engine will mean that you have to break into the engine. That is for this research a too big operation while the ship is already classified by the classification society, which after that operation is not valid any more. Next to that is putting a signal directly on the engine more dangerous, because the EMS is also equipped with different safety features which than will not be active. The reasons given above explain why the input signal will have to go through the control system.

Inside the MCC there is also a feedback system. This feedback line is indicated by the symbol X, but contains several different physical quantities. Some of them are given below:

- Engine speed
- Coolant temperature, pressure and level
- Oil temperature, pressure and level
- Exhaust temperature and pressure

It is assumed that the EMS unit is influenced by each and every different feedback component of the diesel engine, otherwise the feedback would not be there. An educated guess is that these signals are only used when it exceeds a certain value. Next to that, it should be pointed out that during the simplification of the figure some input of different sensors are also left out. For example, the MCU is also receiving sensor information which can lead to a shutdown of the engine via the SDU. Later on in this chapter, the MCC-system is simplified to only a governor and an engine, which than outlined with a light blue background, see figure 6.4.

6.1.3 Measurement system description

The third part contains a measurement system description of the signals during the experiment and will be split up into two different paragraphs. The first paragraph is about the measurement in theory. The second paragraph will be about how the measurements took place in practice and different photographs of the installation will be shown.

The measurement system layout as used during the experiment is shown in figure 6.4. The blue background in this figure is discussed in the previous part. This part discusses the systems shaded in grey (Data acquisition, signal generation). The different symbols that are used to name different signals are listed in table 6.4. Pay attention to the fact that the 'Math Calc' block is in reality inside the logging device (DEWEsoft or imc-TM), but it is chosen to separate them in this schematic diagram to clearly distinguish between raw and calculated signals. Pay attention to the fact that the data is logged on two different devices. The first logging is done by Damen Gorinchem itself and the second logging is executed by JVS B.V., who are specialized in measuring and calculating the vibration and noise levels for maritime installations.

Another point of attention is that only one of the two shaft lines is instrumented and used during the experiments, namely the port side shaft line.

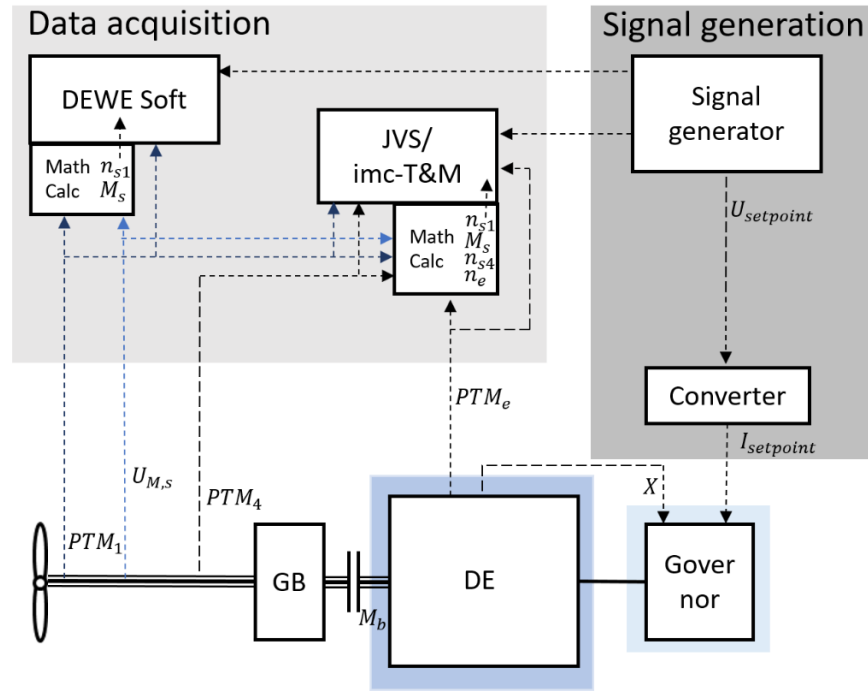


Figure 6.4: Schematic overview measurement set up during the experiments.

Symbol	Physical quantity	Unit
$I_{setpoint}$	Set point current	mA
X	Feedback signal	-
M_b	Engine torque	Nm
M_s	Shaft torque	Nm
PTM_1	Pulse time modulation [1 pulse]	s
PTM_4	Pulse time modulation [4 pulse]	s
PTM_e	Pulse time modulation [engine]	s
n_{s1}	Shaft speed 1 pulse	rpm
n_{s4}	Shaft speed 4 pulse	rpm
n_e	Engine speed	rpm
$U_{setpoint}$	Set point voltage	V
$U_{M,s}$	Shaft torque voltage	V

Table 6.4: Clarification symbols in figure 6.4.

First the different components that are used for the signal set up are elaborated. In the list here down below are the different components types and their product sheet presented. Next to that is a brief description of their output signal.

- The *signal generator* is a RSDG 830, which is used for the input signal and will replace the conventional lever. The signal generator is able to generate a signal between -10V and 10V. More information can be found in the product sheet (31).
- A *signal converter*, Pepperl + Fuchs SC-System S1SD-1AI-1U.2, is used to fulfil the requirements of the MCC system to have a input signal in current, $I_{setpoint}$. The signal converter converts the input signal, of -10V to 10V, to a current between 4 mA and 20 mA. The scaling will

be linear and this is also validated in chapter 6.3. More information about the signal converter can be found at their product sheet (32).

- A temporary 'Binsfeld torque measurement', which is a strain gauge attached to the propeller shaft. This strain gauge is attached on the shaft and transmits with a certain frequency to the receiver, which then sends a voltage signal to the logging device. Next to that, the strain gauge is not bending compensated. So, in the measurement it is possible that there is residue left. More information about the Binsfeld torque measurement can be found on the product sheet. (33)
- A *Remote Optical Laser Sensor (ROLS)* for the detection of the reflectors on the propeller shaft which results in a pulse signal that goes into the logging devices. More information about the laser sensors can be found in the product sheet. (34).
- A *ROLS* for the detection of the four reflectors on the propeller shaft.
- A *ROLS* for the measurement of the engine speed.
- Logging system of imc-TM, type unknown, which is used by JVS for logging the different signals.
- Logging system, DEWESoft SIRIUS, which is used as second logging device. This logging machine was equipped with 8x analogue STG input and 2 counters in total. During the experiments all the signals came trough the analogue STG inputs. More information about the logging device from DEWESoft can be found at (35). The measurements are done with a DEWESoft Dual Core, which involves some consequences on the logging of the data. The logging of the data is explained in more detail on the website of DEWESoft (1). In figure 6.5, it is illustrated how the sampling on the DEWESoft is done. For example, when a sample rate of 2 kHz is used, the signal is internally sampled with sample rate of 2 kHz multiplied by 256. This signal will then go trough a physical 2nd order filter to avoid aliasing. The software will then give only the requested sampling rate, namely 2 kHz.

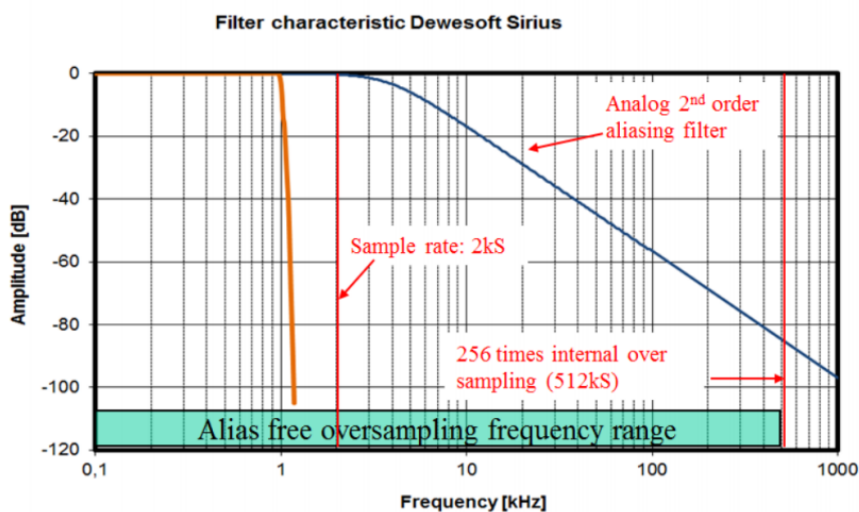


Figure 6.5: Explanation of the sampling rate DEWESoft Dual Core (1).

Some of the components which are used in the signal set up have limitations when it comes to their sampling rate. Next to that, as can be seen in figure 6.4, not every signal goes to every logging device. For this reason a detailed overview is necessary, as presented in table 6.5. Here, it is visible if a signal is logged and with which sample rate the signal is logged.

	JVS	Sample rate [Hz]	DEWEsoft	Sample rate [Hz]
<i>Raw signals</i>				
$U_{setpoint}$	Yes	2000	Yes	5000
PTM_e	Yes	2000	No	-
PTM_1	Yes	2000	Yes	5000
PTM_4	Yes	2000	No	-
$U_{M,s}^*$	No	500-2000	No	500-5000
<i>Processed signals</i>				
M_s^*	Yes	500-2000	Yes	500-5000
N_e	Yes	2000	No	-
N_{s1}	Yes	2000	Yes	5000
N_{s4}	Yes	2000	No	-

Table 6.5: Logged signals on the different logging devices.

The upper note is placed for a point of attention. The transmitter that is used after the strain gauge has a limitation of 500 Hz sampling rate. The receivers output is an analogue signal, so when the logging devices are logging at 2000 Hz and 5000 Hz, then in theory the logging sample will be the same if zero order hold is applied. In practice every sample of the logged data is different, so the output of the shaft torque should be analogue or a filter can cause the different sampling values. According to the specialists of JVS is the bandwidth created in the analogue signal by 2 filters, first by the receiver and second of all by in the input of logging device of JVS.

Now that the symbols, the devices and the signals are clarified, the only thing left is the mathematical calculation blocks in figure 6.4. Their are two different mathematical calculations carried out in the logging devices. The first calculation is the conversion from pulses to shaft- and engine speed, which is illustrated in figure 6.6. In here is T_p depended on when the pulses are above the 2V threshold, which indicated with a dashed line. The pulse width is measured with two 'cond' edges, see equation 6.1.

$$T_p = t_{2,2V} - t_{1,2V} \quad (6.1)$$

With the pulse width is it possible to calculate the shaft speed, this is in general form presented in equation 6.2.

$$n_s = \frac{1}{T_p} \quad (6.2)$$

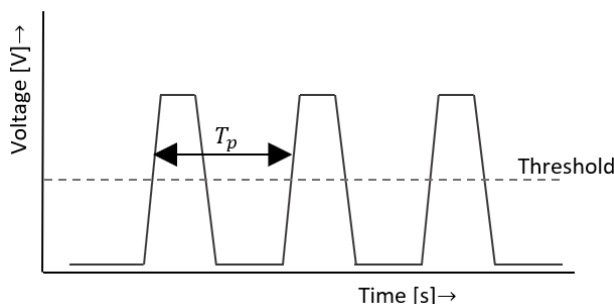


Figure 6.6: Explanation of pulse time modulation (PTM).

The second mathematical conversion that takes place is from voltage signal to the shaft torque. This is quite a simple conversion as the voltage will be multiplied by a factor, which depends on the shaft speed and power. This factor is provided by JVS and implemented in both logging devices and shown in table 6.6.

Symbol	Quantity
C [Nm/mV]	1.059

Table 6.6: Conversion factor provided by JVS B.V.

For a more detailed calculation see Appendix D, which is the file that is provided by JVS.

As stated earlier, the second paragraph contains a more practical description on how the experiments are carried out, so that these kind of experiments can be executed more easily in the future. A lesson learned is that it sounds easier that you log $I_{setpoint}$ instead of $U_{setpoint}$, because $I_{setpoint}$ indicates a lot better what is going into the system. A resistor in parallel is required for a determination of a low current. The reasoning for not doing this is that the converter does not have enough power to overcome the resistance in parallel. A solution would be to purchase more expensive equipment. Because of this, an input signal validation is required.

Figure 6.3 shows that $I_{setpoint}$ goes into the board. In practice the board is a hardware device called a terminal which is presented in figure 6.7, the terminal is shown.

In figure 6.7b a red ellipse is drawn which shows the input for controlling the engine speed, namely A5+ and A5-. As can be seen in figure 6.7a, the two original black wires are disconnected from the terminal and the two green wires are connected to the terminal. The green wires are coming directly from the converter and providing the required current.

In figure 6.8 an illustration is given on how the measurement of JVS is done, these pictures are taken during the experiment. In figure 6.8b the lasers are shown which are counting the pulses from the engine and from the shaft. As can be seen, the lasers are attached to the steel structure of the vessel with a magnet. This can cause vibration of the sensor especially at higher engine speeds.

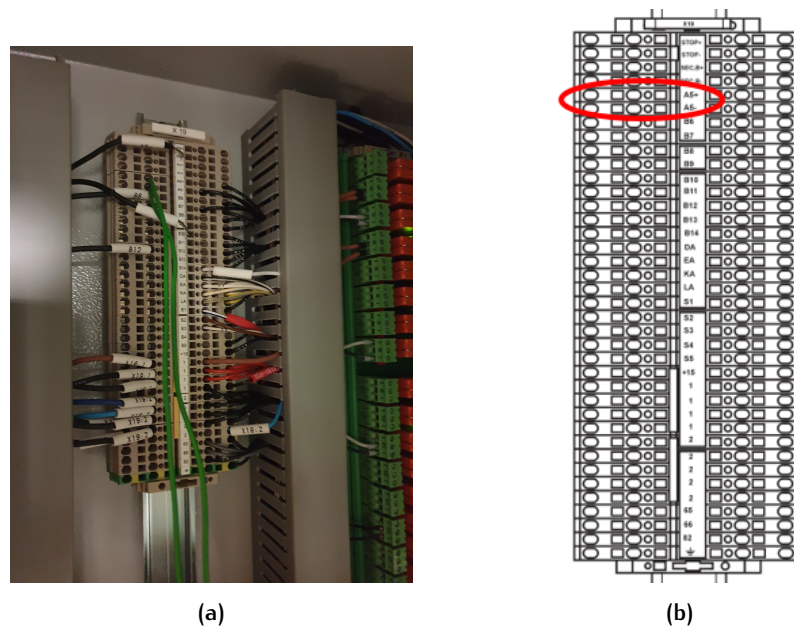


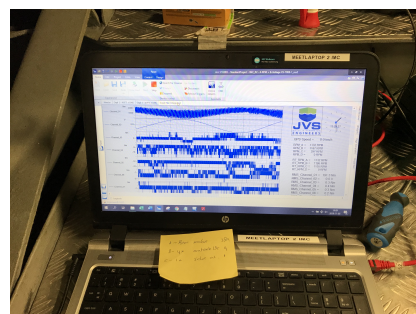
Figure 6.7: Terminal/board of the MCC system. (a) The terminal/board during the experiments. (b) Schematic overview of the board.



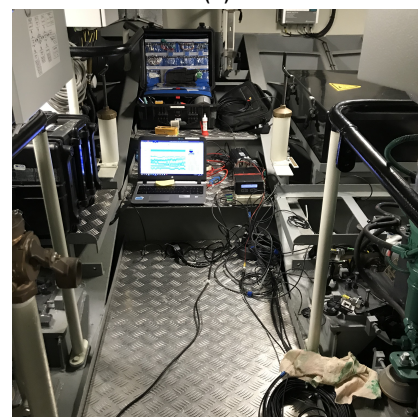
(a)



(b)



(c)



(d)

Figure 6.8: Measurement executed by JVS B.V. (a) Attachment of strain gauge on shaft. (b) Three different pulse measurements. (c) Logging computer of JVS B.V. (d) Complete measurement set up of JVS B.V.

In figure 6.8a, the reflector for the shaft speed is partly visible on the shaft. The strain gauge and the transmitter for the shaft torque measurement are completely visible. The strain gauge is glued on to the shaft and after that wrapped with white tape to make sure it will not move during the experiments.

Figure 6.8c shows the computer logging of JVS, were the yellow sticky note clarifies the different data that is in the pulse signals. And in figure 6.8d the total set up is shown, where you can see two black cables on the floor. These will end up at the DEWESoft logging machine which was placed in the galley of the Stan Tug 1205.

6.2 DESCRIPTION OF EXPERIMENTS

During the experiment multiple measurements were carried out. A list of all the measurements and their different log file names for both logging devices is listed in table 6.7. Three types of experiments are carried out, multiple sine wave experiments, chirp wave experiments and step response experiments. Additionally, the amplitude determination during the experiments is outlined down below.

Signal information				DEWESoft	JVS		
Sinus	Freq [Hz]	-	Ampl. (V)	File	File	Start [s]	Stop [s]
S1	0.0021	-	0.3	'Sin1_0021'	'Run1'	5500	6350
S2	0.0044	-	0.6	'Sin2_0044'	'Run2'	480	1270
S3	0.0092	-	0.6	'Sin3_0092'	'Run2'	1450	1900
S4	0.0193	-	0.6	'Sin4_0193'	'Run2'	1970	2300
S5*	0.0275	-	0.6	'Sin5_0275'	'Run2'	2400	2700
S6	0.0405	-	0.6	'Sin6_0405'	'Run2'	2750	2950
S7*	0.06	-	0.6	'Sin7_06'	'Run2'	3100	3200
S8	0.084	-	0.6	'Sin8_084'	'Run2'	3300	3500
S9*	0.11	-	0.6	'Sin9_11'	'Run2'	3600	3700
S10	0.1778	-	0.6	'Sin10_177'	'Run2'	3800	3950
S11	0.3728	-	0.6	'Sin11_37'	'Run2'	4050	4150
S12	0.7814	-	0.6	'Sin12_78'	'Run2'	4250	4350
S13	1.637	-	0.6	'Sin13_1.6'	'Run2'	4440	4580
S14	3.433	-	0.6	'Sin14_3.4'	'Run2'	4640	4690
S15	7.19	-	0.6	'Sin15_7.2'	'Run2'	4840	4900
S16	15.01	-	0.6	'Sin16_15.0'	'Run2'	5020	5050
S17	31.644	-	0.6	'Sin17_31.6'	'Run2'	5234	5254
Chirp	Start Freq	Stop freq	Ampl. (V)	File	File	Start [s]	Stop [s]
C11	0.001	3.981	0.6	'Chirp11'	'Run2'	8850	9450
C21	0.001	0.02	0.6	'Chirp21'	'Run2'	9600	10150
C22	0.015	0.27	0.6	'Chirp22'	'Run2'	10200	10750
C23	0.1	3.981	0.6	'Chirp23'	'Run2'	10900	11450
Step	Stepsize(V)	Min (V)	Max (V)	File	File	Start [s]	Stop [s]
St1	1	-3	6	'Step1'	'Run2'	7150	7600
St2	2	-3	7	'Step2'	'Run2'	7900	8300

Table 6.7: Overview of executed experiments with the names of the logfiles.

As determined beforehand, the amplitude of the input waves depends on the noise that is found during tests before the 'real' measurements. During the test runs, it was decided to put the amplitude around 150 rpm. At that amplitude the waves are still visible in the noise of all the signals. With an amplitude of 75 rpm, the engine is still quite close to its operating point and when a linearization is made around this point, nonlinear effects are minimized. It was determined beforehand that the operating point is around 1200 rpm. During the test measurements, the bridge display indicated that 1200 rpm required approximately a $-5V$ offset on the signal generator. So the sinus and chirp experiments are carried out with an offset of $-5V$ and the amplitude of the signals is given in the fourth column of table 6.7.

6.2.1 Multiple sine waves

The frequencies of the applied sinusoidal input signal are logarithmic spaced between $0.001Hz$ and $31.6Hz$. The determination of the logarithmic scaling is concluded in previous chapter 5.5. Three additional frequencies have been added, which are marked as * in table 6.7. During the computer simulations most poles and zeros can be found in this frequency range, for this reason are extra sine waves executed around this frequency range. Sine wave S0, which had a frequency of $0.001Hz$ is not carried out, because this would have occupied a lot of measurement time, and during the test measurements beforehand it indicated that the system reacted quite fast on offsets.

6.2.2 Chirp waves

In total, four different chirp wave experiments were carried out; all of them covering a different frequency domain. The chirp signals that are carried out are listed in table 6.7. All the different chirp signals are done with 500 seconds of duration, because this is the maximum time span which can be created by the signal generator. The reason of doing a chirp signal is that its less time consuming than doing experiments with the multiple sine waves. The Chirp signals is the frequency range also logarithmic divided over the time.

The four different chirp waves can be merged into two different chirp signals. The first chirp signal is C11, and the second chirp signal is C21, C22 and C23 added up so that a long chirp signal of $\pm 1500s$ is constructed. The small overlap between the domains is due to settling time of the chirp signals. From these two chirp signal hopefully a conclusion can be withdrawn if a longer chirp input signal has a positive effect on the parameter estimation.

6.2.3 Step responses sequences

The last input that is used during the experiments are two step responses. Table 6.7 shows that there are two different steps set on the drive train. The reason for carrying out these experiments is that once the parameters are estimated in the following chapter they can be validated by implementing these parameters in to simulation model and compare the results of the simulation model with the measured step responses.

The signal generator was not equipped with a step response function that was useful for this experiment. So the step responses are put on the system by putting zero amplitude on the sine wave mode and make the steps with the offset. A disadvantage of this approach is that the step size is limited by 1V, because this was the highest possible instantaneous offset.

6.3 SIGNAL INSPECTION

In the last main section the logged signals are inspected. First, an analysis will be given of complete measured signals and checked if they are in-line with the expectations. This is called a global analysis. The second analysis is more in detail and this will be defined as a detailed analysis. Here, different peaks or noise will be clarified and discussed if there is a physical background or if they are undesired measurement artefacts.

6.3.1 Global analysis

The global analysis is done for three different signals. First is the linearity of the converter discussed. After that the shaft speed measurement and lastly the shaft torque measurement.

Input signal

To check the linearity of the converter, it was tested in isolation on the 23th of October. A picture of the test set up is shown in figure 6.9. Due to the low currents a resistor, $R = 50 \Omega$, is used for measuring voltages over the resistor which can then be rewritten to a current.

The results are shown in figure 6.14, where for certain voltages the current is plotted. Next to that, a line is drawn which represents the theoretical relation according the product sheet. Figure 6.14 shows that the theoretical relation is in-line with the results of the experiment.

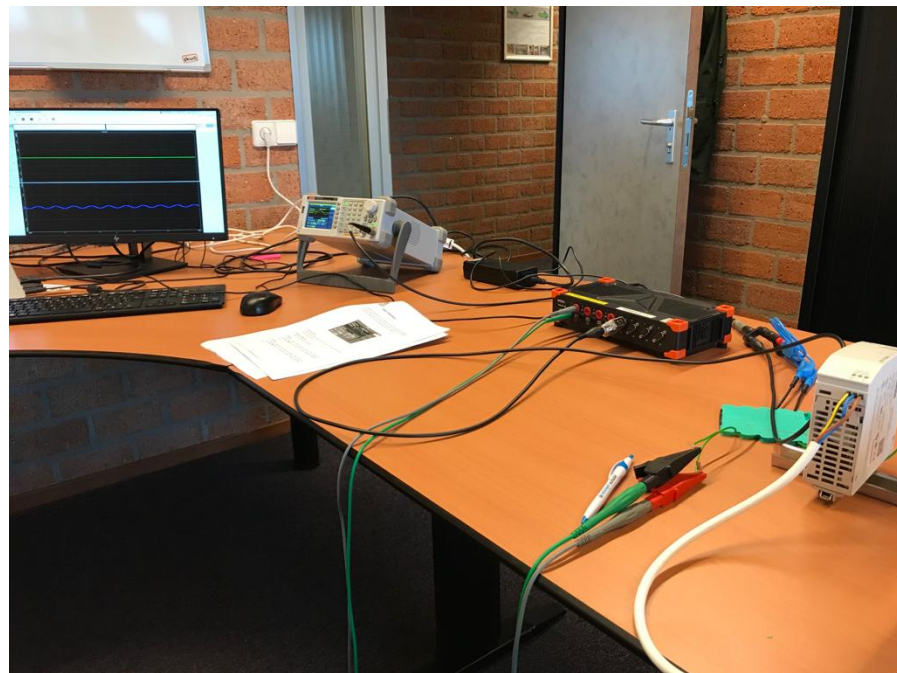


Figure 6.9: Test set up of input signal validation.

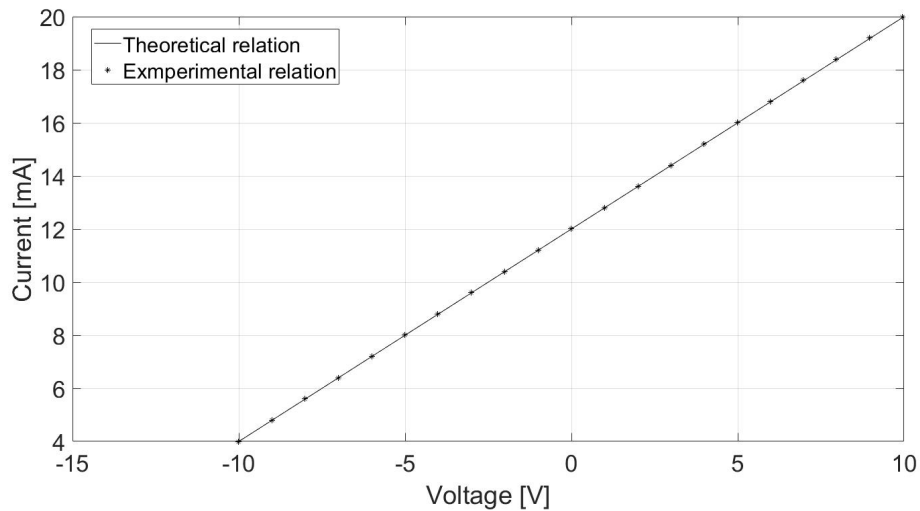


Figure 6.10: Correlation between input voltage and output current.

Shaft speed

The shaft speed validation takes place with JVS data by comparing the one pulse measurement with the four pulse measurement. For a constant input signal, a small time interval is taken and the one and four pulse measurements are plotted, see figure 6.11.

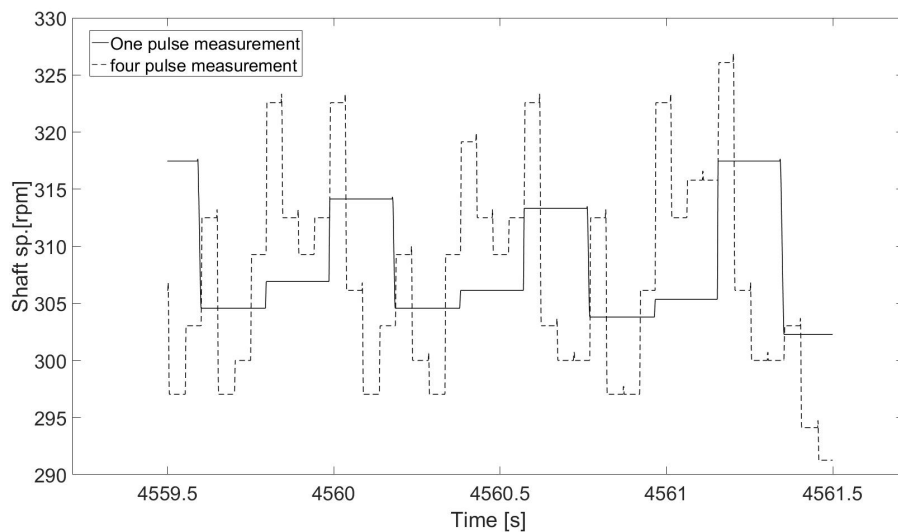


Figure 6.11: Shaft speed comparison between one pulse measurement and four pulse measurement.

In figure 6.11, the one pulse measurement is the solid line and the four pulse measurement is the dashed line. The following can be observed from figure 6.11.

- The four pulse measurement gives in global lines the same values as the one pulse measurement, so from here can be concluded that the measurement for both signals is done properly.

- Another phenomena which is visible is that the fourth measurement of the four pulse measurement is always higher than the previous three measurements. This is illustrated with help of figure 6.13: An error occurs due to the fact that $a \neq b \neq c \neq d$. This effect can be minimized by gluing the reflectors more precisely.

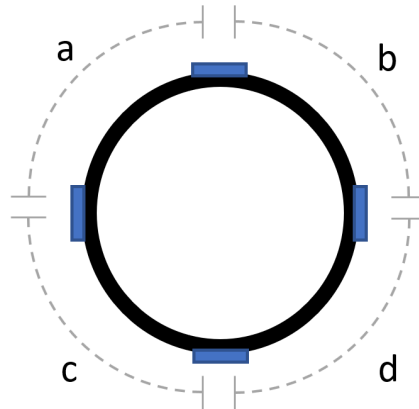


Figure 6.12: Explanation pulse difference with a cross section of the shaft line, where the blue rectangles represents the reflectors glued on the shaft.

- The third phenomena that is visible in figure 6.11, is the zero order hold principle. As presented in table 6.5 the signals are logged with 2000 Hz. This means that there are multiple samplings during the 0.2 seconds constant shaft speed. This also means that the sensor is giving a constant signal until the next reflector is detected. The zero order hold principle then says that for that short moment the shaft speed is constant, but in reality this is not the case. Shaft speed will increase or decrease to the 'next shaft speed'.
- The last phenomena that is visible, is a small peak at the end of every sample. The actual reason is unknown, but most likely it has to do with filters that are in the sensor that a small ringing occurs.

Shaft torque signal

The shaft torque global analysis takes place in two different ways. First of all, the amplitude of the shaft torque is checked. Second of all, the rimping in output shaft torque signal is analysed. The shaft torque signal is illustrated in 6.13

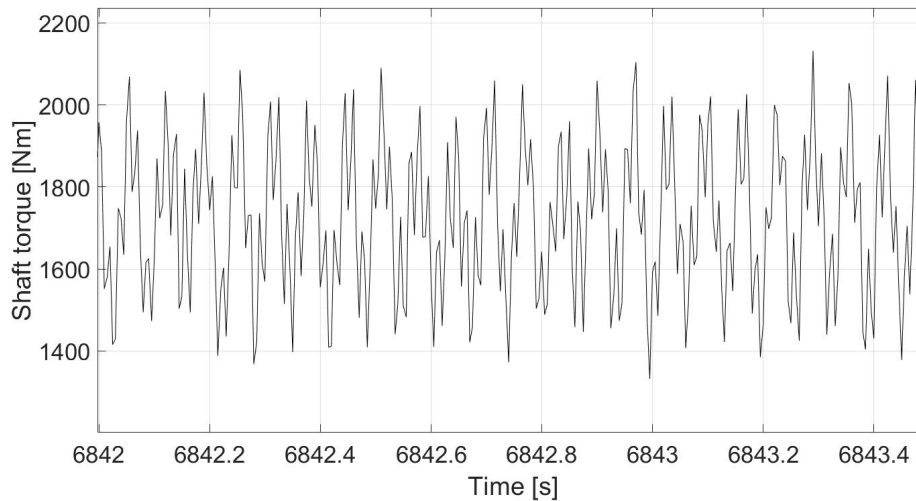


Figure 6.13: Shaft torque signal with constant input signal.

The *offset* of the shaft torque measurement is compared to a static torque calculation. This static calculation is performed for five different operating points. The first step is obtaining the dimensionless torque factor. The ship is operating in backwards bollard push, which means that if you look at an 4 quadrant propeller diagram, the propeller is working between the second and third quadrant. This means that the operating point is $\beta = 180^\circ$. Next to that is assumed that the water in 'Haven Zuid' is fresh water so $\rho = 1000$. The advanced velocity is zero and with this it is possible to fill in equation 6.3 for the different operating points. in this equation is η_r assumed as 1.

$$Q = M_p \cdot \eta_r = C_Q^* \cdot \left(\frac{1}{2} \rho [V_a^2 + (0.7\pi n_s D_p)^2] \right) \frac{\pi}{4} D_p^2 \cdot D_p \quad (6.3)$$

In table 6.8, the comparison is made between the theory and the experiments executed. The second column represents the operating points and the last column, the fifth, contain the errors. From this comparison, it can be concluded that the theory is in-line with the measured value from the experiments for several operating points.

U_{sg} (V)	n_{eng} (rpm)	$M_{s,m}$ (Nm)	Q (Nm)	error (%)
-3	676.5	500	572.1	12.60
-4	927.5	1000	1075.3	7.00
-5	1184	1725	1752.3	0.99
-6	1430	2600	2556.1	-1.72
-7	1684	3550	3544.8	-0.15

Table 6.8: Shaft torque analysis

Now that the amplitude of the shaft torque signal is analysed, the *rimpling* in the shaft torque signal will be investigated. At the shaft torque over time, periodic behaviour can be observed in the signal. A way of making this periodic behaviour clear is by transforming it into frequency domain instead of analyzing it in time domain. A period of 'constant' shaft torque is transformed to frequency domain, which is presented in figure 6.14.

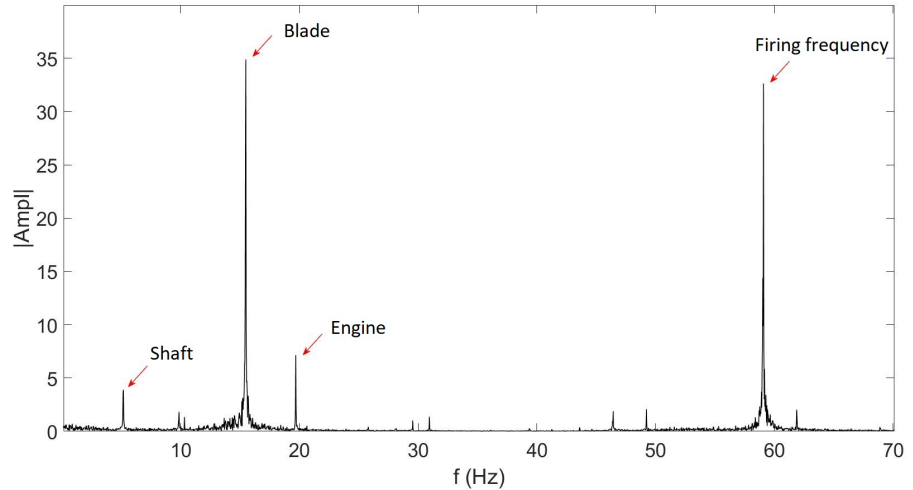


Figure 6.14: Shaft torque in frequency domain, with RMS of torque signal in Nm.

This figure shows peaks in the frequency domain, indicating the periodic behaviour that was mentioned above. These peaks are pointed out with a red arrow and their values are listed in table 6.9.

Peak 1	5.15 Hz ~ rps
Peak 2	15.49 Hz ~ rps
Peak 3	19.68 Hz ~ rps
Peak 4	59.08 Hz ~ rps

Table 6.9: Peak frequencies obtained from figure 6.14.

The frequency peaks in the torque signal are compared to the engine and propeller frequencies. It is checked if the signal contains the correct rimpling according to vibration that is generated by the engine and propeller with which the vessel is equipped. The torque signal in frequency domain is generated while the engine was running at a speed of $n_{eng} = \pm 1184[rpm]$.

As stated the engine is a VOLVO D9, a six-cylinder in-line diesel engine. The propeller is equipped with three blades and the gearbox got a reduction of 3.82 : 1. Pay attention that the engine is a diesel engine, so every 2 rounds an ignition takes place. Also, the cylinders are in-line, which means the cylinders fire after each other. In V shape engines this will be not the case. The most common peak you see is often the engine and the shaft speed. In this case the engine speed is at $n_{eng} = 1184[rpm]$, which equals $n_{eng} = 19.73[rps]$. This value corresponds with peak 3 from table 6.9. The shaft speed is calculated in 6.4, with help of the gearbox reduction factor.

$$n_{shaft} = \frac{n_{eng}}{i_{gb}} = \frac{19.73}{3.82} = 5.16 [rps] \quad (6.4)$$

The shaft speed equals peak 1, so this also aligns with the correct frequencies inside the output torque measurement. Every blade passage of the propeller induces another peak that quite often occurs in the frequency spectrum. The 3 bladed propeller excites the frequency expressed in equation 6.5, z is 3.

$$n_{blade,p} = z \cdot n_{shaft} = 3 \cdot 5.16 = 15.5 [rps] \quad (6.5)$$

The frequency of 15.5 corresponds with peak 2 of table 6.9. The last frequency that can often be seen in torque frequency domain is the firing frequency of the cylinders. The following equation 6.6 is used to calculate the ignition frequency with $k = 2$, because it is a 4 stroke in-line engine.

$$n_{e,cyl}(k = 2) = \frac{Cyl \cdot n_{eng}}{60 \cdot k} = 59.2 [rps] \quad (6.6)$$

The ignition frequency corresponds with peak 4 of table 6.9. From this, it can be concluded that the measured torque signal in time is showing the expected rimpling according to the propeller and diesel engine with which the shaft line is equipped. It is concluded that the torque measurement contains the expected amplitude and frequency and is valid.

6.3.2 Detailed analysis

The detailed error analysis of signals is divided in four different types: A,B,C,D. Table 6.10 lists which error occurs in which signals on one of the two logging systems. This table can be considered as an overview for the errors that are observed in the data. The S represents a sine wave, C represent a chirp signal and St are step responses.

Signal	DEWEsoft	JVS	Signal	DEWEsoft	JVS
S1	A,C	C	S13	A	
S2	A		S14	A	
S3	A		S15	A	
S4	A		S16	A	
S5	A		S17	A	
S6	A		C11	A,C	C
S7	A		C21	A	E
S8	A		C22	A	
S9	A		C23	A	
S10	A		St1	A	
S11	A		St2	A,B,C	D1
S12	A				

Table 6.10: Different signals with their 'errors'.

Type A; Shaft speed peak

As in figure 6.6 is presented is their a threshold in the volt signal, '*Pulse*' > 2 , and when this is achieved a new pulse period is made from the pulse signal. But their is a erroneous determination of pulse period from pulse signals, which can be seen in the upper graph of 6.15. From the lower lower graph

in figure 6.15 can be seen that due to a saw tooth shape of the volt measurements that for one sample the volt signal is below 2 and the next sample above, which is the reason for the high peaks in the shaft speed measurement. A way of resolving this error is by adding a additional threshold, so that an upper cross and lower cross should be made for measuring a pulse. This phenom can also be resolved with a lower sampling rate.

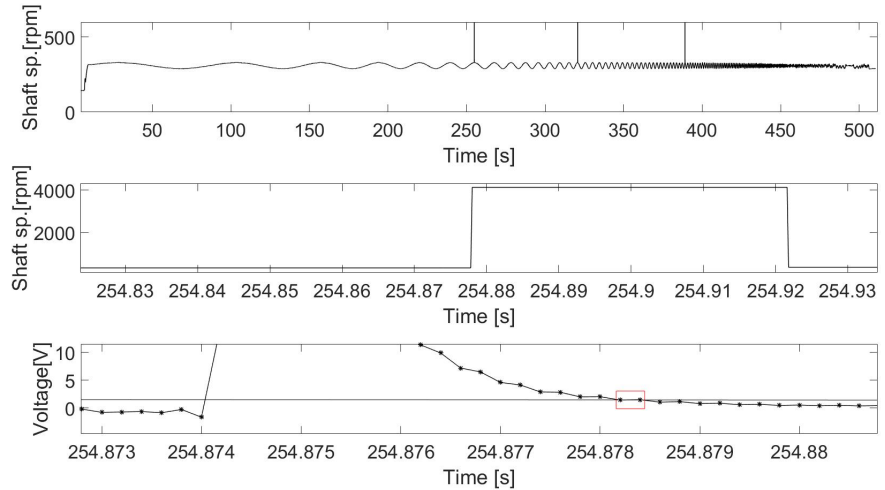


Figure 6.15: Shaft speed in time domain.

Type B; Noise in shaft speed at high engine speeds

At high engine speeds their is also erroneous determination of pulse period from the pulse signals, which is illustrated in figure 6.16. This phenomenon is only visible in the data logged by DEWesoft device. The reason for this phenomena is unknown, but it has to do with an increase of vibrations which disturbs the transfer in the cable.

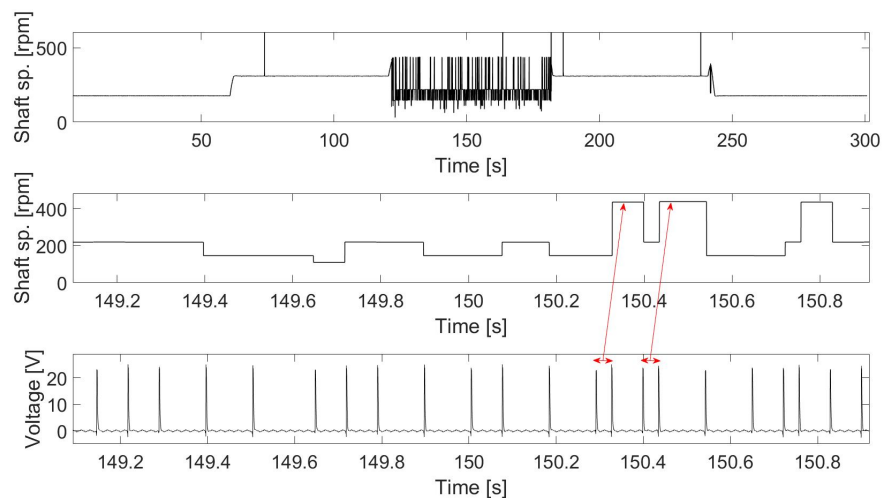


Figure 6.16: Shaft speed in time domain.

Type C; High peaks in torque signal

Erroneous measurement of the torque from the delivered voltage signal due to Electromagnetic compatibility (EMC), such as phone calls. On the shaft is a transmitter connected to the strain gauge, which is received by a stationary receiver and this is connected to the logging device. The receiver can get saturated by EMC, this phenomenon is illustrated in figure 6.17.

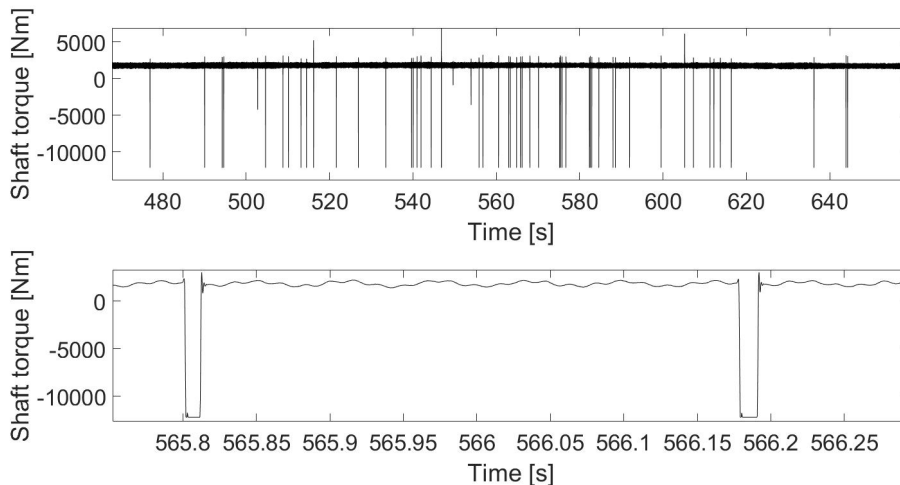


Figure 6.17: Shaft torque in time domain with detailed crest.

Type D; Errors in Input signal

Two unexpected behaviours of the signal generator are detected, which are caused by EMC issues, these errors are visible in upper graph of figure 6.18. First type, defined as D₁, are high jumps in the volt signal of the signal generator, due to wrong relays switches. The error is canceled in a very short period of time and the system is stabilized. These voltage jumps occur under all circumstances, when step responses are set on the system but also in 'normal' running conditions.

The second type of error is defined as D₂. It occurs after ± 8500 s, where a high frequent signal can be observed in the input signal. This error occurs when the 'SWEEP MODE' of the signal generator was turned on. When zoomed in on the disturbance in the signal, seen in the right lower figure 6.18, 5 peaks can be observed in a time period of 0.1s. This means that this disturbance has a frequency of 50 Hz, which matches with the frequency of the electricity net.

The third type of error is defined as D₃. This type of error occurs in input signal 'C₂₁', where a chirp signal is generated for the excitation of the low frequencies in the system. This signal should be a chirp signal, but the frequency does not increase over time, as can be seen in figure 6.19. This is due to incorrectness of the signal generator. What this incorrectness is or what causes it is unknown. After the full-scale experiments, another test with the same frequency domain was executed using the signal generator and again no increase of frequency could be detected.

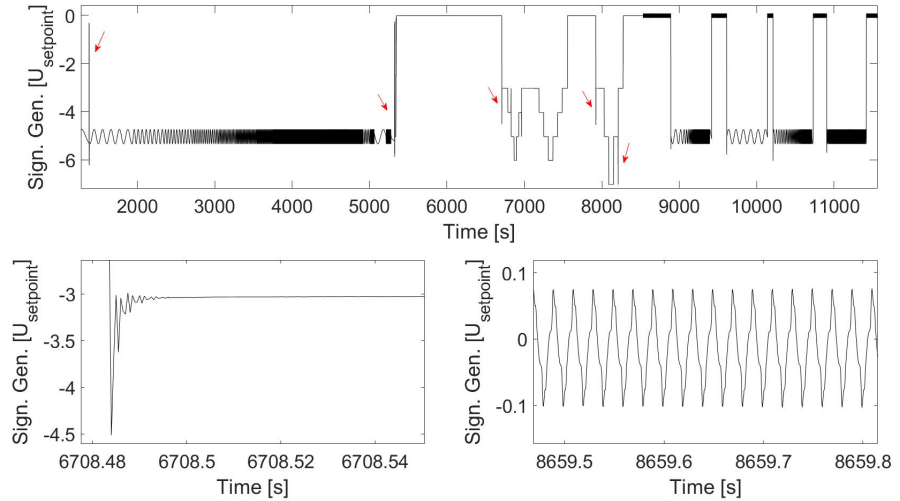


Figure 6.18: Shaft torque in time domain with detailed crest.

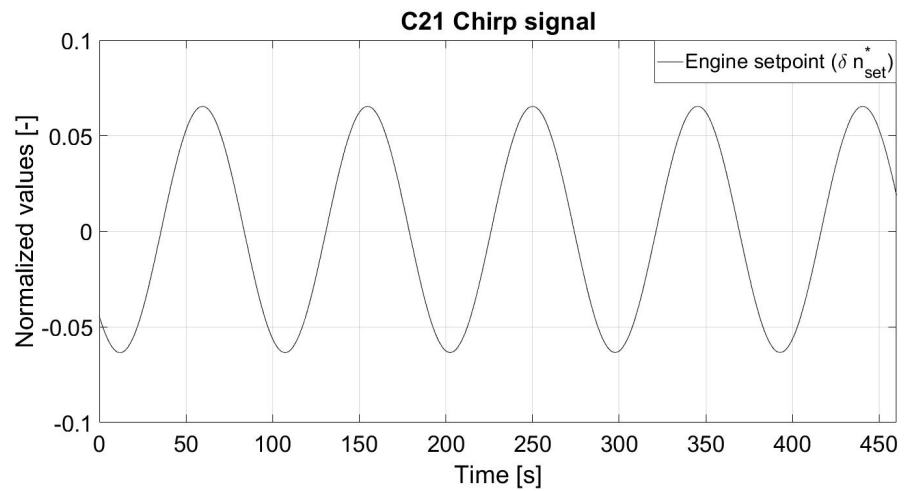


Figure 6.19: Signal 'C21' of table 6.7.

In this main part the different datasets were inspected by first doing a global analysis and, after that, a more detailed analysis. During this inspection several error types were outlined and discussed. The most usable datasets for full-scale parameter estimation are the raw signals from JVS. First of all, it can be seen from figure 6.4, because the JVS measurements logged more signals than the DEWE Soft. Second of all, table 6.10 shows that the JVS measurement contains less error types. A reason to use the raw data instead of JVS would be that the calculation from pulse signal to shaft speed, performed by JVS, is unknown.

6.4 DATA PRE-PROCESSING

In the previous main part it is concluded that the raw JVS data is the most useable data set for the full-scale parameter identification. In this main part is the pre-processing of this data set executed. In practice this is 'Run2' of table 6.7 and the 'error types' in this data set, defined in previous main part are presented in table 6.10. The outliers that are in the torque data measurement are eliminated by taking an average of the neighboring points. Furthermore the following pre-processing operations are discussed: A correlation between the measured voltage and the actual set point engine speed, transformation of measured pulse signal to different shaft and engine speeds, and normalisation of the data.

In the raw data of JVS the set point engine speed is given in voltage. Before the conversion can be made between voltage and set point engine speed, a relationship between those two should be found. This relationship can only be made with stable points, meaning that the set point and shaft speed are constant for a certain time span. At a constant input signal, still some small oscillations are visible in the measured results. These oscillations are cancelled out by taken an average so that the input signal and shaft speed are constant. Some of those stable points are listed below, see table 6.11. The results of table 6.11 are also illustrated in figure 6.20. From this figure is clearly visible that the relationship is linear, so a linear function $n_{e,setpoint} = a \cdot U_{setpoint} + b$ can be derived.

$U_{setpoint}$ [V]	n_{set} [rpm]
-3.0309	676.74
-4.035	927.77
-5.03475	1184.4
-6.0236	1427.9

Table 6.11: Relationship between input signal and engine speed derived from JVS logging.

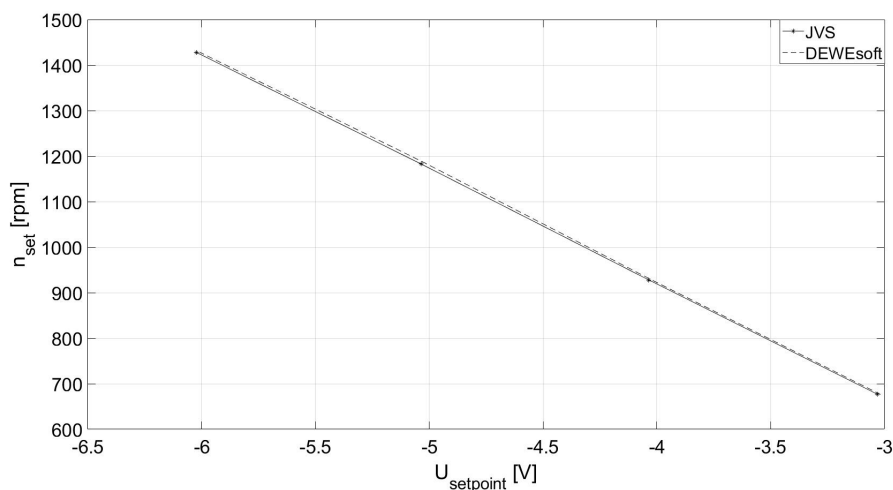


Figure 6.20: Shaft speed as function of input voltage.

Based on figure 6.20 a trend line can be drawn with the following characteristic, see equation 6.7. This characteristic is used for the determination of engine speed set point.

$$n_{set} = -251.38 \cdot U_{setpoint} - 85.29 \quad (6.7)$$

In the second part of the data pre-processing, three different pulse signals are transformed to shaft and engine speeds. Which signals are in the raw data of JVS is illustrated in figure 6.4. In the second main part a general equation of this transformation given, namely equation 6.2 and 6.1. But an equation in more detail is required due to differences in amount of reflectors and placing of the pulse measurement. The transformation Pulse Time Modulations (PTM) to pulse period, illustrated 6.6, is done with the Matlab function 'pulse period'. From this function the pulse periods for one pulse measurement Tp_1 , four pulse measurement Tp_4 and engine speed Tp_e is determined. The engine speed and shaft speeds are calculated according to the pulse period, as presented in following formulas 6.8, were amount of reflectors and were the pulses are measured are taken into account.

$$n_e = \frac{60}{Tp_e}, \quad n_{s,4} = \frac{i_{gb} \cdot 60}{Tp_4 \cdot 4}, \quad n_{s,1} = \frac{i_{gb} \cdot 60}{Tp_1} \quad (6.8)$$

The last pre-processing step that takes place is the normalization of the data sets, because this is required for the model structure. The linearization points are derived from a stable time period, while the system was running at constant $U_{setpoint} = -5V$. The results are shown in table 6.12.

Unit	Value
n_0 [rpm]	1183.8
$M_{s,0}$ [Nm]	1725

Table 6.12: Normalisation points of logging device of JVS, with $U_{setpoint} = -5V$.

Furthermore the JVS raw data is down sampled for two different reasons. First of all it reduces the required computer memory and second of all it speeds up the parameter estimation in the time domain. The data is down sampled to 200 Hz instead of the original 2000 Hz with Matlab function 'interp1'. This is done for all the in- and output data sets.

In end some small statements should be made about the physical limitations of the obtained data sets. The measurement of the shaft speed contains a frequency limitation due to the amount of reflectors installed on the shaft. If the operating point is $\pm 1183.8rpm$ and the gearbox ratio is 3.82, than shaft speed is $\frac{1183.8}{3.82} = 309.89[rpm]$. This can be rewritten to $\frac{309.89}{60} = 5.16rps = Hz$. In total are 4 reflectors glued on the shaft which means that the sensor can receive $5.16 \cdot 4 = 20.65 Hz$ of pulses. For the measurement of a sinus signal you need at least 2 measurement points, according to Nyquist. This leads to a high frequency measurement limitation of $\pm 10Hz$.

From here can be concluded that the data of the shaft speed above $\pm 10Hz$ is incorrect, due to the fact that only four reflectors are installed on the shaft.

6.5 CONCLUSIONS & RECOMMENDATIONS

In the final main part the conclusions from the full-scale experiments are outlined and recommendations for follow-up experiments are presented.

6.5.1 Conclusion

First of all, some conclusion are drawn from the signal inspection.

- The measured signals are all in-line with the expectations, such as shaft torque measurement, shaft speed measurement and input signal measurement. All the measured signals contain errors, which are summarized in table 6.10. However most of the defined 'errors' are outliers, which are easily repairable.
- The most usable datasets are the raw signals from JVS, because the JVS measurements logged more signals than the DEWE soft, as can be seen in figure 6.4. Second of all, it is visible in table 6.10 that the JVS measurement contains less errors and the raw data is chosen, because the calculation performed by JVS from pulse signal to shaft speed is unknown. During the pre-processing the follow tasks are executed.
 - The data is down sampled for several reasons. First of all, it is required to eliminate the errors in the shaft speed calculation. Second of all, it reduces the required computer memory and, thirdly, it speeds up the parameter estimation in the time domain.
 - The data is normalized according to the operation point.
 - The engine speed set point is transformed from measured voltage to engine speed in rpm.
 - The engine and shaft speeds are calculated according to a transformation of measured pulse signal to engine and shaft speed.

The above-mentioned proceedings are required before the data can be used for the full-scale parameter estimation. Doing this provides the user with a valuable dataset, which enables full-scale parameter identification.

- The shaft speed measurement is limited by measurement limitations, so the obtained data from 4 pulse shaft speed measurements above $\pm 10\text{Hz}$ is not useful. The shaft speed measurement with one pulse signal is not useful above $\pm 2.5\text{Hz}$.

6.5.2 Recommendations experiments

Some recommendations are given for follow-up experiments:

- Execute the experiments with a more advanced signal generator, so that for example higher offsets in the step responses can be used for the input signals. It would also be interesting to have the possibility of one long chirp signal, instead of being limited by 500s. Additionally, a more advanced signal generator is able to minimize the 'errors' in the input signal, e.g. low frequent chirp or relay switches.
- Another recommendation is to make one complete input signal in time domain beforehand. This could then contain all the different signals such as sine waves, chirp waves and step responses. This signal can be put on the system, which saves time and it reduces the possibility of human errors during the experiments.
- Shut down or minimize the usage of phones, especially near the stationary shaft torque sensor, during the experiments such that less EMC errors occur in the measurement.
- Logging the input signal $I_{setpoint}$ after the converter may increase the preciseness of what the exact input signal of the system is. Nevertheless, $I_{setpoint}$ should most likely be measured with a resistance and when this is put in parallel with the input signal on the board, the converter is not able to deliver the requested power of this circuit. If in follow-up experiments $I_{setpoint}$ is measured instead of $U_{setpoint}$, then another converter should be used.
- During the signal inspection it is derived that the reflectors of the 4 pulse signal PTM_4 were not positioned equally over the shaft. If the obtained data is used for recalculation or other purposes it is advisable to use a more advanced algorithm that takes the inequality of the reflector positioning into account. The advantage with such an advanced algorithm is that the 4 pulse signal fluctuates less and gives a more realistic presentation of the reality and could improve a future fit.
- It is recommended to pay more attention to the data pre-processing of the shaft torque. In practice, the strain gauge measures the torque between the propeller and the gearbox. The measured shaft torque value should be in-between the propeller torque and gearbox torque depending on the amount of mass moment of inertia on both sides of the strain gauge. However, in the model structure the propeller torque or the shaft torque has to be used. So, because of this, it is advisable to multiply the obtained shaft torque with a correction factor.
- Execute the shaft speed measurement with 8 pulse reflectors on the shaft, such that the shaft speed can be measured still at an input signal of 40 Hz.

7 | FULL-SCALE PARAMETER ESTIMATION

In this chapter the results of the parameter estimation on the full-scale data are discussed. This chapter is divided into four different main parts. In the first main part the pre-processed data from the previous chapter is analysed. In the second main part the used model structure and how this model is fitted on the data for parameter estimation are discussed. In the third main part the full-scale parameter estimation takes place with an additional validation. In the fourth main part the conclusions & recommendations are drawn from this chapter.

7.1 DATA FROM PRE-PROCESSING

The raw data of JVS will be used for the full scale parameter estimation, so the data set 'Run2' of table 6.7 is split up in four different signals.. The four different signals are:

1. Multiple sine waves
2. Short chirp signal
3. Long chirp signal
4. Step responses

Now the input and outputs of these four signals are presented and analysed to see whether they are in line with the expectations.

7.1.1 Multiple sine wave

The multiple sine wave contains different sine wave frequencies, namely S2-S14 of table 6.7. First of all, it should be noted that the amount of periods of every sine wave is random. The input signal is presented in figure 7.1.

The input signal and the response of the shaft speed are plotted in figure 7.2. From Bode Diagram 3.8 is derived that the DC gain for relation $\frac{\delta n^*}{\delta n_{set}^*}$ is 1 and this is also in line with the obtained data. At higher frequencies the shaft speed response should go to zero according to the Bode diagram. A reduction of the shaft speed response is also clearly visible in figure 7.3, which is a zoomed in version at high frequencies of figure 7.2. Nevertheless, it is also visible that the actual shaft speed response is not completely zero at high frequencies. This might be caused due to limitations of the model, see the conclusions of Chapter 3.6, which states that the sampling frequency and step size of the calculations of the engine governor have an influence at high input frequency and causes that the shaft response can not go to zero.

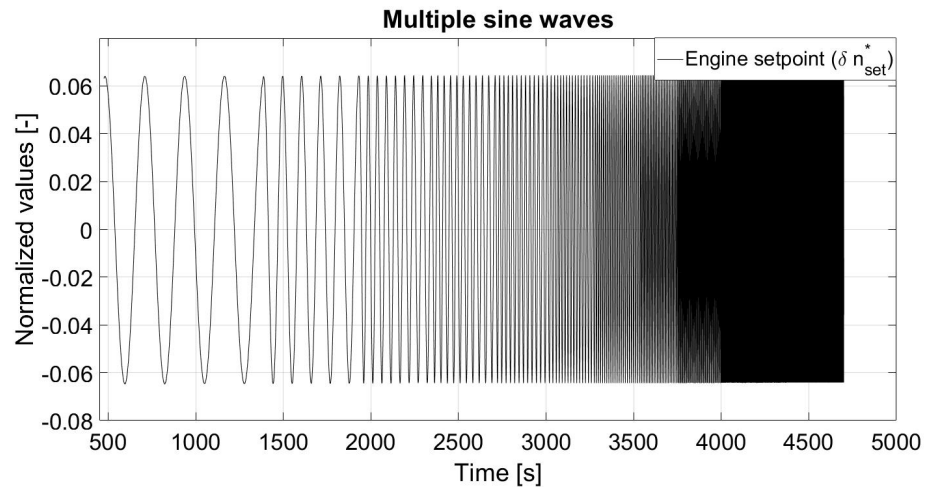


Figure 7.1: Multiple sine wave input signal.

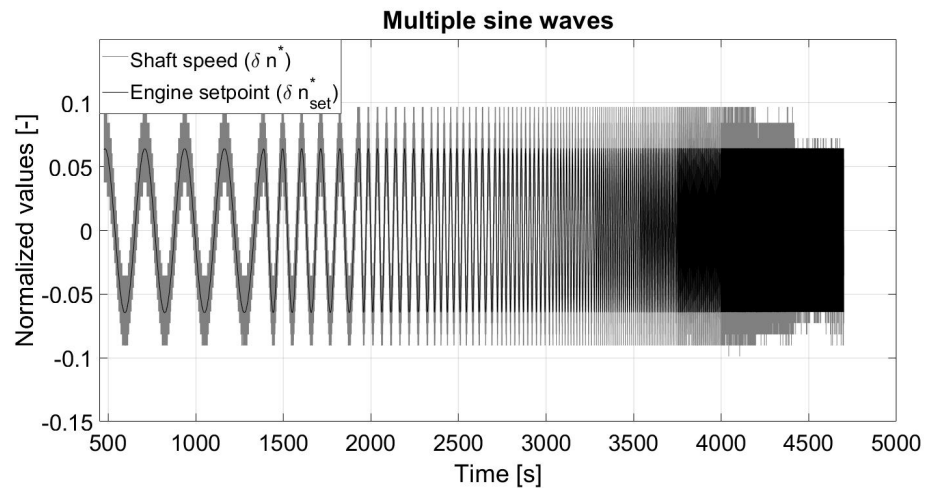


Figure 7.2: Multiple sine wave input signal and shaft speed 4 pulse measurement.

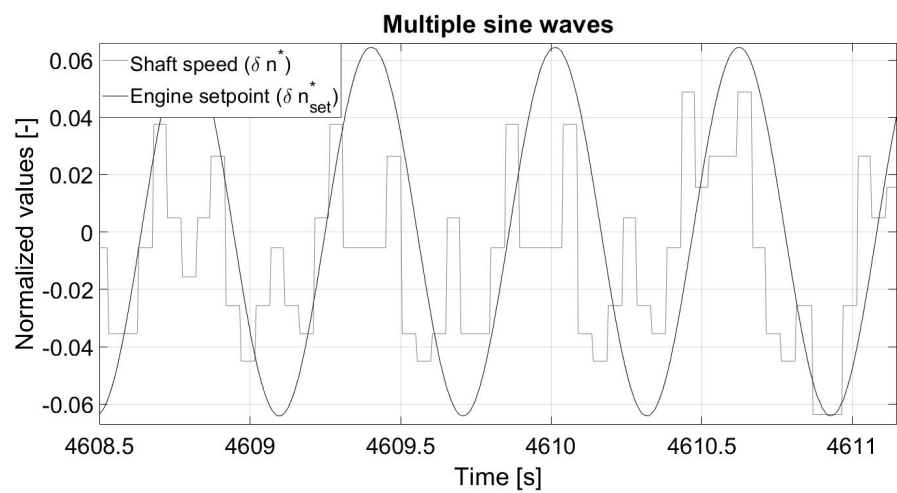


Figure 7.3: High frequency part of multiple sine wave input signal and shaft speed 4 pulse measurement.

The input signal and the response shaft torque are plotted in figure 7.4. From figure 3.9 is known that the DC gain is 2, which is also partly visible in the results of figure 7.4.

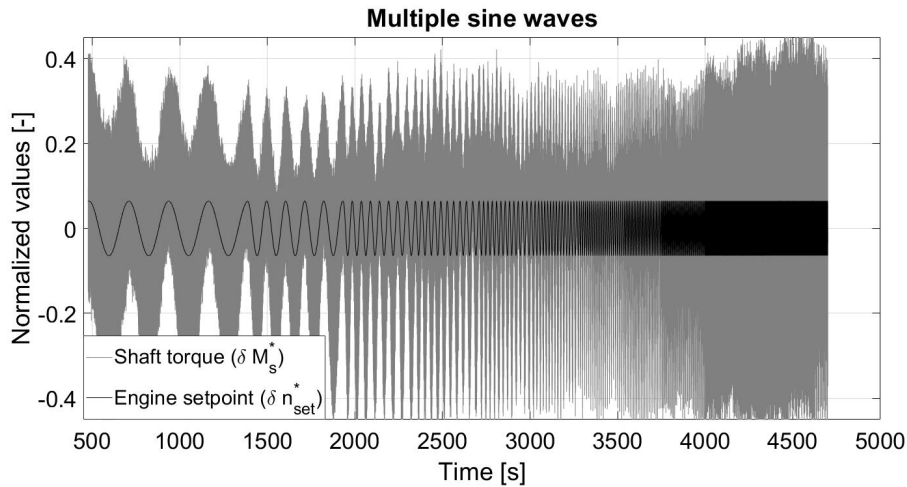


Figure 7.4: Multiple sine wave input signal and shaft torque

At higher input frequencies, the response should increase drastically, according to the Bode diagram. In the obtained data, a small increase is visible, but not the large increase that is expected. The reasons for this reduced increase are most probably also the discrete behaviour in the governor, safety ramps and discrete firing of the diesel engine.

The obtained data is also compared to an expected response graph made by the writer, where the discrete behaviour of the governor, discrete firing of the engine and safety ramps are involved. This is presented in figure 7.5. Please note that the sequence of the events in figure 7.5 is arbitrarily selected, because in reality it is now unknown which event occurs first. The three different events are briefly discussed in the outline here below:

- When the input frequency is above a certain point, the diesel engine can not react physically on this due to the discrete firing. If this is the case, then aliasing occurs, see the grey line. From the shaft torque signal validation the firing frequency of the engine is determined. The different peaks in the shaft torque signal, including the firing frequency of 59.08 Hz, can be seen in figure 6.14. To create a sine wave as input signal it requires at least 2 ignitions, according to Nyquist (36). Then the highest input frequency the system can react on is $\frac{59.08[Hz]}{2} \approx 30[Hz]$. This means that the highest frequency that can be put in the system is a little bit less than 30 Hz, otherwise the signal can not be physically transferred into the drive train. In practice this value is most probably lower due to additional disturbances. The dashed grey line in figure 7.5 indicates the starting frequency of this phenomena.
- A safety ramp is installed in the governor, which limits the shaft torque. It is expected that this ramp is just a constant line, which means that the input frequency can be increased but the output re-

sponse stays constant due to the ramp. The influence of this ramp is illustrated with the red line.

- Sampling frequency of governor, calculation time step sizes of the governor and possibly the engine management system are influencing the shaft torque response. This means in practice that if sampling time of these system is too low, then aliasing occurs. When aliasing occurs, then different output responses are measured and this is illustrated with the yellow line.

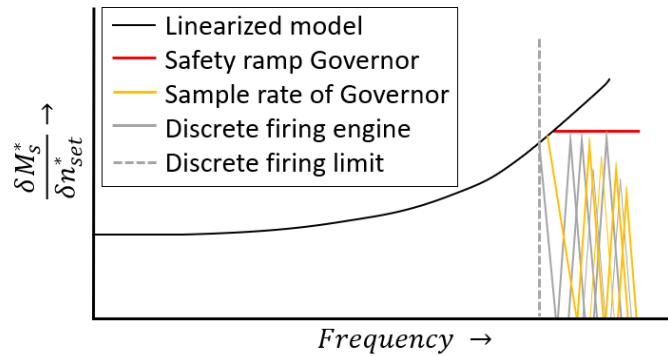


Figure 7.5: Shaft torque response in full-scale measurement.

When looking at the obtained data and figure 7.5, the obtained shaft torque response is in line with figure 7.5. Another way of presenting this data is by putting it in frequency domain.

Earlier in this text, the different sine waves were presented in time domain, but putting the signal into frequency domain has some advantages. Especially the response data contains quite some noise and by putting these signals into frequency domain this noise can be cancelled out. The removal of this noise will most likely influence the parameter estimation positively. The second advantage of putting the data in frequency domain is that less computer memory is required. The third advantage is that using frequency domain data speeds up the parameter estimation drastically. Especially because the multi sine wave signal is a really long measurement with a high sample rate.

The different measured sine signals are summarized to a simple sinus wave, with the Matlab function 'SineFit'. The 'SineFit' function is obtained from Matlab file exchange. This function fits the data into a single sine wave with 4 values: a the offset, b the amplitude, c the frequency and d the phase shift (37). With the use of 'SineFit' it is not necessary to normalize the data, because 'SineFit' determines the normalisation point for every individual frequency, namely the offset.

In global lines, the 'SineFit' works as follows: The data is first transferred to frequency domain and then the algorithm searches for the highest peak in the frequency domain. This is decisive for the frequency that 'SineFit' will return and with too much noise in the measured signal this can lead to a wrong frequency. The amplitude and offset are determined in time domain, with a nonlinear fit. Please note that the phase shift is influenced in multiple

ways, because a cancellation of a negative frequency leads to a phase change.

The results of the 'SineFit' for every frequency and in- and output signals are presented in Appendix E. The end of the appendix contains a small discussion about the obtained results. In the Appendix is concluded that every measurement with a frequency of 3.433 Hz and above are not useful, due to nonlinearities in the data or the conversion from time to frequency domain.

All the different input and output data are defined as simple sine waves by the 'SineFit' for different frequencies, ω_i . The set point engine speed n_{set} , shaft speed measurement n_s and shaft torque measurement M_s are described by the following components a defines the offset, b the amplitude and d the phase shift of the sine wave.

After that the sine waves can be put in complex notations and the absolute magnitude and phase in degrees for the single input and two outputs can be made. This is presented in equation 7.1 and 7.2.

$$H_1(\omega_i) = \frac{n_s^*(\omega_i)}{n_{set}^*(\omega_i)} \quad (7.1)$$

$$H_2(\omega_i) = \frac{M_s^*(\omega_i)}{n_{set}^*(\omega_i)} \quad (7.2)$$

The results are plotted for every frequency, ω_i , in figure 7.6 and 7.7.

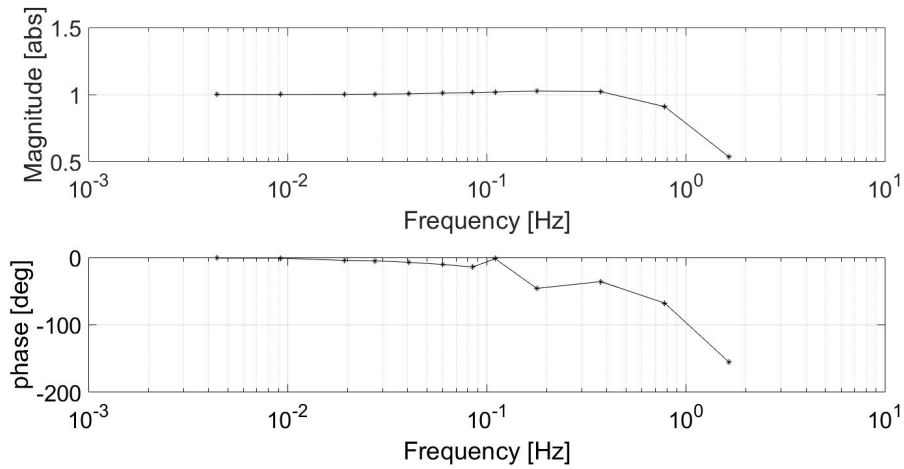


Figure 7.6: Bode plot of $\frac{\delta n_s^*}{\delta n_{set}^*}$.

The shape of the plots are in line with the expectations of chapter 3.5.2, because the results show the same system behaviour as the model structure presented in that chapter. However, it should be stated that the phase in both obtained figures contains some small outliers at a frequency of around 0.1 Hz. Furthermore, the discussion, as outlined for the time domain results, is still applicable for the same data in frequency domain. At higher frequencies, less response in $\frac{\delta n_s^*}{\delta n_{set}^*}$ was expected and more response in $\frac{\delta M_s^*}{\delta n_{set}^*}$. When here a DC gain comparison is made can be seen that the observation in time

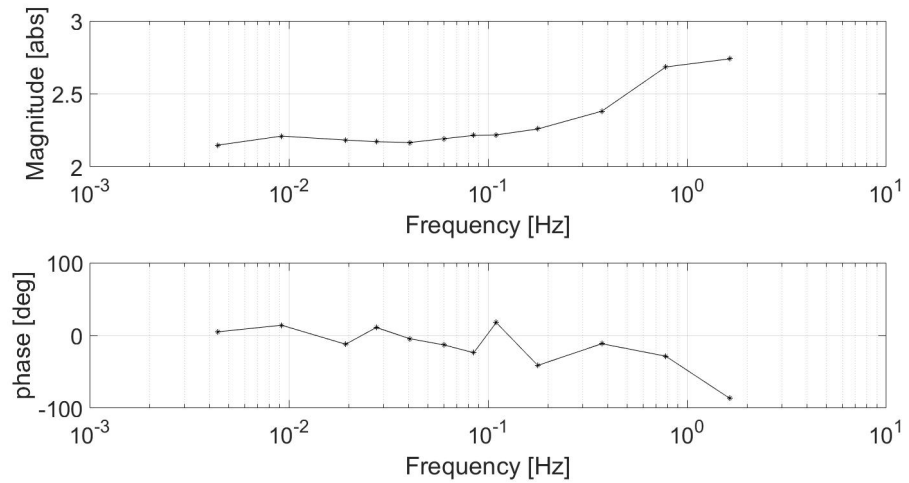


Figure 7.7: Bode plot of $\frac{\delta M_s^*}{\delta n_{set}^*}$.

domain was partly correct while the correct DC gain $\frac{\delta M_s^*}{\delta n_{set}^*}$ is 2.2. The DC gain of $\frac{\delta n^*}{\delta n_{set}^*}$ is 1, which was also expected in time domain.

The data obtained from the multiple sine wave input signal is checked in time and frequency domain. In both domains the lower frequencies are in general in line with the expectations. At really high input frequencies, the influences of sampling frequency and of step size of engine governor calculations are visible, see also Appendix E.

7.1.2 Short chirp signal

The second input signal is a short chirp signal, which is signal 'C11' in table 6.7. The input is presented in figure 7.8, in which the first part of the chirp signal was cut off, because of the disturbances caused by rise time to the operation point on which the chirp signal is executed.

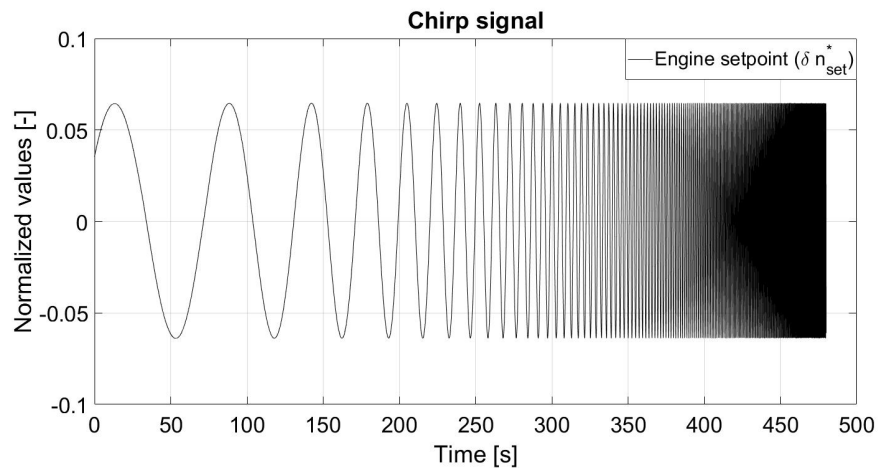


Figure 7.8: Chirp input signal 'C11' of table 6.7.

Figure 7.9 and 7.10 shows that derived responses are identical to the results of the previous signal. The obtained responses for low frequencies are in line with the expected behaviour, but at high frequencies some unexpected behaviour is observed similar to the multiple sine wave case. Nevertheless, the results are in line with expectations. The short chirp signal is not put in frequency domain.

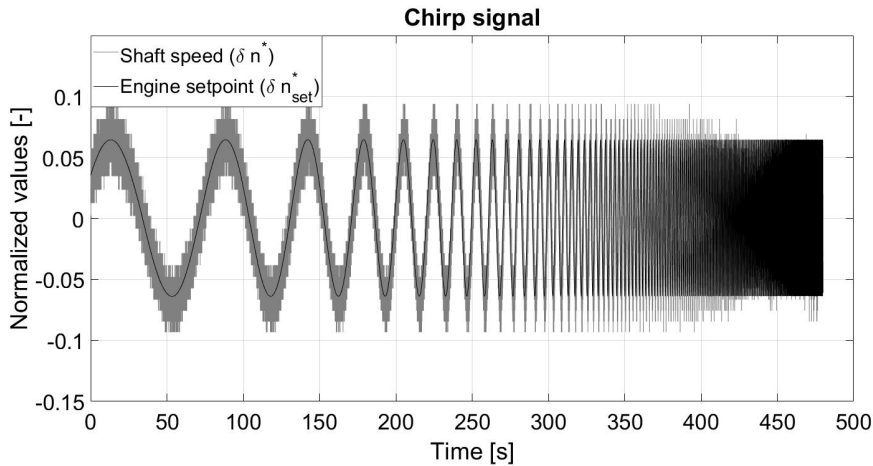


Figure 7.9: Chirp input signal 'C11' of table 6.7 and shaft speed response.

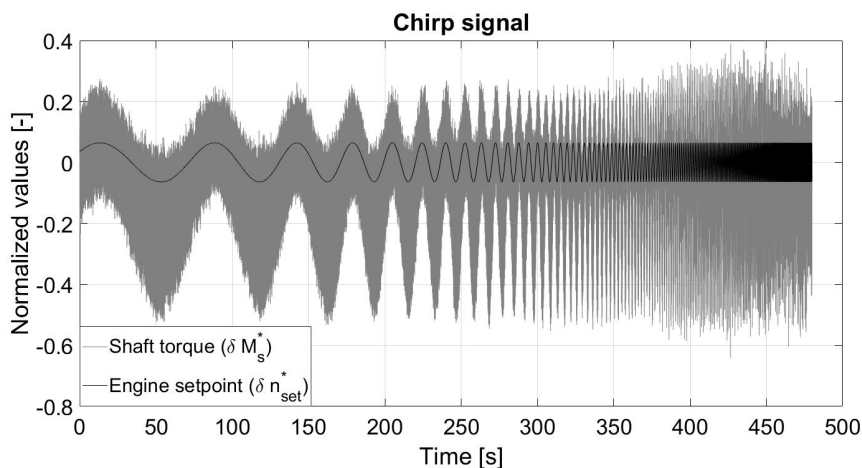


Figure 7.10: Chirp input signal 'C11' of table 6.7 and shaft torque response.

7.1.3 Long chirp signal

The long chirp signals are the signals 'C21', 'C22' and 'C23' from table 6.7. These signals are put after each other by trial and error so that no jumps occur. Nevertheless, when a small jump would occur, then this chirp signal contains a step responses. The signal is presented in figure 7.11. From the detailed signal analysis and from figure 7.11, it is visible that during the first 500 seconds the frequency does not increase. Nevertheless, to excite the low frequencies of the system, the chirp signal 'C21' is still used. In reality this is quite a disadvantage, because the lower frequencies are now only excited by one single frequency instead of a whole range. Figures 7.12 and 7.13

shows the input signal and the shaft speed and shaft torque.

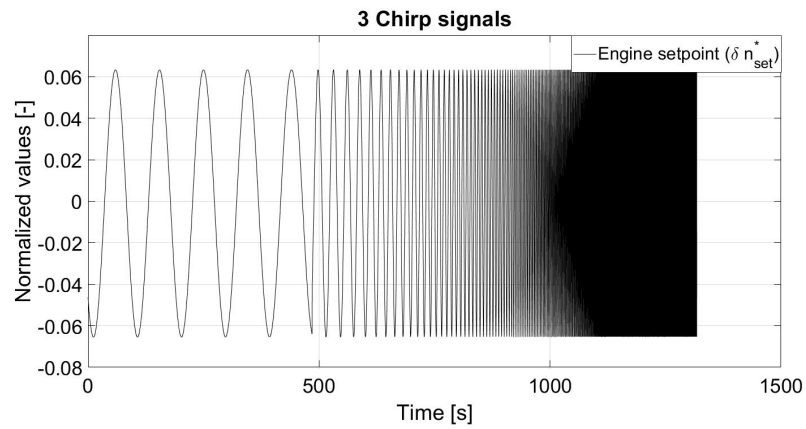


Figure 7.11: Chirp input signal 'C21', 'C22' and 'C23' of table 6.7 and the shaft speed response.

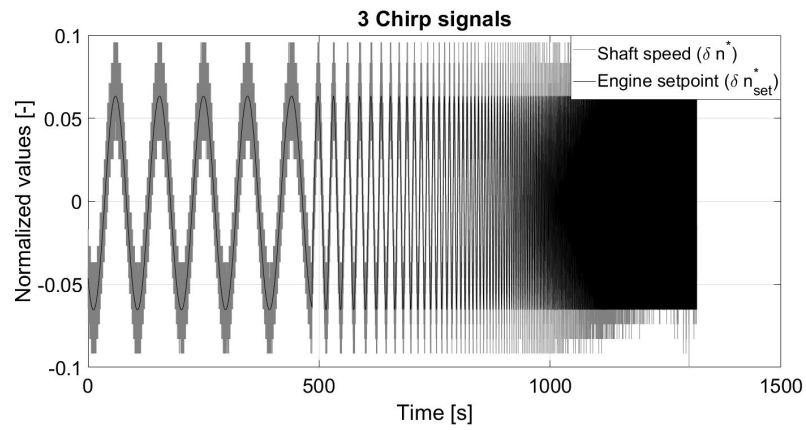


Figure 7.12: Chirp input signal 'C21', 'C22' and 'C23' of table 6.7 and the shaft speed response.

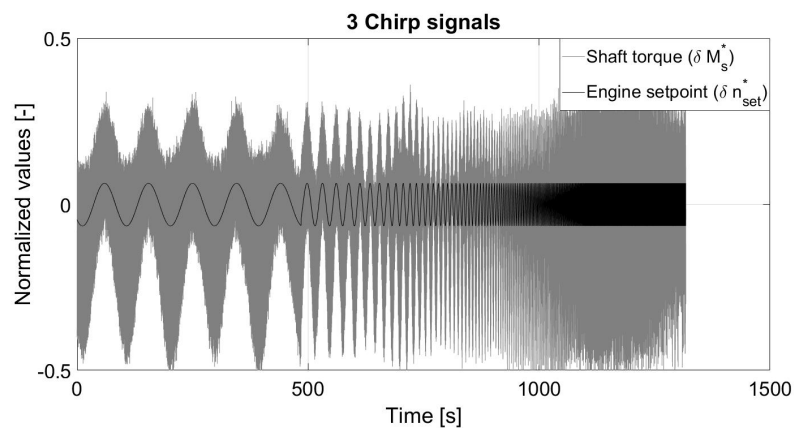


Figure 7.13: Chirp input signal 'C21', 'C22' and 'C23' of table 6.7 and the shaft torque response.

The obtained responses for low frequencies are in line with the expected behaviour, but at high frequencies some unexpected behaviour is observed, similar to the multiple sine wave and short chirp signal cases. Nevertheless, the results are in line with expectations. The long chirp signal is not put in frequency domain.

7.1.4 Step responses

The validation of the different parameter estimations are done according to step responses, such as presented in figure 7.14. The obtained step responses are in line with the expectations.

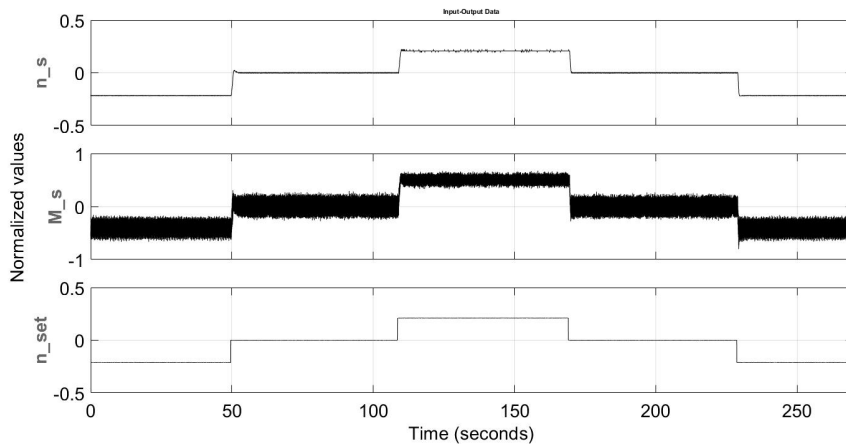


Figure 7.14: Step response data St_1 of table 6.7. Upper graph shaft speed response, middle graph shaft torque response and lower graph input signal.

7.2 MODEL STRUCTURE & SEARCHING ALGORITHM

In the third main part the used model structure and how this model is fitted on the data for parameter estimation are discussed. In the previous part is concluded that the model structure of chapter 5.3 is suitable for the obtained data, so this is also used for the full-scale parameter estimations. Similar to the virtual experiments, two parameters and two relations are estimated during full-scale estimation, namely τ_n , g , $\frac{K_p}{K_i}$ and vK_p .

Nevertheless, pay attention to the fact that in the previous main part, some shortcomings of the model are outlined that influence the response at high frequency input signals. The following events are not in the modelstructure and play most likely an important role only at high input frequencies.

- Safety ramp
- Sample rate governor
- Discrete firing engine

How the model is fitted on the data is identical to the virtual experiments, as was presented in Chapter 5.2. The only difference is that during full-scale parameter estimation noise is involved in the data. So one of the settings is changed, namely the allowance of 'Disturbance' in the data.

7.3 RESULTS PARAMETER IDENTIFICATION

In the fourth main part the results of several parameter estimations are presented, where every parameter estimation is indicated by a small Roman numeral (ii,...,iv). First, the starting conditions are defined, which is followed by a description of the 'three' parameter estimations that have been executed. After that, the results are presented in a table and figures. For parameter estimation a starting parameter set is required, which for the full-scale parameter estimations is defined as follows:

$$\bar{\theta}_0 = [\tau_n \quad g \quad v \quad K_p \quad K_i]^T = [1.2 \quad -0.5 \quad 1 \quad 10 \quad 3]^T \quad (7.3)$$

To speed up the optimization program and to guide the optimization to a feasible solution, different boundaries are set for different parameters. The boundaries are defined in equation 7.4, 7.5, 7.6, 7.7 and 7.8.

$$0.01 < \tau_n < 5 \quad (7.4)$$

$$-3 < g < -0.01 \quad (7.5)$$

$$0.01 < v < 5 \quad (7.6)$$

$$0.01 < K_p < 15 \quad (7.7)$$

$$0.01 < K_i < 10 \quad (7.8)$$

Small Roman numerals (ii,...,iv) indicate different parameter estimations with different input signals and/or settings. All the three parameter estimations (ii,iii,iv) have an input amplitude of $\pm 0.065 \cdot n_0 \approx 77rpm$.

- (i) 'Initial parameter set' $\bar{\theta}_0$ is the set that is used initially for the searching algorithm. Please note that this parameter set is **not** derived by parameter estimation. This initial parameter set is put into a model structure and this initial system is used to see which changes are made compared to a system determined by parameter estimations ii, iii and iv. So this set could also be completely different.
- (ii) 'Multiple sine waves with adjustments' uses the multiple sine waves but some values of the 'SineFit' are manually adjusted. The reason for this is that some of the estimated values are incorrect, which is visible in the figures presented in appendix E. From these graphs, it becomes visible that these adjustments are logical and that at high frequencies an error in the 'SineFit' occurs. The adjustments are listed here below:
 - For the set point engine speed, table E.1, the amplitude at a frequency of 3.433Hz is corrected to 76 instead of 68.
 - For the shaft speed, table E.2, at an input frequency of 3.433Hz the estimated frequency is corrected to 3.433Hz instead of 0.464Hz.
 - For the shaft torque at an input frequency of 3.433Hz, table E.3, the estimated amplitude is corrected to 320 Nm, instead of 96 Nm.
 - All signals with a frequencies of 7.19Hz and above are disregarded, because these are not reliable.

The parameter estimation is executed with the data in frequency domain.

- (iii) 'Chirp signal short' is the input signal as illustrated in figure 7.8. The properties of the used chirp signal can be seen in table 6.7 at 'C11'. The chirp signal is normalized according to the operating points presented in chapter 6.4. The parameter estimation is executed using the time domain data.
- (iv) 'Chirp signal long' is the input signal as illustrated in figure 7.11. The second chirp signal contains exactly three different chirp signals placed after each other, namely signal 'C21', 'C22' and 'C23' from table 6.7. The chirp signal is normalized according to the operating points, presented in chapter 6.4. The parameter estimation is executed using the time domain data.

The results of the three parameter estimations are presented in table 7.1.

	Duration	Parameters				Fitting		Validation	
		τ_n	g	$\frac{K_p}{K_i}$	vK_p	δn^* [%]	δM_s^* [%]	δn^* [%]	δM_s^* [%]
(i)	+	1.2	-0.5	3.33	10	+	+	91.73	63.54
(ii)	$\pm 4250s$	0.275	-0.314	0.0010	0.010	66.64	20.84	95.85	68.27
(iii)	$\pm 480s$	0.5767	-0.01	0.0072	0.035	50.88	18.61	95.85	68.27
(iv)	$\pm 1400s$	1.59	-0.01	1.45	1.93	42.63	10.02	95.85	68.27

Table 7.1: Results of full-scale parameter estimations.

+ The 'initial parameters' are not fitted, so for this reason there is no percentage and no signal time.

In general it can be concluded from table 5.2 that the different parameter estimations are not in line with the expectations. All the three different parameter estimations (ii, iii and iv) show different results. For example, the values of τ_n and g vary a lot. Additionally, the relations of $\frac{K_p}{K_i}$ and vK_p are different for nearly every parameter estimation. The fitting percentages of the obtained parameters are low, especially that of the shaft torque response. Here down below is every parameter estimation discussed in more detail.

Parameter estimation ii shows some unexpected results, e.g. the relation between K_p and K_i . The obtained value for this ratio is low due to the fact that value of K_p is really small, which also results in the low value of the relation vK_p . In practice, a small value of K_p means that an error is cancelled out very slowly. This phenomena is not in line with the results of the input signal and output signals of the multiple sine waves in figures 7.2 and 7.4. From these figures it is visible that the system cancels out errors quite fast, because the responses can follow the input signal for lower frequencies. This then leads to the assumption that the relation between $\frac{K_p}{K_i}$ is wrongly estimated. However, the value of τ_n , which represents the mass moment of inertia for a certain operating point, is also significantly lower than expected.

Parameter estimation iii also shows some unexpected results. First of all, as a result of this parameter estimation the same unexpected relation is visible between the $\frac{K_p}{K_i}$ and vK_p . Nevertheless, the value of τ_n is more in line with the expectations than for parameter estimation ii, but still way too low. It is assumable that the parameters and relations are incorrectly estimated.

Parameter estimation iv is more in line with the expectations when it comes to the estimated parameters and the relations. Nevertheless, the fitting percentages are much lower and the relations and individual parameters are still containing extreme values. It is still assumable that the parameters and relations are incorrectly estimated.

In the following parts the obtained parameter sets are implemented in the used model structure and validated in frequency domain, time domain and the parameter τ_n is compared to a torsion vibration calculation (TVC).

7.3.1 Frequency domain behaviour

First, the relation $\frac{\delta n_s^*}{\delta n_{set}^*}$ is presented in figure 7.15.

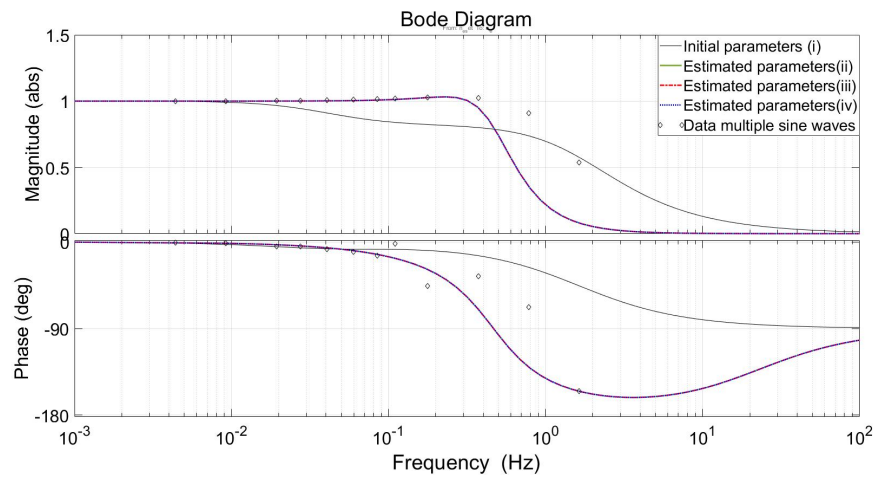


Figure 7.15: Frequency domain comparison $\frac{\delta n_s^*}{\delta n_{set}^*}$.

At first sight of figure 7.15, it can be seen that the responses of the different parameter estimations are identical to each other. Pay attention to the fact that parameter estimations (ii, iii and iv) are on top of each other. Parameter estimations (ii, iii and iv) shows different dynamic behaviour than the initial parameter set implemented in the linearized model. The differences are at which frequency the first decay takes place and the steepness of the decay. However, at lower frequencies the DC gain is 1, which is in line with the expectations derived from the bode plot of $\frac{\delta n_s^*}{\delta n_{set}^*}$. Furthermore are the parameter estimations ii, iii and iv for higher frequencies not in line with the obtained response of the multiple sine wave in frequency domain. The second relation that is plotted, is $\frac{\delta M_s^*}{\delta n_{set}^*}$, see figure 7.16.

Just as in the previous Bode plot, the results of parameter estimations (ii, iii and iv) are on top of each other. The initial parameter set (i) is showing different behaviour than the parameter estimations. At lower frequencies, it can be seen that the parameter estimation sets (ii, iii and iv) have a DC gain of 2, this is in line with the DC gain of $\frac{\delta M_s^*}{\delta n_{set}^*}$, which is also ± 2 . However, at high frequencies the estimated parameters go to zero, while the initial parameter set in the linearized model goes to a certain magnitude. Further-

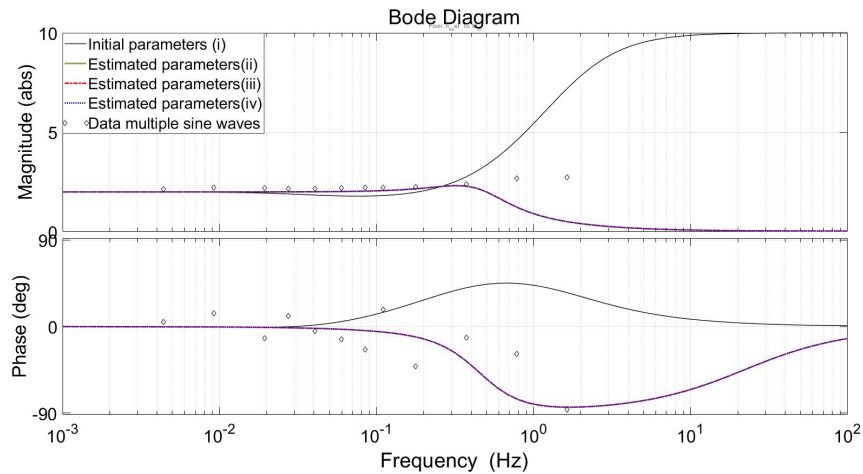


Figure 7.16: Frequency domain comparison $\frac{\delta M_{s}^*}{\delta \bar{n}_{set}^*}$.

more are the parameter estimations ii, iii and iv for higher frequencies not in line with the obtained response of the multiple sine wave in frequency domain, where even a slight increase is visible.

7.3.2 Time domain validation

The previous evaluation is performed in frequency domain. The estimated parameter sets are also compared to another data set to see if the fit in time domain is correct. The ninth and tenth columns of table 7.1 show the fit percentages of the estimated parameters on a different data set, namely step a response defined as 'St1', in table 6.7. From figure 7.17 can be concluded that the parameter estimations (ii, iii and iv) in time domain are correct in global lines. Please note that the parameter estimations (ii, iii and iv) are on top of each other in the graph.

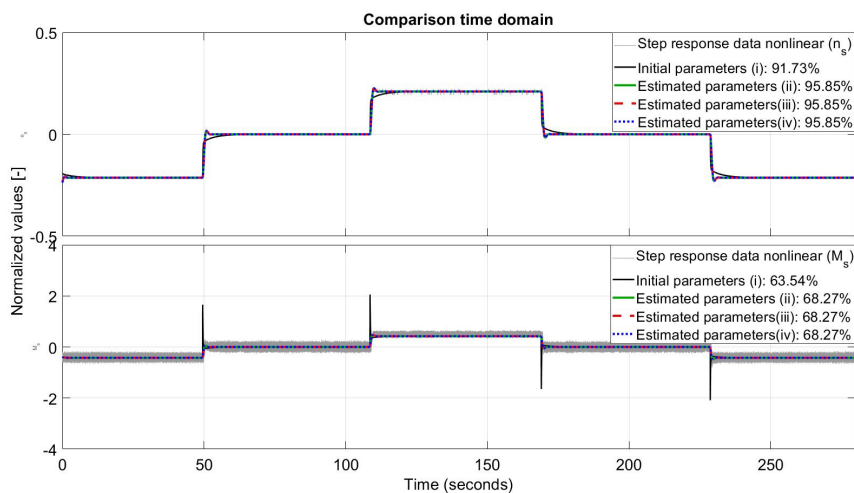


Figure 7.17: Comparison parameter estimation time domain.

The second step is shown in more detail in figure 7.18. From figure 7.18 can be seen that the rise time of the parameter estimations are nearly identical with the actual data. The actual response is identical and a small overshoot is visible in the data and in the estimated simulations. A certain kind of delay can also be observed in the data, namely of 0.5s. For every step that is put on the system, a delay can be observed in the data. The reason for this delay is unknown.

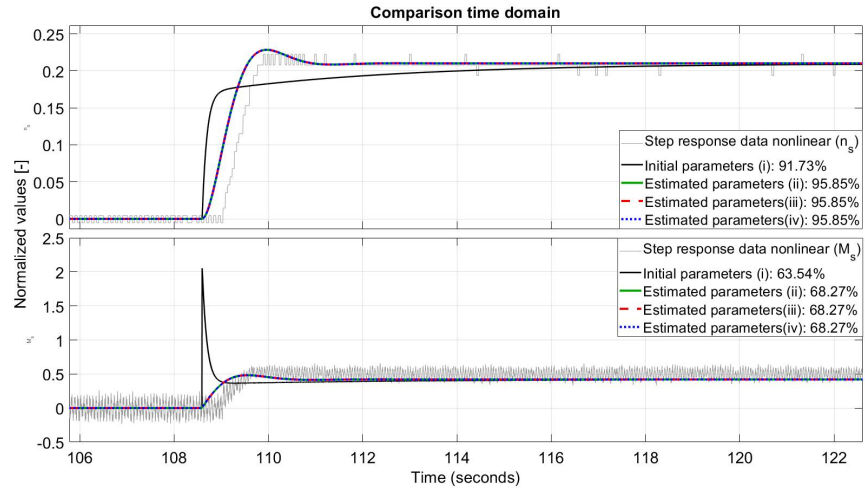


Figure 7.18: Comparison parameter estimation time domain zoomed in on third step

The parameter estimation ii is fitted on the multiple sine waves data, so time domain validation with the multiple sine waves is only done with parameter estimation iii and iv. The results are presented in figure 7.19, where the fit percentages are also presented.

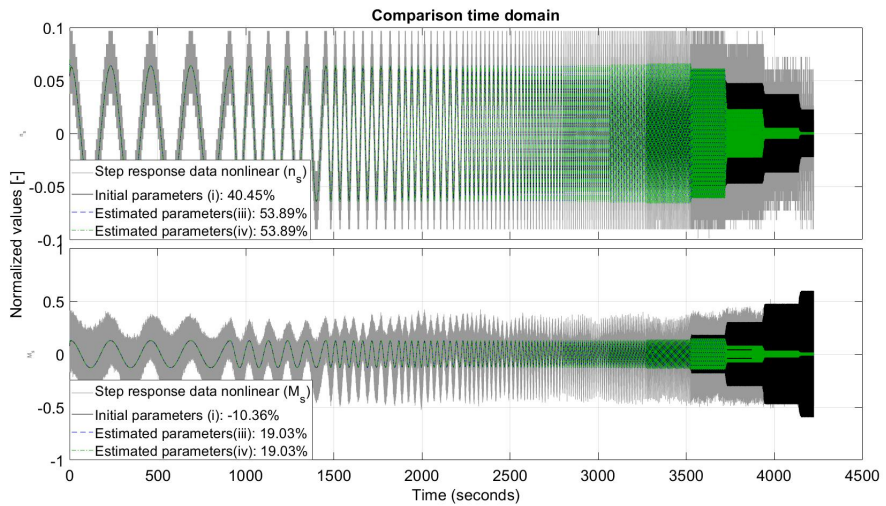


Figure 7.19: Validation parameter estimation iii and iv with multiple sine waves.

From figure 7.19 can be derived that the model with the estimated parameter set has a higher fit percentage than the model with the initial parameters.

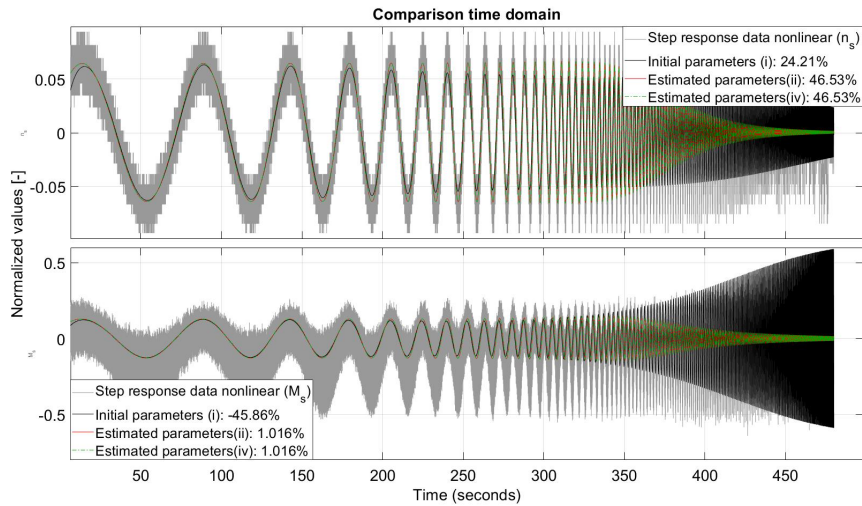


Figure 7.20: Validation parameter estimation ii and iv with short chirp signal.

Most likely, these big difference are caused by response differences at higher frequencies, because at lower frequencies the responses are identical. Furthermore can be noticed that the response of the shaft speed of the estimated parameters (iii and iv) decreases more and also at higher frequency. This is in line with the Bode diagram 7.15, where the response difference is clearly visible.

The parameter estimation iii is fitted on the short chirp signal, so the short chirp signal is used for time domain validation with parameter estimation ii and iv. The results are presented in figure 7.20, where the fit percentages are also presented. The parameter estimations ii and iv are completely in line with the short chirp signal at low frequencies. At higher frequencies there is a difference for the same reason mentioned at time domain validation of multiple sine waves.

The parameter estimations ii and iii are validated with a long chirp signal data set. The results are presented in figure 7.21 where the fit percentages are presented in the legend. The parameter estimations ii and iii are completely in line with the short chirp signal at low frequencies. At higher frequencies there is a difference for reasons explained at the multiple sine waves.

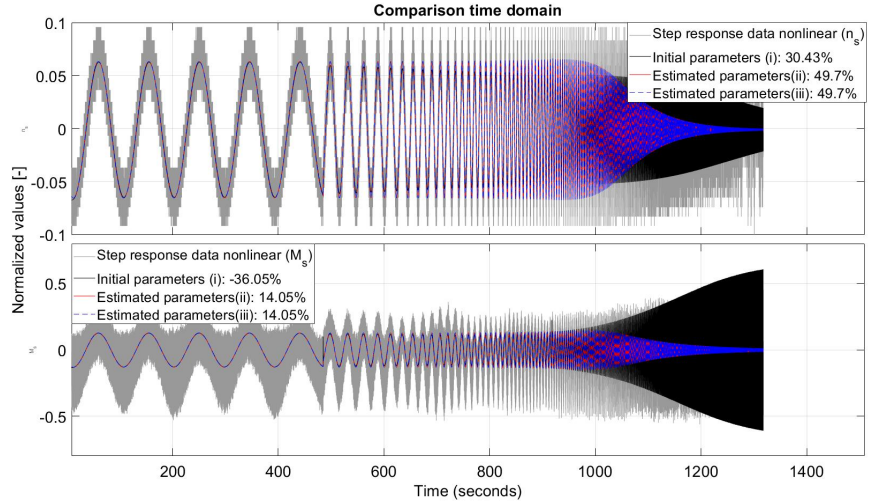


Figure 7.21: Validation parameter estimation ii and iii with long chirp signal.

The results of the different time domain validations from here above are summarized in table 7.2 and 7.3.

	M. sine waves [%]	Short chirp [%]	Long chirp [%]	Step responses [%]
P. est. i	40.45	24.21	30.43	91.73
P. est. ii	fitted	46.53	49.7	95.85
P. est. iii	53.89	fitted	49.7	95.85
P. est. iv	53.89	46.53	fitted	95.85

Table 7.2: Fit percentage shaft speed of different parameter estimations according to different validation sets.

	M. sine waves [%]	Short chirp [%]	Long chirp [%]	Step responses [%]
P. est. i	-10.36	-45.86	-36.05	63.54
P. est. ii	fitted	1.016	14.05	68.27
P. est. iii	19.03	fitted	14.05	68.27
P. est. iv	19.03	1.016	fitted	68.27

Table 7.3: Fit percentage shaft torque of different parameter estimations according to different validation sets.

From tables 7.2 and 7.3, it is not possible to conclude which parameter estimation is the best, because all the fits have the same value. Still, there are differences between the parameter estimations, e.g. the duration of the experiments. If the duration of the experiment is the determining factor than the short chirp signal is the best.

7.3.3 Parameter validation

The validation of an individual parameters is difficult, because the actual value of these parameters are unknown. The only individual parameter that can be partly validated is the value of τ_n . This can be done by making use of the information provided in a torsion vibration calculation (TVC).

The total mass moment of inertia is calculated in the same way as stated in Chapter 3. The total mass moment of inertia for all the different components is $62.3 \text{ kg} \cdot \text{m}^2$, when seen from the propeller. With the normalisation points from chapter 6.4 it is possible to determine the value of τ_n , see equation 7.9.

$$\tau_n = \frac{2\pi I_p n_0}{M_{s,0}} = \frac{2 \cdot \pi \cdot 62.3 \cdot \frac{1184}{3.82}}{60 \cdot 1725} = 1.17 \quad (7.9)$$

In practice the obtained value from the parameter estimation should be lower than the determined 1.17. The reason for this is that the value is influenced by the positioning of the measurement of shaft speed and shaft torque. This is illustrated in figure 7.22, where an arbitrary line is drawn for the build up of total mass moment of inertia as a function of the position on the shaft seen from the propeller. The influence depends on the point where the summation of the moments is taken, which is also decisive for the calculated mass moment of inertia.

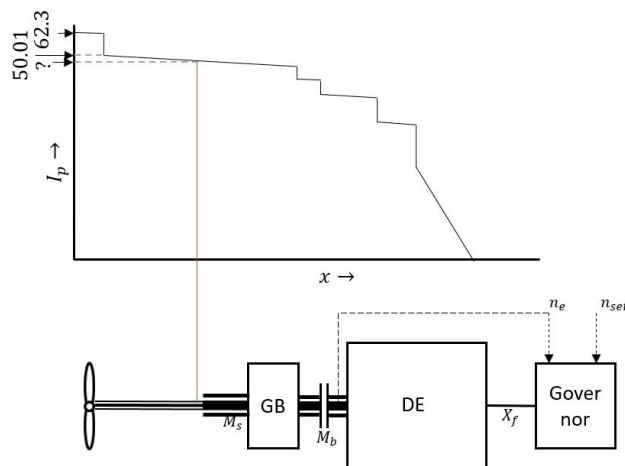


Figure 7.22: Explanation of influence of shaft torque measurement on the value τ_n .

Nevertheless, this influence should not be so big. As can be seen in figure 7.22, this influence is around the $12 \text{ kg} \cdot \text{m}^2$. When this is the case, then the value of τ_n should be around 1. However, none of the parameter estimations result in a value for τ_n between the 1 and 1.17.

7.4 CONCLUSION & RECOMMENDATIONS

In the final main part the conclusions from the full-scale parameter estimations are outlined and recommendations are presented.

7.4.1 Conclusion

The conclusions that can be drawn from this chapter are listed below:

- The pre-processed data sets are in line with the expectations for lower frequencies, because at an increased input frequency the shaft torque responses increases and the shaft speed responses decreases. This is applicable to the input signals: multiple sine waves, chirp signal and long chirp signal.
- The used model structure for parameter estimation derived in chapter 3 is for lower frequencies in line with obtained data sets of the multiple sine waves. But for higher frequencies is noted that the model is too simplified. Surprisingly a lot of dynamic behaviour occurs still at high input frequencies.
- The estimated parameter sets of different parameter estimations show big differences, which makes the results of the different parameter estimations not trustworthy. Additionally, the value of τ_n is individually validated with the help of a torsion vibration calculation and the estimated value is incorrect for all parameter estimations.
- When the obtained parameter estimations are put in the model structure, the system responses are in line with obtained data from full-scale step responses. This result is clearly visible in figure in 7.18, where the rise time and the small overshoot in the system response are clearly visible. Furthermore, step responses are practically the most used input signal of the captain, which makes these parameter estimations with model structure still useful. The obtained step response data contains a delay of $\pm 0.5s$. The reason for this delay is still unknown, but can be caused that the governor will not react on wake differences.
- All three different input signals give the same results when the obtained parameter sets are validated with different obtained datasets, see table 7.2 and 7.3. However, from the introduction can be concluded that the short chirp signal, parameter estimation iii, has the lowest duration. This makes this signal, the best input signal for full-scale parameter identification.
- For further investigation, it is advisable to implement the following in the nonlinear model: Discrete firing, internal sampling time governor and extra ramps. If these elements are included in the nonlinear model, then most likely the obtained full-scale data is more in line with the data obtained from the nonlinear model. Furthermore, it is recommended to execute a parameter estimation with this 'new' nonlinear model, so that the discreteness stays in the model structure and it is not cancelled out due to linearization. With these adjustments, better parameter estimation results can most likely be obtained.

7.4.2 Recommendations full-scale estimation

Figure 7.23 is an extension of figure 1.2, where in the extension multiple events for an unsuccessful model validation are given. For now the estimated models are only able to capture step responses but not any other input signals, such as chirp signals or multiple sine waves. For this reason, the estimated model is not classified as 'ok'. As can be seen in figure 7.23 this can be caused by an unsuitable searching algorithm and/or unsuitable model structure and/or unsuitable data. Down below, recommendations are written for every previously mentioned event to obtain positive model validation instead.

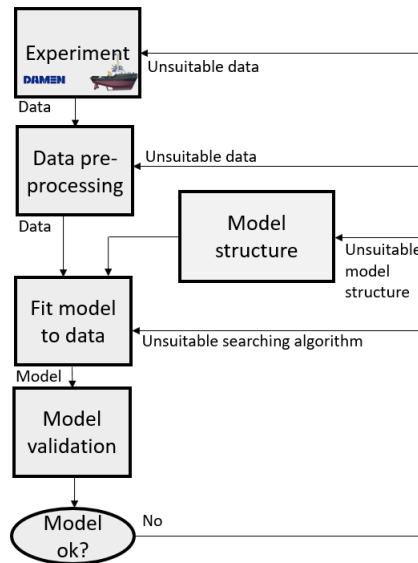


Figure 7.23: Reasons for incorrect parameter estimation

The data obtained during the experiments can be unsuitable due to incorrect measurement or due to incomplete data pre-processing. The recommendations on the experiments themselves, and on pre-processing of the obtained data, are outlined in chapter 6.5.2.

However, it is also recommended that during new experiments more output signals are measured. As one can imagine, if more is known about the output of the system it is also easier to identify the system. This rule is only applicable when there are also more relations available inside the system with the newly measured output signals. Otherwise, one could measure everything, but if there is no relation between input and output, it does not help with the parameter identification. But, for example, during the experiments the reading out of the CAN bus of the diesel engine can lead to information such as fuel rack position, fuel consumption, cylinder temperature.

The searching algorithm can be unsuitable due to wrong settings in the fitting of the model on the data. First of all, it is recommended to execute a more thorough investigation on usage of '*Regularization*', because the influence of this was not notable during the parameter estimations. The advantage of regularization is that it prevents overestimation of parameters,

which is now definitely the case because some parameters are estimated to be extreme.

Another recommendation for linearized parameter estimation is to penalize differently for nonlinear data. This can be achieved by adding a threshold, determined by the user, inside the cost function so that the weights of large errors from quadratic behaviour will be penalized in a linear way instead of quadratic.

The model structure can be unsuitable due to the different simplifications in the nonlinear model and after that due to the linearization. It is recommended to make the governor in the nonlinear model more advanced by implementing a PID regulator instead of a PI regulator and furthermore by implementing discrete behaviour in the governor. Thirdly, it is recommended to implement a time delay which was visible during the step response validation.

Additionally, the nonlinear model contains no discrete firing frequency of the diesel engine. Furthermore, the step sizes of the engine governor calculations and possible engine management system are not implemented. Furthermore, due to the linearization of the engine several engine limitations are not taken into account.

The implementations of these components in the nonlinear model are recommended for two reasons. First of all, the nonlinear model can then be used as model structure for nonlinear parameter estimation. Furthermore, it is possible to see if parameter identification can be executed in a virtual environment when these components are implemented. If more output signals are measured, then it is also recommended that more relations are derived between the input signal and the newly obtained output signals.

8

CONCLUSION & RECOMMENDATIONS

In this final chapter, conclusions are drawn from the findings in this thesis work. In addition to that, some recommendations are given on the future development of full-scale parameter identification.

8.1 CONCLUSION

This thesis aims to answer the main research question: *"How to determine propulsion model parameters with identification techniques on a full-scale propulsion system in limited time?"*. The answering of this main research question is done according to three sub questions.

8.1.1 First sub question

The first sub question is: *"Which parameter identification techniques are suitable for model parameter estimation of a ship propulsion plant?"*. This sub question will be answered with parameter identification in a virtual environment. Parameter identification generally requires three things: an information-rich data set, a model structure and an optimization program. These three components are in following three paragraphs discussed.

The different information-rich datasets are obtained from the nonlinear model which is presented in figure 3.1. The use of this nonlinear model is correct, because it's statically validated in figure 3.2 and 3.3 with data from a sea trail. The two most feasible input signals of the system are multiple sine waves and a chirp signal. The advantage of a multiple sine wave is that the parameter estimation can be 'validated' and it contains a relatively high spectral purity, because it is just a single frequency which also allows the user to filter out noise more easily. The chirp input signal is interesting, because it minimizes the duration of the experiments. Other input signals are not taken into account, because in practice the system can not react to them (pulse signals) or it is unknown whether the signal will be deformed by ramps and/or any other safety mechanism (Band limited white noise). These practical considerations are taken into account, however due to limitations of the nonlinear model it still could work in the virtual environment. More importantly: the input signal needs to contain the correct input frequencies and amplitude, otherwise the parameter estimation is not possible.

The model structure in state space notation, which was used for the parameter estimation, is presented in equation 3.53 and 3.54. This model structure is correct, because it is verified in figure 3.6 and 3.7. Using this model structure it is not possible to determine every parameter individually, because the amount of unique relations between the parameters is not equal to the amount of parameters, presented in table 4.2. This results in the fact that

only the values of g and τ_n and the relations vK_p and $\frac{K_p}{K_i}$ can be individually determined. Nevertheless this model structure is used due to fact that the value v can be derived from a factory acceptance test (FAT) of the engine.

The optimization program takes the following things into account: Weighted cost function, regularization, stopping criteria and constraints to the parameters so that a feasible solution is obtained.

With the information-rich data sets, model structure and optimization program, different parameter estimations are executed and the results are promising due to high fit and validation percentages, see table 5.2. During the virtual experiments, the two input signal types are used multiple times with different properties. The used signals are: Multiple sine waves (ii), a chirp signal where the frequencies are linearly divided over time (iii), a chirp signal where the frequencies are logarithmically divided over time (iv) and a chirp signal with an increased amplitude (v). There is a good fit between the nonlinear data and the simulated response using the estimated parameters. Additionally, validated percentages are obtained by comparing the obtained simulated response using the estimated parameter set compared to a different nonlinear data set, namely step responses. These validated percentages are promising, due to the high percentages. The estimated parameter sets ii, iii and iv only differ from the actual value by a small percentage, max $\pm 2\%$. From this can be concluded that parameter estimation ii, iii and iv are correct. For parameter estimation v, the maximum obtained error in the parameters increases to a maximum of $\pm 22\%$. This is a point of attention for the full-scale experiments due to the fact that an increased amplitude influences the parameter estimation a lot and is the reason for this error. However, this parameter estimation is classified as correct especially if the simulated response using the whole estimated parameter set is taken into account. This is shown in the time domain with several step responses in figure 5.17 and in the frequency domain in figures 5.15 and 5.16. In both domains, all parameter estimations are showing the same simulated response as the response of actual parameters.

So, with the given model structure, information-rich data sets and optimization program, it is possible to execute parameter estimation on a ship propulsion plant in a virtual environment. Still, the answering of the first sub question is incomplete, namely which techniques are suitable. Parameter identification requires three things, model structure, information-rich data set and optimization program. During this research, only the information-rich data sets are varied by using different input signals. So, virtual parameter estimation is possible with multiple sine waves and chirp signals as input signal. For executing parameter estimation on full-scale, similar input signals and the same optimization program will be used as outlined above.

8.1.2 Second sub question

The second subquestion is: *"Which experiments are suitable for the full-scale determination of model parameters?"*. The full-scale limitations are already taken into account in the choice of the input signals, as discussed in the previous subquestion. This subquestion is thus already partly answered. Still, it is unknown whether it is possible to obtain full-scale model parameters. To an-

swer this question, the same approach is used as for the virtual experiments, with some minor changes to the optimization program, model structure and information-rich data sets.

The optimization program is identical as during the virtual experiments. The only difference is that disturbances need to be added, because the measured data contains noise. For full-scale parameter estimation, the same model structure is used as for the virtual model parameter simulation, equation 3.53 and 3.54.

In Chapter 6 is concluded that the obtained information-rich data sets are derived correctly. However, some important remarks were made. First, the shaft speed obtained from single pulse measurement is only valid for input frequencies lower than $\pm 2.5\text{Hz}$. The shaft speed obtained with the four pulse measurement is only valid for input frequencies lower than $\pm 10\text{Hz}$.

The following parameter estimation on full-scale are executed: Multiple sine waves, chirp signals short and chirp signal long. The results of the full-scale parameter estimation, shown in table 7.1, do not look promising. First of all, the fitting percentages are not high and the estimated parameters are all different. However, the validation percentages are high and this is achieved by comparing the parameter estimation with another data set, namely step responses. Please note that these percentages are so high, because a big part of this signal is constant. Because of this it's better to make a validation where the results are visually compared. The results of this validation are presented in figures 7.17 and 7.18. From these figures, it is concluded that the parameter estimation responses are in line with measured data, namely step responses. Additionally, a 0.5 s delay is observed in the propulsion drive train, the reason for this is unknown.

The answering on the second sub question is as follows: So far no suitable experiments are found that can determine the full scale individual parameters and relations. However, it is possible that in the near future the executed experiment is suitable and that only a more advanced searching algorithm and/or model structure leads to correct parameter estimation. However, with the executed experiment and the explained model structure and searching algorithm it is possible to estimate the model response quite well compared to full scale step response. This is quite relevant, because in practice the most given input signals by the captain are step responses.

8.1.3 Third sub question

The third research question is: *"What is the uncertainty of an estimated full-scale model parameter?"*. The goal of this question is to look at the uncertainty of the estimated parameters. Determining the uncertainty of the estimated parameters is a difficult task, but possible. With the correct mathematical approaches the variance and bias of the estimated parameters can be determined. However, the influence on the uncertainty of fitting a linearized model on the nonlinear data is unknown and makes determining the uncertainty difficult. Because the parameters are not estimated correctly, no in-depth uncertainty analysis is executed. For this reason, an answer in the precision of the estimation is more useful than the uncertainty.

So, the value of τ_n is obtained from a different experiment, namely $\tau_n = 1.17$. If this value is compared to the results of the parameter estimation in table 7.1, it is clear that none of the parameter estimations are correct and the precision is low. However, the simulated response of the three different estimated parameter sets are identical when they are compared to different validation data sets, see figure 7.18 and 7.17. From this, it is concluded that the simulated response using the estimated parameters sets is more precise.

Nevertheless, before an uncertainty analysis is done, it is advisable to start with a sensitivity analysis, where five Bode plots are made and in every Bode plot one single parameter is varied. This shows the influence of a certain parameter on the complete estimate response.

8.2 RECOMMENDATIONS

This final section contains the recommendations for future work on full-scale parameter identification. Please note that only the main recommendations are outlined here and that all the recommendations can be found in Chapter 6.5.2 'Recommendations experiments' and Chapter 7.4.2 'Recommendations full-scale estimation'.

- If another nonlinear simulation model would be built (discrete engine firing, sampling time governor and discrete steps in the governor), it is recommended to do this based on a Damen Stu1205, because dynamic data exists for this vessel which enables the user to do a dynamic validation of the simulation model.
- The results of the virtual parameter estimations are executed without any noise in the data. A recommendation for future work is to see if parameter estimation is also possible when noise is included, and to see what the influence is on the results. This approach might reduce the gap that is between full-scale experiments and virtual experiments.
- After a comprehensive analysis of the data, it is concluded that at higher frequencies the obtained data is not in line with the nonlinear model data. A possible reason for this could be that an incorrect assumption is made in chapter 2, where is stated that the simplifications such as discrete engine firing frequency, sampling frequency governor and engine management system can be made. Also, the assumption that the governor is equipped with a PI regulator instead of a PID regulator can have influence. However, it is recommended to add and change these components in the nonlinear model. Then, first of all, to see if it is possible to execute parameter identification with this new, more complex nonlinear model(virtual experiments). Second of all, this nonlinear model can be used as a 'model structure', so that discrete steps and limits are involved during the parameter estimations. When the nonlinear model is used as model structure, this leads to nonlinear parameter estimation.
- It is recommended in follow-up experiments to measure the shaft speed with eight pulses instead of four pulses. Furthermore, it is recommended to measure more output signals than only the shaft speed and shaft torque, e.g. CAN bus of the diesel engine, because this can

offer a solution in identifying all the parameters instead of only relations. For example, the relation of fuel rack over engine set point can be used.

- It is recommended to pay more attention to the data pre-processing of the shaft torque. In practice, the strain gauge measures the torque between the propeller and the gearbox. The measured shaft torque value should be in-between the propeller torque and gearbox torque depending on the amount of mass moment of inertia on both sides of the strain gauge. However, in the model structure the propeller torque or the shaft torque has to be used. So, because of this, it is advisable to multiply the obtained shaft torque with a correction factor. Second of all, it is advisable to take into account the 4 pulse signal PTM_4 , not all of the reflectors were positioned equally over the shaft. If the obtained data is used, it is recommended to use a more advanced algorithm that takes this inequality of the reflector positioning into account, so that the model is not fit on noise of the imperfection of the shaft speed measurement.
- It is also recommended to take a closer look at the searching algorithm and the usage of regularization, so that overestimation can be avoided. Furthermore, if a linearized parameter estimation is used, then penalize nonlinear data differently. This can be achieved by adding a threshold, determined by the user, inside the cost function so that the weights of large errors from quadratic behaviour will be penalized in a linear way instead of quadratic.
- A separate recommendation from a more practical point of view is to execute the parameter estimation with a simpler model structure, so that the parameters v and g are cancelled. This leads to a three parameter model structure, which can maybe capture the shaft dynamics and can be easily used for simulations.
- The above-mentioned recommendations contain contradictions, because it is recommended to increase the level of detail of the model structure and afterwards it is recommended to simplify the model. Which to follow depends on the purpose of the research or application, as some require simplicity, while other purposes require additional complexity.

BIBLIOGRAPHY

- [1] DEWESoft Dual Core. https://d36j349d8rqm96.cloudfront.net/3/6/SIRIUS-DC_and_HD_filtering.pdf. Accessed: 2019-12-20.
- [2] A. Vrijdag. Potential of hardware-in-the-loop simulation in the towing tank. Proceedings Oceans MTS/IEEE Monterey:1–6, 2016.
- [3] M. Altosole, G. Benvenuto, and U. Campora. Real-time simulation of a cogag naval ship propulsion system. Journal of engineering for the maritime environment, 223, 2009.
- [4] F. Cipolini, A. Oneto, L. Coraddu, A.J. Murphy, and D. Anguita. Condition-based maintenance of naval propulsion systems with supervised data analysis. Ocean Engineering, 149:268–278, 2018.
- [5] A. Coraddu, L. Oneto, A. Ghio, S. Savio, D. Anguita, and M. Figari. Machine learning approaches for improving condition-based maintenance of naval propulsion plants. Journal of Engineering for the Maritime Environment, 230:136–153, 2016.
- [6] M. Martelli. *Marine Propulsion Simulation methods and results*. De Gruyter, 2015.
- [7] N. Makrygiannis. Propulsion system control in ships sailing in waves. MSc-thesis, Delft University of Technology, 2018.
- [8] A. Vrijdag and D. Stapersma. Extension and application of a linearised ship propulsion system model. Ocean Engineering, 143:50–65, 2017.
- [9] J. Carlton. *Marine Propellers and Propulsion*. MPG Books Ltd, Bodmin Cornwall, 2007.
- [10] P. Matic and R. Antonic. Marine diesel engine governor identification. Volume 40:385–389, IFAC Proceedings Volumes, 2007.
- [11] L. Ljung. *Systems identification Theory for the user*. Prentice Hall PTR, 1999.
- [12] G.J. Olsder and van der J.W. Woude. *Mathematical Systems Theory*. VSSD, 2004.
- [13] J. Schoukens and L. Ljung. Nonlinear system identification a user-oriented roadmap . IEEE Control System magazine:1–2, 2019.
- [14] D. Stapersma and A. Vrijdag. Linearisation of a ship propulsion system model. Ocean Engineering, 142:441–457, 2017.
- [15] A. Vrijdag and D. Schuttevaer. Exploration of a systems and control approach to reduce propeller cavitation in a seaway. 182:174–187, 2019.
- [16] T. Westwick and R. Kearney. *Identification of nonlinear physiological systems*. Wiley-IEEE Press, 2003.
- [17] M. Verhaegen and Vincent. Verdult. *Filtering and System identification: A least squares approach*. Cambridge University Press, 2007.

- [18] V.A. Golikov. A simple technique for identifying vessel model parameters. 4th International Scientific Conference SEA-CONF, 172, 2018.
- [19] R. Skjetne, O. Smogeli, and T. I fossen. A nonlinear ship manoeuvring model: identification and adaptive control with experiments for a model ship. *Modeling, Identification and control* 25(1), 2004.
- [20] R. Skjetne, O. Smogeli, and T. I fossen. Modeling identification and adaptive maneuvering of cybership ii: A complete design with experiments. *IAFC Proceedings Volumes*, 2004.
- [21] Y. Sang. Parameter identification, simulation, linearization and validation of a ship propulsion system. MSc-thesis, Delft University of Technology, 2018.
- [22] A. Vrijdag and Y. Sang. Fingerprinting the ship propulsion system: low hanging fruit or mission impossible. *Proceedings of INEC/ISCSS*, Glasgow, UK, 2018.
- [23] Wei-Yuan Hwang. *Application of system identification to ship maneuvering*. PhD thesis, 1980.
- [24] Gengshen Liu. *Measurement of ship resistance coefficient from simple trials during a regular voyage*. PhD thesis, 1988. Eindverslag.
- [25] Stan Launch 804 product sheet. <https://products.damen.com/en/ranges/pushy-cat/stan-launch-804>. Accessed: 2019-06-03.
- [26] Bollard pull calculation. <https://www.wartsila.com/encyclopedia/term/bollard-pull>. Accessed: 2019-06-13.
- [27] B. Girod and R. Rabenstein. *Signals and systems 2nd*. Wiley, 2001.
- [28] H. Bozdogan. Model selection and akaike's information criterion (aic): The general theory and its analytical extensions . *Psychometrika* 52(3):345-370, 1987.
- [29] System identification toolbox. <http://citeseerx.ist.psu.edu/viewdoc/download?doi=10.1.1.461.1702&rep=rep1&type=pdf>. Accessed: 2019-07-2.
- [30] Installation marine commercial control d9 d12 d16. https://muldermotoren.nl/SalesGuidedec2014/prosales.penta.volvo.net/vpprosales/sst/marine_genset_asp/html_pdf/7745527.pdf. Accessed: 2019-09-09.
- [31] Signal generator. <https://docs-apac.rs-online.com/webdocs/1568/0900766b81568ea8.pdf>. Accessed: 2019-11-02.
- [32] Signal converter. https://files.pepperl-fuchs.com/selector_files/navi/productInfo/edb/264352_eng.pdf. Accessed: 2019-11-02.
- [33] Binsfeld. <https://binsfeld.com/wp-content/uploads/2019/08/tt10-users-guide.pdf>. Accessed: 2019-11-05.
- [34] ROLS. <https://monarchserver.com/Files/pdf/InstrumentBrochure.pdf>. Accessed: 2019-11-04.

- [35] DEWEsoft. https://d36j349d8rqm96.cloudfront.net/3/6/SIRIUS_technical_reference_manual_EN.pdf. Accessed: 2019-11-03.
- [36] L. Balmer. *Signals and Systems: An introduction*. Prentice Hall, 1997.
- [37] Sinefitting. <https://www.mathworks.com/matlabcentral/fileexchange/66793-sine-fitting>. Accessed: 2019-12-17.

A | LINEARIZATION

A.1 NORMALIZATION OF GOVERNOR

For small increments can be said that the error in the governor is the difference between the set point of the lever and the 'real' engine speed, see the equation A.1.

$$\delta e_n = \delta n_{set} - \delta n_e \quad (\text{A.1})$$

This can be normalised by dividing both sides by the operating point.

$$\frac{\delta e_n}{n_0} = \frac{\delta n_{set}}{n_0} - \frac{\delta n_e}{n_0} \rightarrow \delta e_n^* = \delta n_{set}^* - \delta n_e^* \quad (\text{A.2})$$

The PI controller in normalised conditions in the same way:

$$\frac{\delta X_{set}}{X_0} = \frac{K_p \delta e_n}{n_0} + \frac{K_i \delta E_n}{n_0} \rightarrow \delta X_{set}^* = K_p \delta e_n^* + K_i \delta E_n^* \quad (\text{A.3})$$

Were the integral of the error is capital error:

$$\delta E_n^* = \int_0^t \delta e_n^* dt \quad (\text{A.4})$$

A.2 DERIVATION SHAFT TORQUE AND ENGINE SET POINT

First of all can the nonlinear model be summarized into figure A.1, were every component now equals one or more equation from the DAE. All the different components in the figure A.1 are also defined with a letter, so the governor is defined as C , the diesel engine defined as D , and the core propulsion system is H_{ship} . It eases the math when these letters used instead of the whole equation.

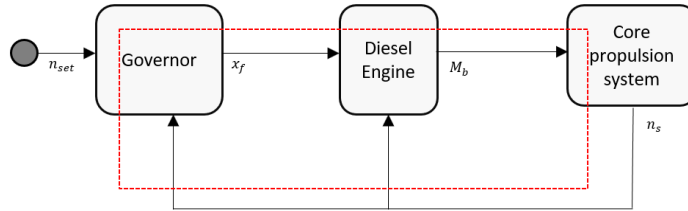


Figure A.1: Closed loop linearization

Equation A.5 is a Laplace transform from the shaft loop equation 3.14. This is also the only equation that is in the core propulsion system.

$$\tau_n s \delta n^* = M_s^* - 2 \delta n^* \quad (\text{A.5})$$

The core propulsion system can be rewritten so that the actual shaft speed is in relation with the shaft torque, see equation A.6. Next to that can the governor component also be written as in equation A.7.

$$H_{ship}(s) = \frac{\delta n^*}{\delta M_s^*} = \frac{1}{\tau_n s + 2} \quad (\text{A.6})$$

$$C(s) = K_p + \frac{K_i}{s} \quad (\text{A.7})$$

When the efficiency of the gearbox is constant then A.8 is applicable.

$$\delta M_s^* = g \delta n^* + v \delta X^* \quad (\text{A.8})$$

Then the normalised fuel rack set point, δX^* , is equal to the governor, C multiplied by the error, where the error, $\delta n_{set}^* - \delta n^*$. This leads after some mathematical manipulations to equation A.9.

$$\delta M_s^* = (g - vC) \delta n^* + vC \delta n_{set}^* \quad (\text{A.9})$$

Equation A.6 can be rewritten were the shaft speed is a function of H_{ship} and δM_s^* . This can be implemented in equation A.9, were after some additional mathematical manipulations the transfer function A.13 is derived.

$$\delta M_s^* = (g - vC) H_{ship} M_s^* + vC \delta n_{set}^* \quad (\text{A.10})$$

$$\frac{\delta M_s^*}{\delta n_{set}^*} = \frac{vC}{(vC H_{ship} - g H_{ship} + 1)} \quad (\text{A.11})$$

$$\frac{\delta M_s^*}{\delta n_{set}^*} = \frac{vK_p s + vK_i}{s (vH_{ship} K_p + vH_{ship} \frac{K_i}{s} - g H_{ship} + 1)} \quad (\text{A.12})$$

$$\frac{\delta M_s^*}{\delta n_{set}^*} = \frac{vK_p s^2 + \frac{vK_i \tau_n + 2vK_p}{\tau_n} s + \frac{2vK_i}{\tau_n}}{s^2 + \frac{vK_p - g + 2}{\tau_n} s + \frac{vK_i}{\tau_n}} \quad (\text{A.13})$$

B | RELATIONS MODELSTRUCTURE

As defined in transfer functions 4.14, 4.15 and 4.16 the values in the denominator are all equal so, this is defined as a and b , see equation B.1.

$$\frac{2 - g + vK_p}{\tau_n} = a \quad \frac{vK_i}{\tau_n} = b \quad (\text{B.1})$$

In the named transfer functions are the relations in the numerator presented in B.2 and B.3.

$$\frac{vK_p}{\tau_n} = c \quad \frac{vK_i}{\tau_n} = d \quad \frac{2 - g}{\tau_n} = e \quad (\text{B.2})$$

$$vK_p = f \quad \frac{vK_i\tau_n + 2vK_p}{\tau_n} = h \quad \frac{2vK_i}{\tau_n} = i \quad (\text{B.3})$$

C | STAN TUG 1205

Product sheet STAN TUG 1205 'TOR'



STAN TUG 1205
"TOR"

GENERAL

Yard number 502520
 Delivery date December 2017
 Basic functions Towing and mooring operations
 Bureau Veritas
 Classification I * HULL * MACH Seagoing Launch
 Sweden
 Flag
 Owner Marin & Haverikonsult KA AB

DIMENSIONS

Length overall 13.08 m
 Beam overall 5.28 m
 Depth at sides 2.30 m
 Draught aft 1.80 m
 Displacement 54 t
 (98% consumables)

TANK CAPACITIES

Fuel oil 5.60 m³
 Fresh water 0.35 m³
 Sewage 0.33 m³
 Bilge water 0.30 m³

PERFORMANCES

Bollard pull 9.1 t
 Speed 9.9 kn

PROPULSION SYSTEM

Main engines 2x Volvo D9 MH
 Total power 442 bkW (600 bhp) at 1800 rpm
 Gearboxes Twin Disc MG 5091 / 3.82:1
 Propellers 2x Kaplan fixed pitch 1050 mm diameter
 Nozzles 2x Van de Giessen 'Optima' with stainless steel innerrings
 Engine control Volvo EVC
 Rudders 2x double plate high performance
 Steering gear Powered-hydraulic 2x 50° + rudder indicator

AUXILIARY EQUIPMENT

Battery sets 2x 24 V 230 Ah, changeover facility
 Generator Onan MDKBR-eQD 230 V, 17.5 kVA, 50 Hz
 Alarm system Engines, gearboxes and bilge alarm
 General service/ bilge pump SIWI VWSI 5013, 15 m³/h at 2.3 bar
 Fuel oil system Water separator, filters and SOS valve
 Cooling system Closed cooling channels
 Sanitary system Speck 24 V pressure set, Rheinstrom 24 V sewage discharge pump
 Engine room ventilation Mechanical ventilation 8000 m³/h
 Fire extinguishers 2x 5 kg CO₂ and 2x 6 kg dry powder

DECK LAY-OUT

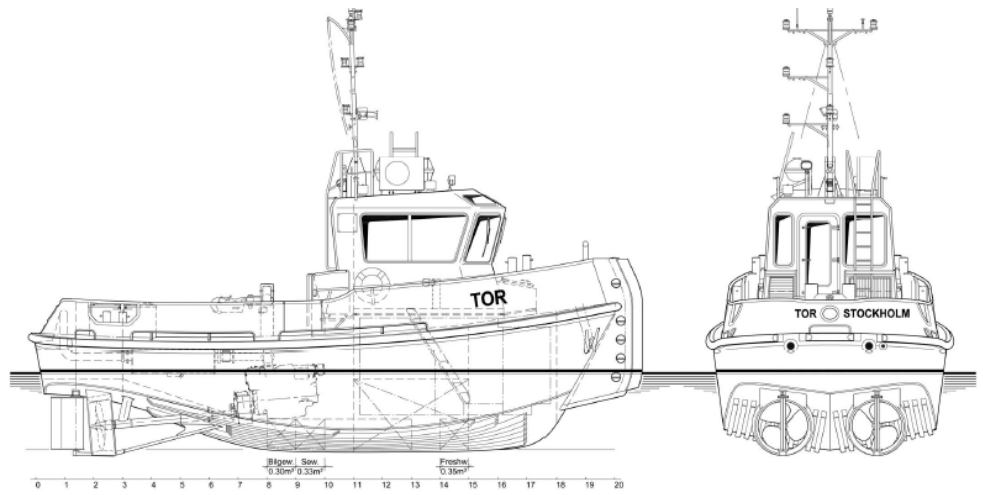
Anchor winch Electrically driven 24 V
 Towing hook Mampaey Disc type, 15 ton SWL
 Side/astern fender Rubber D-fender 150 x 150 mm
 Push bow Cylindrical rubber fender 380 mm

ACCOMMODATION

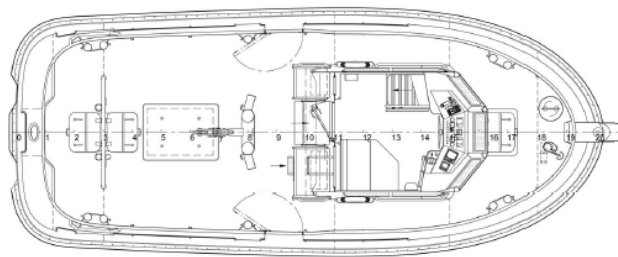
The air-conditioned wheelhouse is resiliently mounted and has an extremely low noise level of approx. 55 dB(A). The wheelhouse and below deck accommodation are completely insulated and finished with durable modern linings and composite synthetic floor. Wheelhouse with a bench for two persons and a table. Windows are fitted in aluminium frames. Below deck a kitchen unit, shelves and 4 lockers are arranged.

NAUTICAL AND COMMUNICATION EQUIPMENT

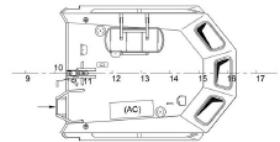
Searchlight Den Haan 250 W, 24 V
 Compass fluxgate Cassens & Plath, type Kotter
 GPS Furuno GP-32
 Echosounder Furuno LS-6100
 VHF radio telephone Sailor Compact 6248, 25 W
 Navigation lights Navigation lights incl. towing and side lights
 Floodlight 150 W on aft deck



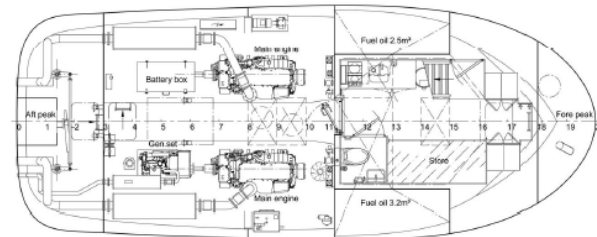
Main deck



Top deck



Below Main deck



DAMEN

D | SHAFT TORQUE FACTOR

Provided by JVS B.V. conversion factor shaft torque.

Berekening asfactor			
project:		Datum:	4-11-2019
Input installatie			
Vermogen =	221	kW	
RPM =	1800		
Reductie =	3,820	1/i =	I= 0,261780105
T motor =	1,17	kNm	
T as =	4,48	kNm	Mv= 4229
Invoer meetapparatuur			
Rstr =	350	[ohm]	
Rijk =	437400	[ohm]	
K =	2,080		
U =	2000	[mV]	
G =	7,700E+10	[n/m2]	
Duitw. =	90	[mm]	
Dinw. =	0	[mm]	
C =	1,059	Nm/mV	
IMC =	9,441E-04	V/Nm	
<p>Blaue cellen zijn in te vullen velden. Rode uitkomst zijn berekende waarden</p>			

E

TIME TO FREQUENCY DOMAIN

In this appendix the results of the 'SineFit' function for the different frequencies ω_i and the different measured input and output signals are discussed. In practice this means that the time domain measurement is put into frequency domain. This is done with help of a Matlab function 'SineFit'. Only the obtained data of multiple sine waves S2-S16 are put into frequency domain. The 'SineFit' function determines four values, first of all 'a' the offset, 'b' the amplitude, 'c' the frequency, 'd' the phase shift, as presented in E.1.

$$a + b \cdot \sin(ct - d) \quad (\text{E.1})$$

In tables E.1, E.2 and E.3 the results are presented of the 'SineFit', where in the first column the input frequency of the signal generator is presented. In the second column the value 'a' is presented, in the third column value 'b', in fourth column value 'c' and in the fifth column value 'd'.

Freq_input [Hz]	Offset [rpm]	Amplitude [rpm]	Frequency [Hz]	Phaseshift [Phi]
0.0044	1181	76	0,0044	0,8063
0.0092	1181	76	0,0092	3,0402
0.0193	1181	76	0,0193	5,882
0.0275	1181	76	0,0275	4,692
0.0405	1181	76	0,0405	3,087
0.06	1181	76	0,0600	2,268
0.084	1181	76	0,0848	6,079
0.11	1181	76	0,1100	5,12
0.1778	1181	76	0,1778	3,98
0.3728	1182	76	0,3728	3,028
0.7814	1182	76	0,7814	5,091
1.637	1182	76	1,6370	4,3933
3.433	1182	68	3,432	1,2377
7.19	1182	76	7,1899	2,501
15.01	1182	76	15,0099	1,809
31.644	1182	76	31,644	4,29

Table E.1: Setpoint engine speed determined by 'SineFit'

Freq_input [Hz]	Offset [rpm]	Amplitude [rpm]	Frequency [Hz]	Phaseshift [Phi]
0.0044	1180	76	0,0044	0,79
0.0092	1180	76	0,0092	3,022
0.0193	1180	76	0,0193	5,81
0.0275	1180	76	0,0275	4,61
0.0405	1180	76	0,0405	2,96
0.06	1180	76	0,05996	2,09
0.084	1180	77	0,0848	5,832
0.11	1180	77	0,10998	5,17
0.1778	1181	78	0,17781	3,18
0.3728	1180	77	0,37277	2,40
0.7814	1178	69	0,78134	3,91
1.637	1176	41	1,63689	1,69
3.433	1171	24	0,46446	5,82
7.19	1179	62	0,70541	4,482
15.01	1173	21	2,04048	2,05
31.644	1179	4	0,77896	0,16

Table E.2: Shaft speed determined by 'SineFit'

Freq_input [Hz]	Offset [Nm]	Amplitude [Nm]	Frequency [Hz]	Phaseshift [Phi]
0.0044	1685	233	0,0044	0,8929
0.0092	1651	235	0,0092	3,2854
0.0193	1672	235	0,0193	5,6700
0.0275	1699	237	0,0275	4,8836
0.0405	1703	237	0,0405	3,0079
0.06	1706	240	0,060	2,0408
0.084	1712	244	0,0848	5,6642
0.11	1706	243	0,110	5,5086
0.1778	1713	249	0,1778	3,2608
0.3728	1719	263	0,3728	2,8288
0.7814	1690	292	0,7813	4,5919
1.637	1705	300	1,6369	2,882
3.433	1695	96	3,0510	2,8923
7.19	1691	253	0,7054	0,2885
15.01	1698	234	15,3584	0,232
31.644	1721	304	15,4423	2,3834

Table E.3: Shaft torque determined by 'SineFit'

Already, by looking at the values in the tables E.1, E.2 and E.3, some errors and outliers from the 'SineFit' can be observed. In the coming three parts, every signal is discussed in more detail for different frequencies. Please note that only the errors and outliers of the 'SineFit' estimation are discussed in the parts here below,.

SETPPOINT ENGINE SPEED

From table E.1 setpoint engine speed, is visible that at an input frequency of 3.43 Hz the amplitude is most likely not estimated correctly. This is illustrated in figure E.1, because in this graph is clearly visible that the amplitude of the data is higher and is also around $\pm 76 \text{ rpm}$ (red line), but the 'SineFit' estimates the amplitude lower (blue line), the reason for this occurrence is partly unknown. In frequency domain is namely visible that at the input signal of 3.43 Hz some lower frequent noise (3.1 Hz) can be distinguished, which most probably influences the estimated amplitude.

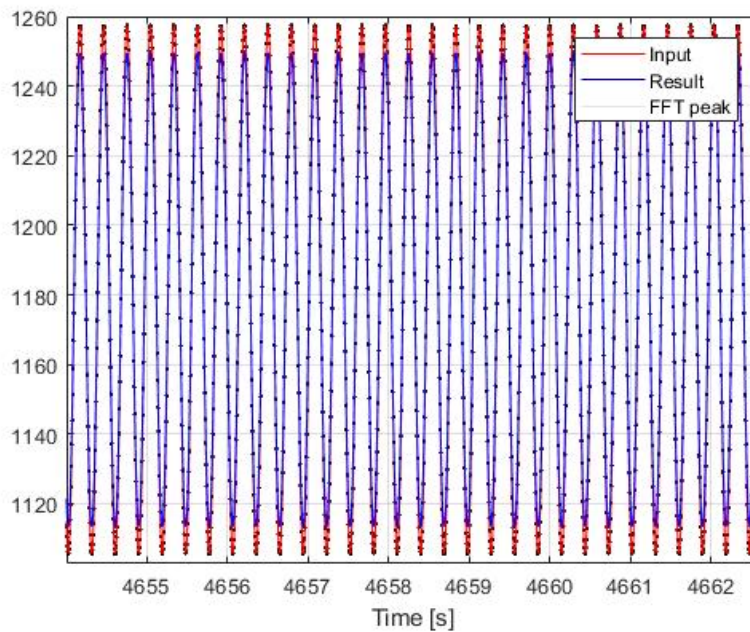


Figure E.1: Input signal validation 3.433 Hz in time domain

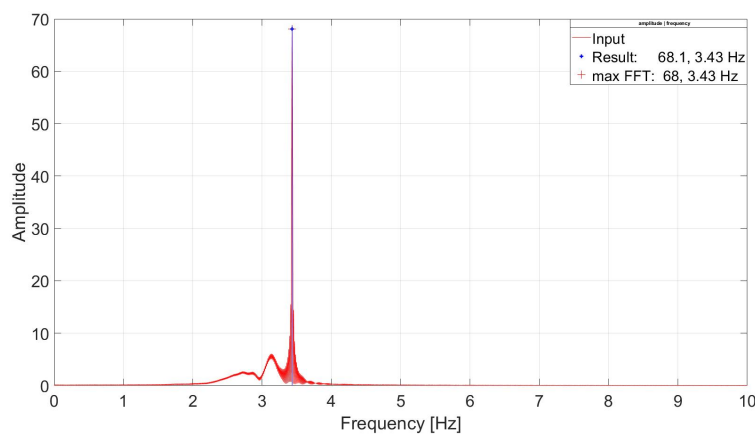


Figure E.2: Input signal validation 3.433 Hz in frequency domain

SHAFT SPEED

The results of the sine fits on the shaft speed are presented in table E.2. It is visible that at an input frequency of 3.433Hz the estimated frequency is incorrect, 'c'. This can be easily checked, because the input frequency is known. In figure E.3 the error is illustrated and the high frequent input signal is visible in the output, but unfortunately the lower frequency component in the signal is more dominant. This is clearly illustrated in figure E.4, where in frequency domain a big peak can be observed at 0.7 Hz . A reason for this is most probably aliasing or nonlinearities inside the system.

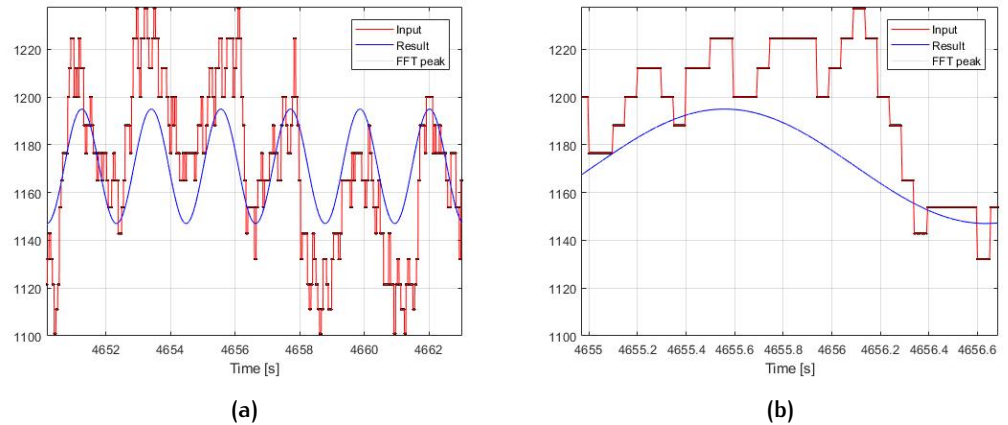


Figure E.3: Measurement shaft speed frequencies 3.433Hz in time domain.

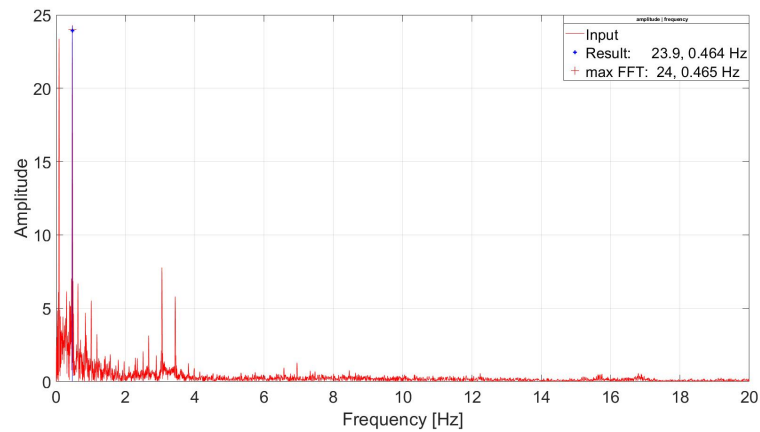


Figure E.4: Input signal validation 3.433 Hz in frequency domain.

The shaft speed measurement with an input frequency of 7.19Hz is presented in figure E.5, where can be seen that most probably due to aliasing the measured response is a lot lower. This means that the SineFit is correctly fitted on the data, but the data just does not contain the high frequent component of 7.19Hz . This becomes clear when the results are put in frequency domain see figure E.6.

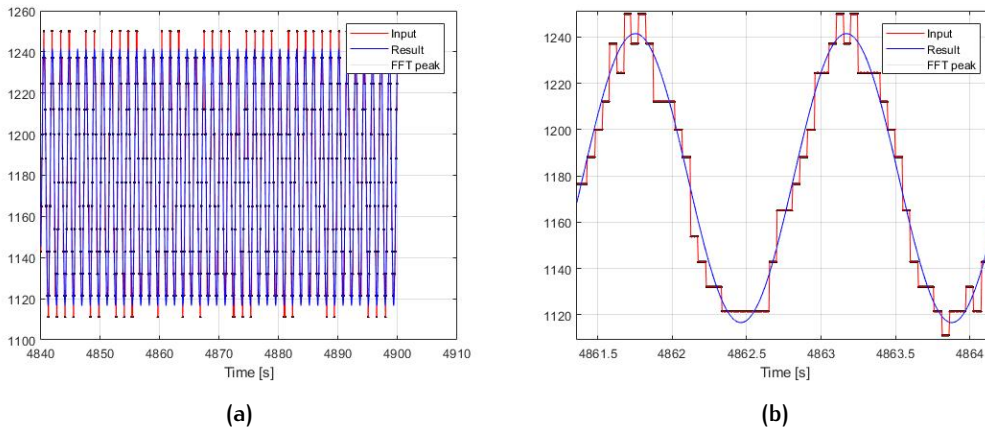


Figure E.5: Measurement shaft speed frequencies 7.19Hz in time domain.

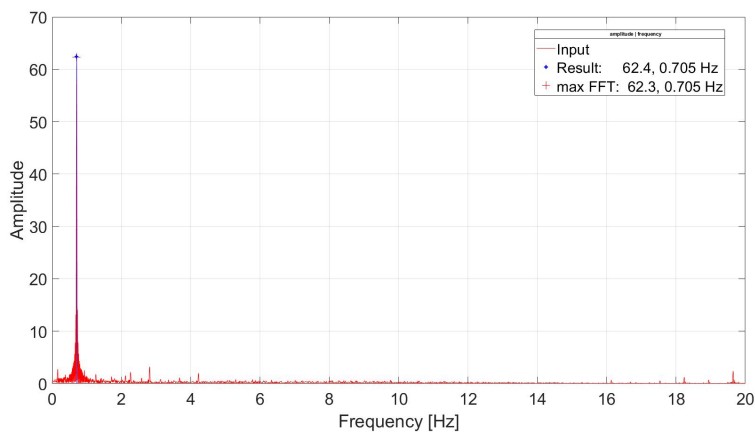


Figure E.6: Input signal validation 7.19 Hz in frequency domain.

SHAFT TORQUE

The results of the 'SineFit' on the shaft torque is presented in table E.3. In this table can be seen that at input frequency of 3.433Hz the amplitude is estimated quite low. This problem is also illustrated in figure E.7. The fitted blue line is not coping with the input data, namely the red line. Again, the lower frequency noise is dominant in the total signal, which is clearly visible in figure E.8. In frequency domain also the blade, engine and firing frequencies are visible.

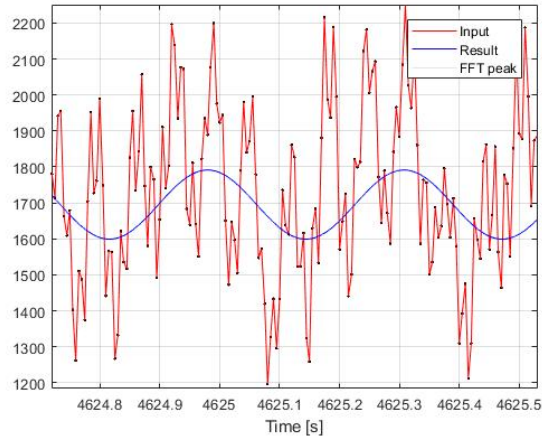


Figure E.7: Torque signal wrongly estimated amplitude at input frequency 3.44 Hz in time domain.

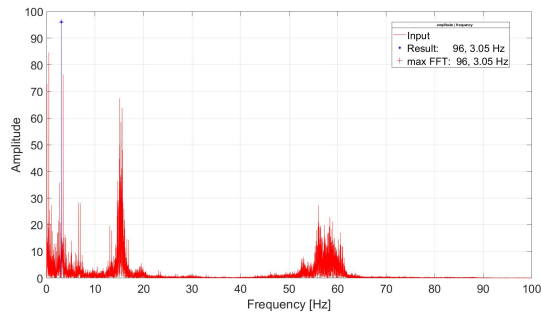


Figure E.8: Torque signal wrongly estimated amplitude at input frequency 3.44 Hz in frequency domain.

At an input frequency of 7.19 Hz is clearly visible that the 'SineFit' of the shaft torque is incorrect, e.g. frequency is estimated significantly lower. In figure E.9 is clearly visible that a lower frequency is most dominant in the signal. Only the blade, engine and firing frequencies are visible.

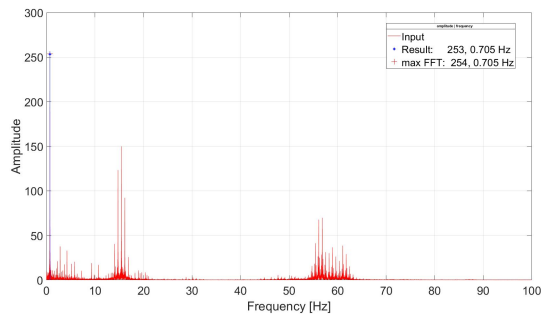


Figure E.9: Torque signal wrongly estimated amplitude at input frequency 7.19 Hz in frequency domain.

